MANUFACTURING OF AGAROSE-BASED CHROMATOGRAPHIC MEDIA WITH CONTROLLED PORE AND PARTICLE SIZE

by

Nicolas Ioannidis

A thesis submitted to

The University of Birmingham

for the degree of

DOCTOR OF PHILOSOPHY

School of Chemical Engineering

College of Engineering and Physical Sciences

The University of Birmingham

2009

ABSTRACT

Chromatography remains the most commonly employed method for achieving high resolution separation of large-sized biomolecules, such as plasmid DNA, typically around 150-250 nm in diameter. Currently, fractionation of such entities is performed using stationary phases designed for protein purification, typically employing pore sizes of about 40 nm. This results into a severe underexploitation of the porous structure of the adsorbent as adsorption of plasmid DNA occurs almost exclusively on the outer surface of the adsorbent. In this study, the effect of two processing parameters, the ionic strength of agarose solution and quenching temperature, on the structure of the resulting particles was investigated. Three characterization methods, Atomic Force and cryo-Scanning Electron microscopy, as well as mechanical testing of single particles where used to quantify the effect of these parameters on the pore size/size distribution and mechanical properties of the adsorbent. In the presence of salt, it was found that agarose fibres tend to aggregate, leading to a gel with large pore size and wide pore size distribution. In fact, for the narrow range of ionic strength used (0-0.1m), a five-fold increase in pore size of the gel was observed. The same type of enlarged agarose structures was observed when slow cooling was applied during the gelation of agarose. The increase in pore size of the gel was also accompanied by an increase in the compression strength and the elastic modulus of the particles, i.e. particles with 200 nm pore size were found to have higher compression strength (1.5-fold difference) than those with 40 nm pore size.

ACKNOWLEDGEMENTS

First of all, I would like to thank my supervisor at the University of Birmingham, Prof. A.W. Pacek, for his enormous patience and excellent guidance throughout the last four years. I would also like to thank Prof. A. Lyddiatt for his vital contribution to this work.

I would like to expresses my acknowledgement to the EPSRC and Millipore who provided the funding for this work. I would also like to express my sincere gratitude to Prof. Z. Zhang, and Dr. W. Liu for providing me with Micromanipulation equipment and expertise, essential for the completion of my work.

Essential for the completion of my work was also the contribution of Dr. J. Bowen in Atomic Force Microscopy, and of Dr. P. Ding in Micromanipulation.

Many thanks to all the technical staff at the University of Birmingham and especially to Mr. T. Edleston, Ms. H. Jennings and Mrs. E. Mitchell for technical assistance as well as Mr. P. Stanley and Mrs. T. Morris for their assistance with Scanning Electron Microscopy

Last but not least, I would like to thank Poppy for standing by me and encouraging me through this difficult time.

To my parents, Poppy, and my aunt Thalia who is no longer with us

LIST OF ABBREVIATIONS

AFM: Atomic force microscopy

C–IP–I: Capture, intermediated purification, polishing

CM: Carboxy methyl group

DEAE: Diethylamino ethanol

DNA: Deoxyribonucleic acid

EBD: Electron-beam deposition

HETP: Height of equivalent theoretical plate

HGMF: High gradient magnetic fishing

HLB: Hydrophilic-lipophilic balance

HSM: High shear mixer

ISEC: Inverse size exclusion chromatography

MW: Molecular weight

NMR: Nuclear magnetic resonance

O / W: Oil-in-water

pDNA: Plasmid DNA

Q: Quaternary ammonium

RNA: Ribonucleic acid

SALS: Small angle light scattering

SANS: Small angle neutron scattering

SAS: Small angle scattering

SAXS: Small angle neutron scattering

SEC: Size exclusion chromatography

SEM: Scanning electron microscopy

SP: Sulfopropyl

STM: Scanning tunnelling microscopy

TBE: Tris base, boric acid and EDTA buffer solution

TEM: Transmission electron microscopy

UV: Ultra-violet

W / O: Water-in-oil

LATIN SYMBOLS

A: Constant relating to eddy diffusion and mobile phase mass transfer

$\mathbf{A_d}$: Total area of dispersed phase (m^3)

$\mathbf{A_{min}}$: Minimum area occupied per molecule (m^2)

$\mathbf{A_s}$: Specific surface area of dispersed phase ($m^2\ m^{-3}$)

B: Constant relating to longitudinal diffusion

b: Material-depended constant

c.m.c: Critical micelle concentration (mol kg^{-1})

C, C': Constants relating to stagnant mobile phase diffusion

c: Material-depended constant or surfactant concentration in the bulk (kg m^{-3})

$\mathbf{C_A^0}$: Initial concentration of surfactant in the continuous phase prior emulsification (kg m^{-3})

$\mathbf{C_A^{eq}}$: Eq. concentration of surfactant in the continuous phase after emulsification (kg m^{-3})

$\mathbf{C_n}$: Flory characteristic ratio (-)

$\mathbf{C_s}$: Initial surfactant concentration in the emulsion (kg m^{-3})

D: Diameter (m) or diffusion coefficient (m^2s^{-1})

$\mathbf{d_{32}}$: Sauter mean diameter (μm)

$\mathbf{d_{max}}$: Particle maximum diameter (μm)

$\mathbf{d_{min}}$: Particle minimum diameter (μm)

$\mathbf{d_p}$: Particle diameter (μm or m)

E: Young's modulus (Pa) or constant relating to adsorption kinetics

F: Force (N)

$\mathbf{f_{HB}}$: Correction factor

g: Gravitational acceleration (m s^{-2})

G: Shear modulus (Pa)

G': Elastic modulus (Pa)

G'': Viscous modulus (Pa)

h: deformation (m)

H: Height (m)

K: Consistency index (N s^n m^{-2})

l: length of bond along the polymer backbone (nm)

L_c: Column length (m)

m: Meters (m)

M_c: Molecular weight between crosslinks

M_r: Molecular weight

$m_{s,i}$: Mass of surfactant adsorbed in the interface (kg)

$m_{s,t}$: Total mass of surfactant in emulsion (kg)

N: Rounds per minute (rpm) or Avogadro's number (-) or number of crosslinks per chain (-)

n: Flow behaviour index (-)

p_c: Capillary pressure (Pa)

r: particle radius (m)

$(r_0^2)^{1/2}$: root-mean-square, end-to-end distance of the polymer between to crosslinks (nm)

R: Gas constant (-)

Re: Reynolds number (-)

R_h: Hydraulic radius (m)

T: Absolute temperature (°K)

t_{br}: Breakage time (s)

u: Linear velocity (m s^{-1})

V: Volume (L or m^3)

$v_{2,s}$: Polymer volume fraction (-)

V_d: Volume of dispersed phase (m^{-3})

We: Weber number (-)

Y: Yield (%)

z_i: Number of charges in the ion (-)

GREEK SYMBOLS

α: Cone angle (°) or elongation ration of polymer chains in any direction

$\dot{\gamma}$: Shear rate (s^{-1})

Γ: Surface excess concentration of surfactant (mol kg^{-1})

$\boldsymbol{\Gamma_s}$: Surfactant mass surface coverage (kg m^{-2})

$\boldsymbol{\delta_{gap}}$: Rotor-stator gap (m)

ε: Voidage (%) or energy dissipation rate (W kg^{-1})

η: Apparent viscosity (Pa s)

Θ: Surface coverage (-)

λ: Viscosity ratio (-)

μ: Viscosity (Pa s)

ν: Poisson's ratio (-)

ξ: Pore size (nm)

ρ: Density (kg m^{-3})

σ: Interfacial tension (N m^{-1}) or normal stress (Pa)

ϕ: Dispersed phase volume fraction (-)

TABLE OF CONTENTS

LIST OF FIGURES

LIST OF TABLES

INTRODUCTION

i. Background

Chromatography remains the high-resolution method for the separation of biopharmaceuticals. In parallel, with the application of gene vectors as vaccines and medical therapies for improving human health appearing very promising (Levy *et al*. 2000), a considerable demand for chromatographic adsorbents suitable for the isolation of such biomolecules is arising.

In 2009 (until March) the number of approved / initiated gene therapy clinical trials reached 1537 (Fig. 1.1a). Most of these are in Phase I (Fig. 1.1b), while their majority concerns the treatment of cancer diseases (Fig. 1.1c) (http://www.wiley.co.uk/genmed/clinical/). At present, these clinical trials are predominantly concerned with the use of viruses, but plasmid DNA constantly gains ground as gene vector, as it is considered safer and simpler to use in said therapies (Fig. 1.1d) (Kepka *et al*. 2004, Diogo *et al*. 2005, Tiainen *et al.* 2007).

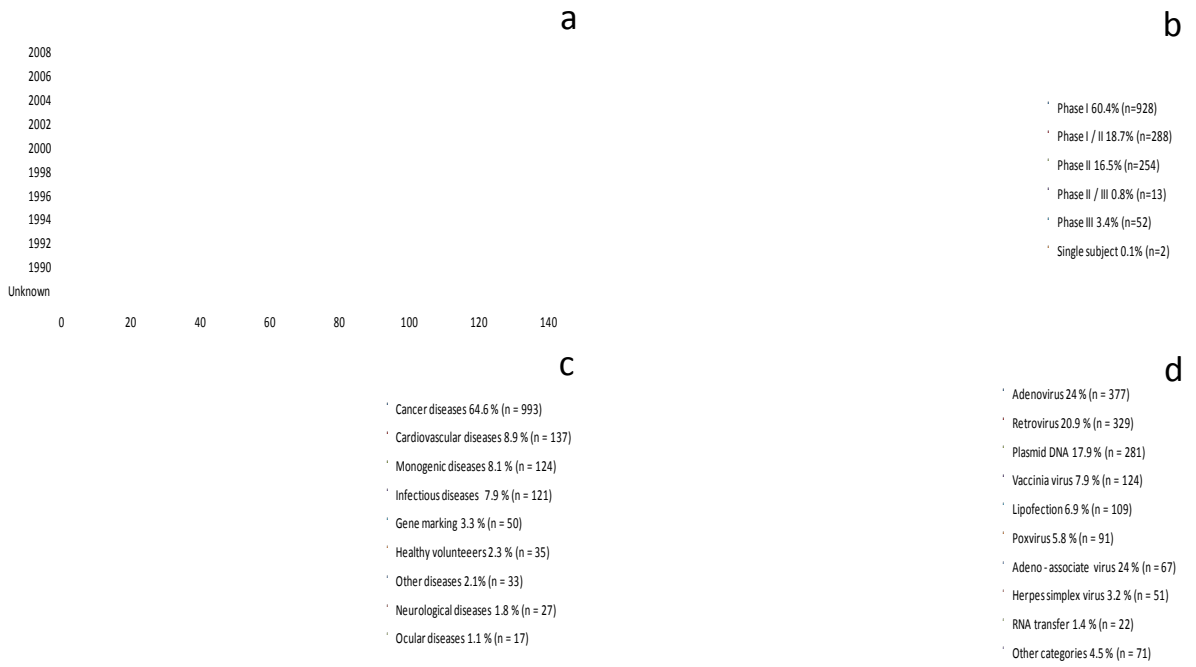

Figure 1.1. *(a) clinical trials approved/initiated in the last 20 years, (b) trial phases, (c) indications, (d) vectors (data from http://www.wiley.co.uk/genmed/clinical/).*

Release of bioproduct from host usually involves alkaline lysis of *E. coli* for plasmids (Kepka *et al*. 2004, Diogo *et al.* 2005) and multiple freeze-thaw cycles for disruption of infected cells for viruses (Peixoto *et al.* 2006). Following clarification, further purification of viruses is typically achieved with CsCl or sucrose gradient centrifugation but this method is associated with low purity, loss of infectivity, time consumption and scalability issues (Peixoto *et al.* 2006, Chahal *et al*. 2007). For plasmids, methods such as precipitation with polycations or spermidine, cross-flow filtration and aqueous two-phase system have been used (Kepka *et al*. 2004). Besides said methods, chromatography, being a high-resolution technique, is commonly employed for the separation of both plasmid DNA and viruses, from contaminating proteins, host nucleic acids, pyrogens, etc. (Lyddiatt and O' Sullivan 1998,

Diogo *et al.* 2005, Peixoto *et al.* 2006, Tiainen *et al.* 2007). In fact, it is rather unlikely that gene vectors of the quality required for therapeutic purposes can be produced without the use of chromatography (Levy *et al.* 2000).

Most of these new-generation bioproducts are nanoparticulates between 20-300 nm in size (Lyddiatt 2002). Representative examples of such entities include supercoiled plasmid DNA (typically around 150-250 nm depending on solvent conditions) (Tiainen *et al.* 2007) and inactivated adenoviral, adeno-associated and retroviral vehicles (typically around 30-120 nm) (Lyddiatt and O' Sullivan 1998), whilst there is strong evidence that the size of these vectors will increase, as demands for molecular targeting and effectiveness are growing (Levy *et al*. 2000).

Due to their 'unusual' size, chromatographic purification of said entities using conventional stationary phases designed and optimized for protein purification, is faced with a major limitation, which is in fact one of the most commonly reported problems (shear-sensitivity, high viscosity feedstocks leading to high pressure drop in packed beds , poor selectivity and simultaneous elution of product and impurities, and particle aggregation) (Lyddiatt and O' Sullivan 1998, Theodossiou *et al.* 2001, Diogo *et al.* 2005). Most commercially available chromatographic media for protein purification have an average pore size of generally less than 400 nm (Lyddiatt 2002) and typically around 30-60 nm (Jungbauer 2005, Tiainen *et al*. 2007). These dimensions are well suited for macromolecular proteins that have typical sizes in the range of 2-10 nm (Thwaites *et al.* 2001, Theodossiou *et al.* 2001, Jangbauer 2005), but in the case of plasmids and viruses, adsorption occurs almost exclusively on the outer surface of the adsorbent. This results in low binding capacities

(typically 2-3 orders of magnitude less than proteins), low recoveries and generally underexploitation of the full potential of a porous structure (Theodossiou *et al.* 2001, Lydiatt 2002). Besides poor chromatographic performance, the exclusion of such large-sized biomolecules (particularly plasmids) from the interior structure of the adsorbent has been observed by confocal microscopy means (Ljunglof *et al*. 1999, Thwaites *et al.* 2001). In addition to the superficial adsorption and the low unit operation performance associated with it, the internal structure of the adsorbent tends to accommodate small size impurities that need to be washed-out prior to product elution, thus increase process time, costs and compromise the reusability of the adsorbent (Thwaites *et al.* 2001, Zhang *et al.* 2001, Lyddiatt 2002).

To circumvent the limitations presented in the purification of nanoparticulates using conventional chromatographic setups intended for protein purification, several approaches have been suggested. The most obvious solution would be the use of small-sized particles in order to increase the external surface area available for adsorption (15 μm anion exchangers have given up to 2 mg pDNA/mL capacitites) but this is clearly limited by the associated high pressure drop in the packed bed (Diogo *et al.* 2005, Tiainen *et al.* 2007). Monolithic beds consisting of channels that allow the convective transport of nanoparticulates to binding sites (pDNA capacity in the area of 8 mg/mL) offer an alternative, but scale-up and industrial application of such stationary phases is restricted mainly by the exothermic nature of the polymerization reaction during manufacturing which makes the preparation of high-volume monolithic columns with uniform pore size difficult (Przybycien *et al.* 2004, Tiainen *et al.* 2007). Plasmid DNA adsorption (1-4 mg/mL) though convective flow with large pores is offered with superporous agarose (Tiainen *et al.* 2007) but manufacturing of such

adsorbents is rather complicated and expensive, while inclusion of densifiers for application in expanded beds complicates production even further (Lyddiatt and O' Sullivan 1998). Expanded bed adsorption, using prototype, small, near solid dense particles, coated with a thin (3-5 μm) layer of agarose appears a promising alternative as it circumvents the issue of pressure drop (through bed expansion due to suitable density) and adsorption of impurities (through inclusion of a solid core) in the internal structure of the adsorbent, while exhibiting near identical binding capacity for plasmid DNA (1-3.5 mg/mL) with traditional stationary phases used in expanded beds (Lyddiatt and O' Sullivan 1998, Theodossiou *et al.* 2001, Zhang *et al.* 2001). However, it terms of operating capacities, even with said prototype stationary phases it is difficult to cost-effectively meet the multi-gram quantities needed for gene therapy (Thwaites *et al.* 2001).

Based on the above, it is clear that the bioprocess industry lacks a stationary phase that can be routinely used in the purification of newly emerging large-sized bioproducts. This chromatographic support should overcome the capacity and diffusion limitations, presented by currently available matrices, (commonly designed, optimized and used in protein purification) by employing a sufficiently large porous structure to allow intraparticle diffusion of large-sized bioproducts. In parallel, its manufacturing, preferably continuous, should be simple and inexpensive.

Probably the most commonly used chromatographic support is beaded agarose gel (a review on agarose-based chromatographic adsorbents, as well as on the structure of the raw material itself can be found below, see sections *1.3.1* and *1.4*). This is due to its great physical and chemical stability, hydrophilic environment and macroporous structure that can

facilitate the transport of protein molecules in its interior structure (Gutenwik *et al*. 2004). The pore size of the matrix is a continuous function of the agarose concentration in the gel and currently, the latter is the only means by which the structure of the adsorbent is controlled. In effect, agarose concentration has been limited to a discontinuous series of arbitrary concentrations (e.g. 2, 4, 6 % (w/w)) and pore sizes (30-60 nm) (http://www.soonersci.com/catalog/page46.html). This approach to control the structure of the gel presents two important issues: First, the number of possible structures that can be manufactured is rather limited. Second, when open structures are desired, this is at the expense of mechanical strength, although the latter can be partially overcome by chemically cross-linking the gel.

The *US patent no. 5,009,759* (Serwer and Griess 1991) states that the pore size of agarose gels, designated for electrophoresis, can be controlled by means of ionic strength of the agarose solution, to produce gels having variable pore size. To this day, no information regarding the extension of this application, to agarose-based chromatographic adsorbents for packed or expanded beds, has appeared in the open literature. In addition, there is a considerable body of information regarding the effect of cooling rate on the structure of agarose (for references see following Chapters), but similarly to ionic strength, no information relating to the manufacturing of agarose beads for bioseparations.

It appears therefore, that beaded agarose structure can be controlled by means other than altering the polymer concentration in the gel, and as ionic strength and cooling rate can be essentially treated as process variables, this type of structural control can be

incorporated in the currently applied manufacturing procedures (w/o emulsification of agarose into hot mineral oil) without significant impact on process complexity and/or cost.

ii. Objectives

The four main objectives of this work were:

- To quantify the effect of two process parameters (ionic strength of agarose solution, quenching temperature) during manufacturing of agarose beads on the porous structure (pore size/pore size distribution) of the adsorbent.
- To quantify the effect of these parameters on the mechanical properties (compression strength at given deformations/Young's and shear moduli/viscoelastic properties) of the resulting particles.
- To identify a fast and reliable characterization method of agarose-based chromatographic adsorbents in terms of pore structure and the properties depending/resulting from the latter.
- To assess whether the above parameters can be used for producing a tailored end-product that can be used for the purification of large-sized biological entities.

iii. Layout of the Thesis

This Thesis consists of six chapters. *Chapter 1* is a literature review mainly focusing on the development and availability of commercial chromatographic adsorbents, the requirements for ideal adsorbents and available methods for manufacturing agarose beads and characterizing agarose-based media. Additionally, the reasons for selecting the particular characterization techniques used in this work are also discussed. In *Chapter 2*, the materials, equipment and experimental procedures used in this work are described. In *Chapter 3* the effect of processing parameters, such as ionic strength, quenching temperature, surfactant concentration and type, and energy dissipation rate, on the macroscopic properties of the adsorbent (particle size/particle size distribution) are presented and discussed. *Chapter 3* also contains results of the physical (density, interfacial tension) and rheological (gelation temperature of agarose, viscosity and flow curves) properties of the dispersed (agarose solution) and continuous phase (mineral oil) of the emulsion. The effects of ionic strength of agarose solution and quenching temperature of the emulsion on the resulting pore size/pore size distribution of the adsorbent, as obtained with the aid of AFM and cryo-SEM, are presented and discussed in *Chapter 4*. In *Chapter 5*, the effects of said processing parameters on the resulting mechanical properties of the adsorbent are discussed. Finally, the conclusions of this work as well as recommendations for future work are presented in *Chapter 6*.

CHAPTER 1

-

LITERATURE SURVEY

1.1. Biotechnology and downstream processing

Since the 1970s, biotechnology has attracted much attention among other technologies, by substantially affecting healthcare, improving wealth and holding promising future prospects (Gavrilescu and Chisti 2005). Biotechnology involves the exploitation of microorganisms and cell cultures to produce high purity compounds for treating diseases, thus generating the need for developing cost effective methods for rapid product purification from complex process environments. The innovations in biological sciences, started 15 years ago, promoted the development of efficient production processes and new separation techniques (Asenjo and Andrews 2008). In today's highly competitive environment, R&D-supported production focuses on good manufacturing practises and improved purification processes to gain regulatory approval for a drug before its market rivals and benefit from its sales by gaining a significant share of the market. For example, biopharmaceutical industries (in USA, Europe and Japan) employ a variety of improved purification techniques to meet the stringent demands of drug safety and purity demanded by the regulatory authorities (Kalyanpur 2000). As a consequence, in the current ground of downstream processing, there is not only a constant need for 'mining' the bioseparation technology and exploring new alternative bioseparation routes, but also for the use of mathematical models to optimise the existing production techniques and experimental procedures (Asenjo and Andrews 2008).

The bioprocess technology is divided into upstream (fermentation, bioreaction) and downstream (product recovery, bioseparation) steps. During fermentation, the bioproduct is produced by microbial, animal or plant cells within the fermenter environment. Following fermentation, bioseparation takes place, which consists of a sequence of recovery and separation steps that aim to maximise the purity of the final product while minimizing processing time, yield losses and costs (Ladisch 2001).

Depending on the type of bioproduct, the recovery characteristics and unit operations employed change. Furthermore, as most of these products are sensitive to conditions such as temperature and pH, the separation processes differ from normal process used in other industries. There are three main categories of products after fermentation: whole cells (eg. single cell proteins and baker's yeast), intracellular macromolecules (protein in inclusion bodies from recombinant fermentation) and extracellular macromolecules (antibiotics, organic acids, alcohols). In most of these cases the cells must be removed from the broth (clarification). Yeast and bacterial cells that are quite rigid are normally separated by flocculation, mechanical filtration and centrifugation. On the other hand, mammalian cells are much more sensitive and fragile, therefore can be separated by disk-stack centrifugation and cross-flow microfiltration. The protein of interest can be in soluble form within the cell or often in the form of an insoluble refractive mass (inclusion body). Mechanical cell disruption is then used to lyse the recovered cell mass and obtain the desired product. Afterwards, the lysate is clarified using appropriate membrane equipment. The soluble proteins pass through the membrane and are further purified, while inclusion bodies are solubilised by adding an agent (e.g. urea), renaturated, then separated from particulates by

ultrafiltration. A similar procedure is used for viral vectors and plasmid DNA (Kalyanpur 2000, Lightfoot and Moscariello 2004).

Once the target biomolecule is obtained in a particulate-free process stream, the product is obtained at a high level of purity by further purification. An efficient, multistep process based on the purification strategy of '*Capture, Intermediated Purification,* and *Polishing*' (*C-IP-P*) (Amersham Biosciences 2004) is commonly employed. There are three main categories of techniques involved in the Capture and Intermediate Purification: membrane based methods (ultrafiltration and nanofiltration), liquid-liquid extraction using aqueous two-phase systems, and a variety of chromatographic procedures (discussed below) (Kalyanpur 2000, Lightfoot and Moscariello 2004, Przybycien *et al*. 2004).

Finally, depending on the product and its intended use, polishing is required to remove contaminants such as viruses or endotoxins for safety reasons, where size exclusion chromatography and membrane filtration are commonly employed. Adsorptive membranes are proving attractive in this step and their use seems to be increasing rapidly (Lightfoot and Moscariello 2004).

The overall yield of purification ($Y_{\text{purification}}$) for a recovery depends on the number of steps n of the fractional yield *Y*i (Ladisch 2001):

$$Y_{purification} = (Yi)^n \quad (1.1)$$

When each step has different yield losses, the overall yield is the product of these fractional yields:

$$Y_{purification} = \prod_{i=1}^{n} Yi \quad (1.2)$$

Capital and operating costs increase with the required purity of the product and the number of steps of the process. The overall cost is even higher due to losses of yield during each individual stage, and as a consequence, there is a need to reduce the number of steps or to increase the step yields. As bioseparations is a serial process, optimisation of the individual purification steps and yields may contribute to higher final yield at lower cost. In the biopharmaceutical industry, where more than 50 % of the purification costs lie on the chromatographic steps and where the upstream productivity is increased tremendously in a continuous manner (in pace with bioprocessing yields improvement), the capacity bottleneck is being pushed downstream (Ladisch 2001).

1.2. Process chromatography

Chromatographic separations play a very important role in the purification of therapeutic compounds. These are highly versatile and selective techniques that serve well in the downstream processing of bioproducts (Kalyanpur 2000). From the processing steps available for bioseparations, chromatography is the one that achieves high resolution of biomolecules. None of the other steps, such as filtration (micro-, ultra-, and reverse osmosis), centrifugation, flocculation, flotation, precipitation etc. can reach the purity of a product that biopharmaceutical products need for compliance with regulations.

In broad terms, chromatographic separations are based on the principle of passing the liquid containing the target biomolecule through a column packed with a porous adsorbent. Good adsorbents should effectively capture the bioproduct allowing contaminants to pass

through. After completion of the separation the target biomolecule is eluted from the matrix and it is available for further processing

In chromatography, convective flow is responsible for the transport of bioproducts in the interparticle void of the porous adsorbent, whereas diffusion (influenced by the relative size of solutes and pores as well as particle size) governs transport of molecules within the porous structure of the adsorbent. Pressure drop across and flowrate throught the column depends on particle size and column length (Lyddiatt 2002). Currently, seven different techniques are employed for the adsorption of biomolecules. These exploit some physical, chemical or biological characteristic of the target molecule in order to achieve separation (Kalyanpur 2000, Jungbauer 2005):

- Ion exchange (surface charge)
- Size exclusion or gel filtration (molecular size and shape)
- Normal phase (solubility/hydrophobicity)
- Reverse phase (solubility/hydrophobicity)
- Hydrophobic interaction (surface hydrophobicity)
- Affinity (stereoselective binding activity)
- Metal chelation (coordination complex formation)

As mentioned above, separation in chromatographic applications is primarily achieved by diffusion and subsequent adsorption of biomolecules onto the stationary phase. An exception is size exclusion chromatography. In the latter, a mixture of biomolecules is applied from the top of the column. Entities larger in size than the exclusion limit of the

adsorbent, which defines the maximum size of molecules that can enter the pores of the gel, quickly pass through the bed. Smaller molecules diffuse in and out of the porous network thus will need more time to elute (Amersham Biosciences 2002). Consequently, the mixture is separated in order of decreasing molecular size. Therefore in size exclusion chromatography, the process of adsorption onto the stationary phase is not only unfavourable, but is considered as an issue in the application of the technique.

Following diffusion and adsorption of the target biomolecule onto the porous support, the former is removed from the matrix by elution. During elution, the physiochemical or biological characteristic of the biomolecule exploited during adsorption, are utilized in a reversed manner. For example, ion exchange chromatography takes advantage of the fact that the relationship between net surface charge and pH is unique for a specific protein. In a given separation, reversible interactions between charged molecules and the stationary phase are controlled in order to favour binding or elution of specific molecules and achieve separation (Amersham Biosciences 2004). During affinity separations, conditions that favour the specific binding of the target molecule to the ligand are applied. In order to obtain the product, conditions are changed to favour elution of the bound molecule. Elution can be performed specifically, using a competitive ligand, or non-specifically by changing pH, ionic strength or polarity (Amersham Biosciences 2004). In hydrophobic interaction chromatography, protein binding is promoted by moderately high concentrations of anti-chaotropic (structure-forming) salts. Elution is achieved by decreasing the salt concentration in the elution buffer (Amersham Biosciences 2000). In general, elution can be performed in linear gradient (change in buffer composition occurs linearly) or step (change in buffer composition occurs step-wise) manner. The former is favoured in analytical and optimization

applications where high resolution is of primary importance, while the latter is used for well -established, large-scale applications where short separation times and reduced buffer consumption are essential (Amersham Biosciences 2004).

All the above chromatographic techniques offer a balance between resolution, capacity, and recovery of bioproduct as well as speed of operation (Fig. 1.2a). Depending on the stage of the purification (see above, *C-IP-P*) said parameters have different gravity. During the *Capture* stage (Fig. 1.2b) isolation, concentration and stabilization of the target biomolecule take place. This is concentrated and transferred to an environment that retains its biological activity. In order to achieve stabilization and retention of biological activity, contaminants such as proteases must be removed. Other impurities such lipids, prions and culture media are also removed during *Capture.* For said reasons, *Speed* of operation and *Capacity* (the amount of target product that can be loaded to the column) are of primary importance during *Capture*, therefore favoured at the expense of *Resolution and Recovery*. During *Intermediate purification* (Fig. 1.2c) most of the bulk impurities, such as cellular proteins, nucleic acids, detergents and inhibitors, are removed. Since the target bioproduct is in a stable environment, *Speed* is less significant (but not insignificant) during *Intermediate Purification,* while *Resolution* (depending by the selectivity of the technique and the efficiency of the chromatography matrix in producing narrow peaks during elution) and *Capacity* are important. Finally, in the *Polishing* stage (Fig. 1.2d) most of the impurities have been removed except trace impurities and closely related substances, such as aggregates, fragmented product, similar cellular proteins as well as leaked affinity ligands. The purpose of *Polishing* is to remove said substances and achieve final purity demanded by regulations. In general, *Resolution* is most difficult to achieve in the final stages of purification when

impurities and target protein are likely to have very similar properties. *Recovery* becomes increasingly important as the purification proceeds because of the increased value of the purified product. *Recovery* is influenced throughout purification by destructive processes in the sample and by unfavourable or harsh conditions of the column (Amersham Biosciences 2004).

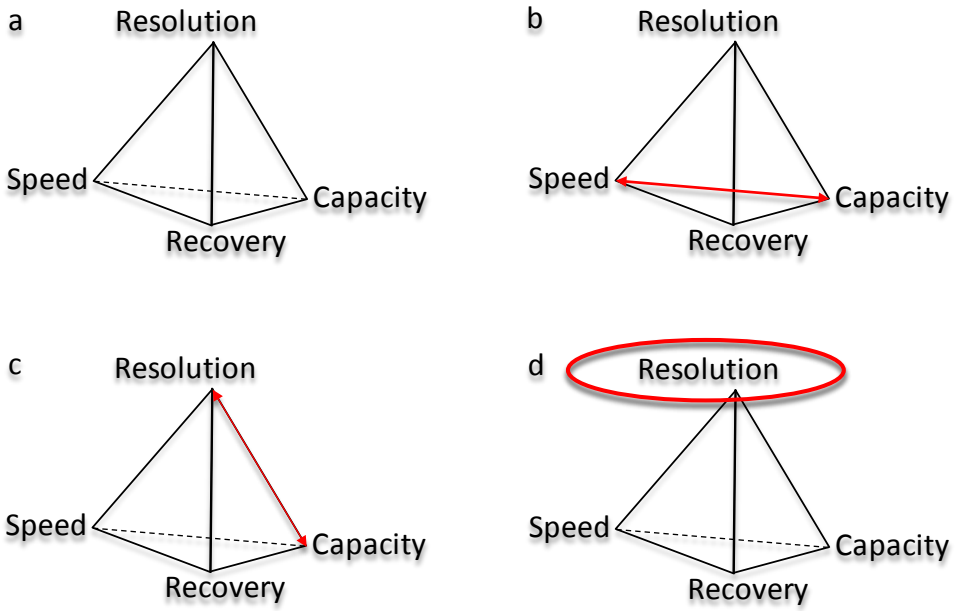

***Figure 1.2**. (a) balance between speed of operation, resolution, capacity and recovery of bioproduct during (b) capture, (c) intermediate purification and (d) polishing (redrawn from Amersham Biosciences 2000).*

Besides the different modes described above, chromatographic applications can be employed in different types. The most commonly used is the packed bed where clarification of the fermentation broth prior to its application is mandatory, as cell debris will deposit in the interparticle void thus clogging the column (Lyddiatt 2002). Typically, membrane filtration and/or centrifugation are employed for the removal of cells. However, the two

techniques exhibit limitations. Microfiltration is associated with low transmembrane fluxes and partial rejection of the target molecule. Large scale centrifugation of fermentation broths is not as effective as in lab applications, consequently a second pass is required or a combination of centrifugation and microfiltration. Therefore, both unit operations are associated with long processing times (Amersham Biosciences 1996, Anspach *et al.* 1999). To overcome the mandatory clarification of fermentation broths, expanded bed adsorption (EBA) can be employed. In the latter, the increase in the interparticle void allows particulate matter present in the feedstock to pass thought the column, thus providing the possibility of incorporating clarification and initial purification into one direct capture step (Peixoto *et al.* 2005). A stable classified bed is obtained by choosing a stationary phase of appropriate density and particle size (Balasundaram and Harrison 2007). Increase of particle density is achieved by inclusion of densifiers in the stationary phase. The size of the adsorbent is usually larger than those used in packed beds and consequently column performance is low (Anspach *et al.* 1999). In principle all of the aforementioned modes (affinity, ion exchange etc.) of packed bed chromatography can be employed in EBA (Lyddiatt 2002).

Adsorption of bioproducts can also be exploited in batch contactors. Besides the actual process of separation, the adsorption-desorption kinetics of biomolecules onto the stationary phase can be evaluated in a batch adsorber. The measured model parameters, such as adsorption equilibrium parameters and effective intraparticle diffusivity, are used to predict the performance of industrial processes such as packed and expanded beds (Lyddiatt 2002, Li *et al*. 2003). In terms of unit operations, there are two distinct applications of batch adsorption:

Stationary phases traditionally used in packed beds, as well as cheaper materials that lack geometrical and/or physical characteristics can be used in mechanically agitated batch contactors for the separation of biomolecules. Following dispersion of the media into crude or clarified broth, adsorbent particles can be recovered by settling, centrifugation or filtration (type of operation which is popular with blood plasma fractionation). Another way of separating particles, following adsorption, is termed 'suspended bed chromatography'. Following adsorption the suspended chromatographic media are pumped into a chromatography column where the residual steps are performed. The same principles (affinity, ion exchange etc.) used for the separation of bioproducts onto stationary phases in packed and expanded beds can be used for batch contactors (Lyddiatt 2002, Jungbauer 2005).

The second distinct application exploiting batch adsorption of bioproducts is termed 'high gradient magnetic fishing' (HGMF). It combines commonly employed principles for separation in packed/expanded beds and batch adsorption with magnetic separation used in the chemical and mineral processing industries. In HGMF, tailor-made, submicron non-porous magnetic supports, coated with appropriate ligands, are mixed with crude feedstocks in a batch contactor, followed by magnetic capture of the adsorbents in magnetic field and subsequent elution of bioproduct (Hubbuch 2000, Heeboll-Nielsen 2002, Lyddiatt 2002).

1.3. Chromatographic media

1.3.1. Development

For the past fifty years the properties of chromatographic adsorbents have been constantly improved. The first natural material in beaded form suitable for protein purification, introduced by Peterson and Sobers in 1956, was cellulose with ion exchange functionalities. Only three years later, in 1959, the first cross-linked, dextran-based Sephadex G-25 and G-50 beads, developed by Porath and Flodin, were commercially available. The first dextran-based ion exchangers were introduced in 1960-62, whereas 1961 saw the introduction of polyacrylamide by Hjerten (Jungbauer 2005, Curling 2007). He was also the first to use beaded agarose as a chromatographic support in 1962 (Janson and Jonsson 1998, Curling 2007).

Currently, agarose beads are available under several commercial names denoting different concentrations, compositions and applications. Most of these products are designed and optimized for protein purification and their pore size dimensions are typically in the range of 30-60 nm (Jungbauer 2005). GE Healthcare has launched Sepharose 2B, 4B, 6B and CL-2B etc. which is made of pure agarose. The number before the letter *B* is an indication of the agarose concentration in the gel: 4B is 4 % (w/w) agarose etc. The *CL* denotes the cross-linked with epichlorohydrin counterpart of Sepharose. The flow properties and particle size of Sepharose and Sepharose CL (40-160 µm) make them suitable for analytical applications. Sepharose Fast Flow (GE Healthcare) is an agarose-based adsorbent obtained from Sepharose by cross-linking the gel matrix to a much higher degree than Sepharose CL. The resulting flow properties of Sepharose Fast Flow after chemical cross-

linking make it suitable for preparative applications. Sepharose HP (GE Healthcare) is a nearly monodispersed agarose matrix of similar rigidity to Sepharose FF but with smaller average particle size (34±10 µm). Sepharose Big Beads (6 % (w/w) agarose) (GE Healthcare) with ion exchange functionalities is a gel equivalent to Sepharose Fast Flow in terms of rigidity. What differentiates Sepharose Big Beads is the large particle size (100-300 µm) allowing the application of viscous feedstocks. Superose (GE Healthcare) is a highly cross-linked monodispersed (10 µm) agarose matrix available in two different agarose concentrations, 6 and 12 (6 and 12 % (w/w) respectively) and it is designated for both analytical and preparative applications. (http://www1.gelifesciences.com/APTRIX/upp01077.nsf/Content/bioprocess). Ultrogel A (Pall) has a composite matrix (40-160 µm) consisting of agarose coupled with acrylamide at equal or greater concentrations than agarose (http://labfilters.pall.com/catalog/laboratory_35870.asp, Janson and Jonsson 1998). BioGel A (Bio-Rad) is an agarose-based matrix available in sizes ranging from 55-220 µm in diameter (http://www.chromdata.net/ChromMedia.php?id=100&PageID=Ligand, Janson and Jonsson 1998). Enhancement of density (and particle size) by inclusion of inert densifiers (quartz, ceramic, etc.) extends the applicability of packed-bed adsorbents to expanded bed operations. For example, Steamline Quartz Base Matrix (GE Healthcare) is such an adsorbent. Its quartz core (adsorbent density 1300 kg m^{-3}) and large particle size (100-300 µm) make it suitable for the initial purification of unclarified feedstocks (http://www1.gelifesciences.com/APTRIX/upp01077.nsf/Content/bioprocess). Most of the above products are either available as base matrices for subsequent chemical derivatization

by the end user or are sold with ion exchange, affinity, hydrophobic interaction, normal and reversed phase, etc, functionalities.

A relatively new agarose product under development is superporous agarose beads (Fig 1.3). This type of bead has two sets of pores and a fairly large particle size (300-500 μm). The first set consists of typical mesopores found in agarose gels, while the second set consists of superpores (typically around 30 μm). This material can be prepared by a double emulsification technique including an O/W emulsion followed by a W/O emulsion. In the first emulsion the oil (dispersed) phase acts as porogene for the formation of superpores while the droplet size of the former determines the size of the superpores (Gustavsson and Larsson 1996). A second method for preparing superporous agarose beads involves the inclusion of a suitable solid porogene (such as $CaCO_3$) in granule form in the agarose solution with subsequent removal of the former with a suitable solving agent (such as HCl) (Zhou *et al.* 2007).

Flow through the superpores (or flow pores) is governed by convection rather than diffusion while the walls of the pores provide additional surface area increasing the binding capacity of the adsorbent. Such extreme geometry is suitable for large sized molecules such as plasmids and viruses (Tiainen *et al.* 2006). Numerous applications of superporous agarose beads found in the literature include affinity separation of bovine lactate dehydrogenase and rabbit IgG (Gustavsson *et al.* 1997), hydrophobic interaction separation of lysozyme and bovine serum albumin (Gustavsson *et al.* 1999) and anion exchange separation of plasmid DNA (Tiainen *et al.* 2006). The applicability of superporous agarose has being extended to monolithic beds (Gustavsson and Larsson 1999), dense pellicular agarose-glass composite

beads for expanded bed adsorption (Zhou *et al.* 2007) and beaded solid supports for microfluidic immunoassay (Yang *et al.* 2008).

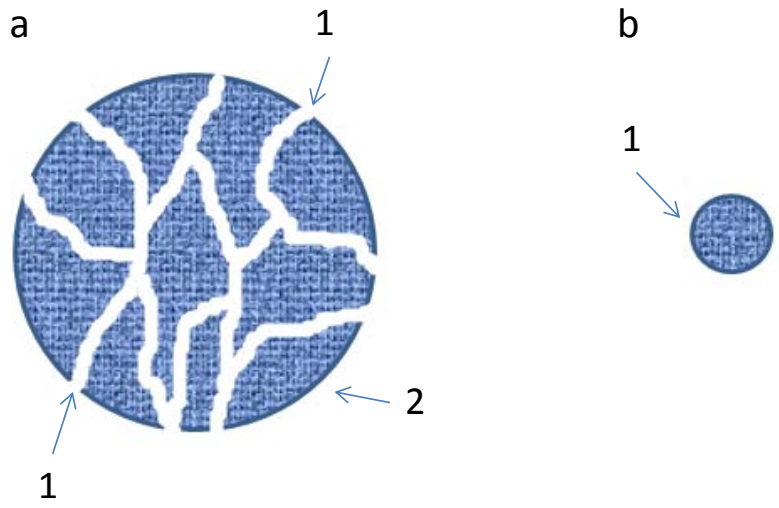

Figure 1.3. *(a) superporous agarose bead: (1) flow pores, (2) normal diffusion pores, (b) conventional agarose bead (redrawn from Gustavsson and Larsson 1996).*

Chromatographic media are not exclusively made of natural polymers (agarose, cellulose, dextran, chitosan); synthetic and inorganic materials have also been used. In fact, the very first material used as chromatographic support, even prior to natural cellulose, was $CaCO_3$, although this material is unsuitable for protein purification. Tiselius (Jungbauer 2005, Curling 2007) introduced hydroxyapatite for protein chromatography. The original material was in microcrystalline form with poor flow properties but excellent selectivity. A modification by sintering the powder into ceramic particles with large pores led to a breakthrough in terms of flow properties. Currently it is used for large-scale industrial production of recombinant monoclonal antibodies (Jungbauer 2005, Curling 2007). The most commonly used inorganic material for protein chromatography is silica (Jungbauer 2005). It

was introduced by Stober *et al.* in 1968 (Walcarius *et al*. 1998). These spherical particles can be obtained by a two-step emulsion polymerization and control of the structure is easily achieved by varying the reaction conditions (Unger 1973). Besides its pure application, silica has been used to produce composite adsorbents by coating with dextran, agarose, cellulose, polystyrol and poly(alkylaspart-amide) (Jungbauer 2005). An example of commercial silica product for chromatography is LiChrospher (Merk). It is a monodispersed base matrix in beaded form made of pure silica. It is available in two particle sizes (12 and 15 µm) and two pore sizes (6 and 10 nm) designated for both analytical and preparative applications. LiChrospher is available as base matrix as well as with a range of functionalities. (http://www.financialreports.merck.de/servlet/PB/menu/1139910/index.html). Silica beads exhibit a high concentration of hydroxyl groups on their surface. The -OH groups can interact with proteins especially at high pH. For this reason it is required to react the residual Si-OH groups in order to inactivate them (end-capping). This material is known as *bonded silica* (Walcarius *et al*. 1998). LiChroprep (Merk) is an amorphous matrix made of bonded silica and it is available in the ranges of 5-20, 15-25 and 25-40 µm and with different functionalities. Another inorganic material exploited as chromatographic support is glass, more commonly known as 'controlled porous glass'. Its first application as a chromatography material was proposed by Haller in 1964 (Schnabel and Langer 1991). ProSep A, an amorphous affinity matrix is commercially available by Millipore for industrial affinity separations (Jungbauer 2005). It is available in a particle size range of 74-125 µm with two pore sizes, 50 and 100 nm. The strong adsorption properties, especially for charged molecules like proteins, initially restricted the use of glass. Nowadays, controlled porous glass is available with reduced adsorption properties or with bonded reactive groups allowing the applicability of this

material to size exclusion and adsorption chromatography. Pores size can be controlled in the range of 10 to 400 nm while pore volume can be up to 70 %. These two properties are controlled by heat treatment and leaching of porogenes respectively. These particles are amorphous after production but can be refined to glass beads by subsequent heat treatment in an inclined rotating tube furnace (Schnabel and Langer 1991). Synthetic polymers have also been used as chromatographic adsorbents. The most important materials of this class are: vinyl polymers, polyacrylamide polymers and polyvinylstyrene. Commercial products manufactured from synthetic polymers, suitable for protein chromatography include the following: Trisacryl (polyacrylamide derivative), Toyopearl (hydrophilic cross-linked polymer), CIM (polymethacrylate) (Jungbauer 2005). Typical particle size ranges for synthetic adsorbents are 10-530 µm while pore sizes are in the range of 10-60 nm (Adachi *et al*. 2002, Adachi and Isobe 2004). A significant advantage obtained with the use of synthetic polymers is their resistance to extreme chemical conditions such as high or low pH (Jungbauer 2005).

Besides porous particulate adsorbents, a relatively new class of chromatographic media are the *monoliths*. Such stationary phases can be prepared in various shapes using polymerization chemistry and can be derivatized with traditional chromatography ligands (Przybycien *et al.* 2004). The material is usually cast into a chromatography column as a continuous block interlaced with channels (Jungbauer 2005). Another format of monoliths is conjoint liquid chromatography where numerous small scale disks of different chemistries are placed in the same housing providing multiple separation mechanisms in one unit separation (Przybycien *et al.* 2004). Typical materials for manufacturing monolithic media are silica and synthetic polymers such as polyacrylamide (Josic and Clifton 2007). In general the major advantage of monolithic supports, regardless of the application, is the fast mass

transfer that is achieved between mobile and stationary phase (Buchmeiser 2007). This is because transport of solutes in the medium is achieved by convection rather than diffusion. Further advantages over conventional particulate chromatographic media are the ability to be manufactured in with a wide variety of pore sizes (up to 5000 nm (Jungbauer 2005)) and the low back-pressure even at high flow rates. Because of their wide variety of pore sizes monoliths can be used for the purification of large sized biological entities such as viruses, cells, proteins complexes etc. (Josic and Clifton 2007). Scale-up and industrial application of monolithic stationary phases has been restricted mainly by the exothermic nature of the polymerization reaction during manufacturing which makes the preparation of high-volume monolithic columns with uniform pore size difficult (Przybycien *et al.* 2004).

1.3.2. General characteristic and requirements for an ideal adsorbent

Chromatographic adsorbents are essentially the centrepiece of chromatographic applications since their role is to capture the biomolecule of interest while unbound material is washed out prior to elution. Generally, the nature of the mobile phase (e.g. clarified fermentation broth) determines the nature of the stationary phase (chromatographic adsorbent), while the chemical nature and size of the proteins determine the surface characteristics and physical properties respectively, of the adsorbent matrix (Jungbauer 2005). There are several requirements for an ideal adsorbent and in some cases compromises need to be made (e.g. unhindered diffusion vs. surface area available for adsorption). From the available materials for manufacturing chromatographic adsorbents,

agar (and agarose, the fraction of agar with the lowest possible charge) is the natural product that meets most of the requirements for an ideal adsorbent (Porath *et al*. 1971).

Spherical shape*:* Optima beds for chromatographic applications are obtained with hard, spherical particles (Porath *et al*. 1971) The need for this expensive geometric refinement derives from the better flow characteristics (lower pressure drop, minimization or absence of 'dead' zones) that spheres offer compared to e.g. amorphous particles of the same apparent size. An exception is preparative applications employing large amorphous particles (e.g. ProSep A for industrial affinity separations). Due to the large particle size the pressure drop due to the deviation from spherical shape is negligible (Jungbauer 2005).

Large surface area: In adsorption chromatography the intraparticle surface area determines the surface area available for adsorption of biomolecules and hence the dynamic binding capacity of the adsorbent after ligand immobilization. Large intraparticle surface area can be obtained in an adsorbent with small pores. On the other hand, very small pore size suggests diffusion hindrance, especially when the ratio between pore size and molecules is less than 10 (Jungbauer 2005). In other situations where large biological entities (viruses, plasmids, protein complexes etc.) are to be separated, large pore size is essential for their adsorption, therefore reduction in the surface area per gram of adsorbent is unavoidable. Hence a compromise must be made between large surface area and pore size (or in other words between area for adsorption and diffusion).

Hydrophilicity and availability of functional groups: Chromatographic adsorbents must be hydrophilic in order to allow reversible adsorption (desorption) of bound bioproducts. The property of hydrophilicity is readily obtained with the use of natural polymers such as

agarose, dextran and cellulose that have a plethora of -OH while enough groups are available for the introduction of ligands to specifically modify them according to the intended use (Porath *et al*. 1971, Poole 2003, Jungbauer 2005).

Chemical stability: Any chemical modification of the adsorbent and ligand immobilization should result in a chemically stable matrix during operation and cleaning (Porath *et al*. 1971, Jungbauer 2005). Unsubstituted Sepharose products (Sepharose 4B, Sepharose CL-4B, Sepharose 4B Fast Flow) as well as substituted (Q, DEAD, CM, SP, Phenyl and Octyl Sepharose 6 Fast Flow) have been tested under static conditions (incubation) with respect to the release of organic compounds (Andersson *et al.* 1998). In the unsubstituted media it was found that chemical cross-linking with epichlorohydrin of the particular chromatographic media increases the chemical stability of the matrix, especially under extreme acidic or basic conditions. With respect to substituted media and ligand leaching it was found that supports with coupled ligands can either reduce or increase the chemical stability of the matrix, depending on conditions. The increase in chemical stability of the matrix with increasing degree of cross-linking is not independent of the nature of the cross-linker. For example it has been shown (Porath *et al*. 1975) that chemical cross-linking with divinyl sulphone results in a chemically unstable matrix.

Low unspecific adsorption: Unspecific adsorption can reduce the binding capacity of the matrix for the target protein (Amersham Biosciences 2004). In general, unspecific adsorption reduces with hydrophilicity. Agarose and cellulose are the two natural materials with the lowest unspecific adsorption. The introduction of cross liking agents in order to improve the

mechanical properties of the natural polymers result into a more hydrophobic medium and the therefore increase in unspecific adsorption is unavoidable (Jungbauer 2005).

Mechanical stability: Besides specific surface characteristics, chromatographic adsorbents should also possess mechanical strength. The latter determine the deformation of particles caused by the weight of the bed and pressure drop during operation. Therefore the understanding of the mechanical properties of chromatographic adsorbents is essential to the successful design and operation of chromatographic applications (Muller et al. 2005). The main drawback of natural polymers is their soft structure (Jungbauer 2005). Rigid particles can be obtained by chemical intra- and inter- molecular cross-linking (Porath *et al.* 1975) using agents such epichlorohydrin or divinyl sulphone. Although chemical cross-linking dramatically increases the mechanical stability of matrices, it is sometimes at the expense of other properties, such as chemical stability and hydrophilicity (see above: Chemical stability, Low unspecific adsorption).

Reusability and low cost: Some adsorbents can be used up to 2000 purification cycles (Muller *et al*. 2005). It is therefore of critical importance that adsorbents can mechanically and chemically withstand such extended use. In addition, adsorbents (and buffers) can be very costly (e.g. £ 30550 / 10 L of protein G-activated agarose particles (GE Healthcare 2009)) and hence, reconsideration of operational strategies in process chromatography is essential (Lyddiatt, 2002).

1.3.3. Structure-diffusion relationships

The chromatographic efficiency of a packed bed defines its ability to produce narrow symmetrical peaks during elution of bioproducts (Amersham Biosciences 2002). One of the parameters commonly used to describe this efficiency is the plate number *N*. The plate number as well as the corresponding height of an equivalent theoretical plate (*HETP*) is a common measure for ideal mass transfer within packed beds (Schmidt-Traub 2005).

The quantity *N* is proportional to the column length L_c, so that, with other factors being constant, an increase in column length results in an increased plate number and better separation. These quantities relate by (Snyder and Kirkland 1979):

$$N = \frac{L_c}{HETP} \tag{1.3}$$

HETP measures the efficiency of a given column (operated under a specific set of operating conditions) per unit length of column. Small *HETP* values suggest more efficient columns and large *N* values. A central goal in chromatographic applications is the attainment of small *HETP* values for maximum *N* and highest column efficiencies (Snyder and Kirkland 1979).

The *HETP* quantity is related to the contribution of various band-broadening processes during separation by (Snyder and Kirkland 1979, Gustavsson and Larsson 1996):

$$HETP = Au^{0.33} + \frac{B}{u} + Cu + Eu \tag{1.4}$$

where *u*: the linear velocity of the mobile phase

A: constant relating to eddy diffusion and mobile phase mass transfer

B: constant relating to longitudinal diffusion

C: constant relating to stagnant mobile phase diffusion

E: adsorption kinetics

The term *C u,* relating to diffusion of macromolecules into the porous network of the gel, is dominant in most chromatographic separations, i.e. when the separation is diffusion-controlled. In such cases, Eq. (1.4) reduces to (Gustavsson and Larsson 1996):

$$HETP = Cu \tag{1.5}$$

C u can be expanded to:

$$HETP = \frac{C'(d_p)^2 u}{D} \tag{1.6}$$

where *C'*: constant

d_p: particle size

D: macromolecule diffusion coefficient

It can be seen from Eq. (1.5)-(1.6) that chromatographic efficiency depends on particle size and the *C'* constant relating to stagnant mobile phase diffusion. The value of *C* depends on the nature and structural characteristics of the adsorbent. An optimized adsorbent in terms of pore accessibility and diffusion path-length will result in smaller *C* values thus

reducing the height of equivalent theoretical plate (*HETP*) and increase chromatographic efficiency (Schmidt-Traub 2005).

1.4. Agarose

Agar is a natural polysaccharide obtained from red sea weeds (Zhou *et al*. 2007). This material has two main constituents: agarose and agaropectin, a composition similar to starch, which is composed of amylose and amylopectin. Agarose (Fig. 1.5) is a linear polysaccharide consisting of 1, 3-linked β-D-galactopyranose and 1,4-linked 3, 6-anhydro-α-L-galactopyranose, while agaropectin is a more complicated polysaccharide containing sulphuric and uronic acid residues (Araki 1956). Because of its electrically neutral character, agarose is superior to agar as an agent for electrophoresis and packed bed chromatography (Hjerten 1971). X-ray diffraction studies indicate that agarose has a double helix structure with 0.95 nm axial periodicity. Each chain in the double helix forms a left-handed threefold-helix of 1.9 nm pitch and is translated axially relative to its partner by exactly half this distance (Amsterdam *et al*. 1975). The gelation of agarose (Fig. 1.4) involves a shift from a random coil in solution to a double helix in the initial stages of gelation, and then to bundles of double helices in the final stage (Quali 2001). A more detailed discussion on the gelation of agarose can be found in sections *3.2.3* and *4.1.2.*

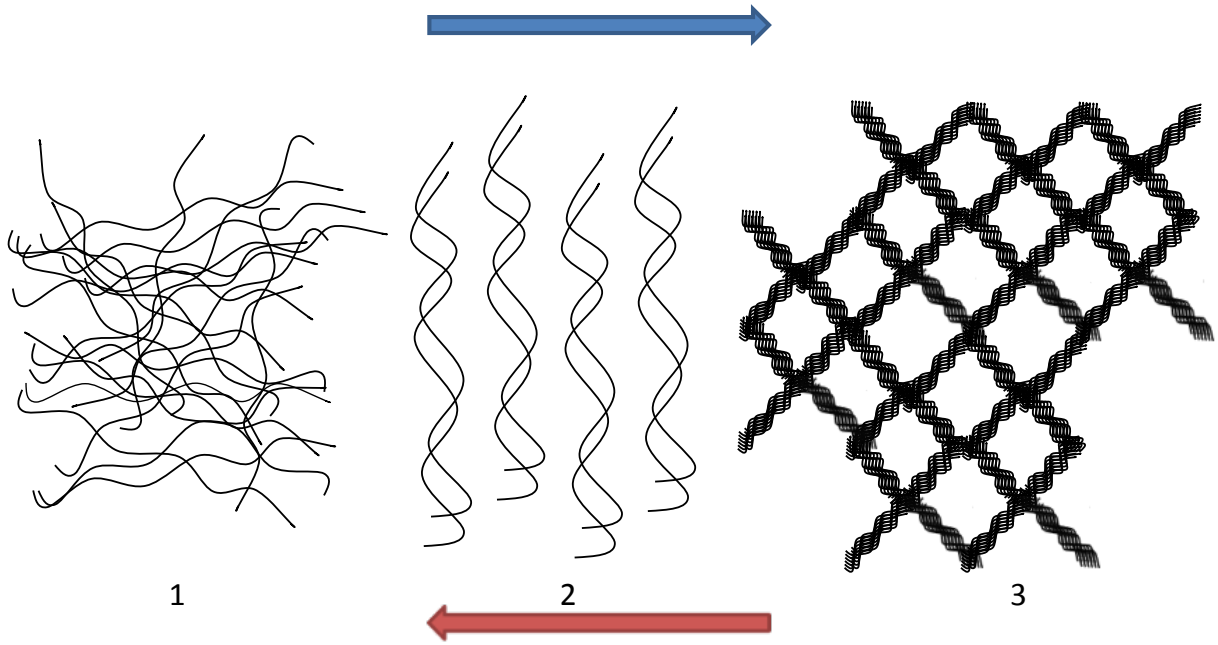

Figure 1.4. *Gelation of agarose: (1) random coil conformation, (2) double helix formation, (3) aggregation of helices into porous network (blue and red arrows indicate decrease and increase in solution temperature respectively).*

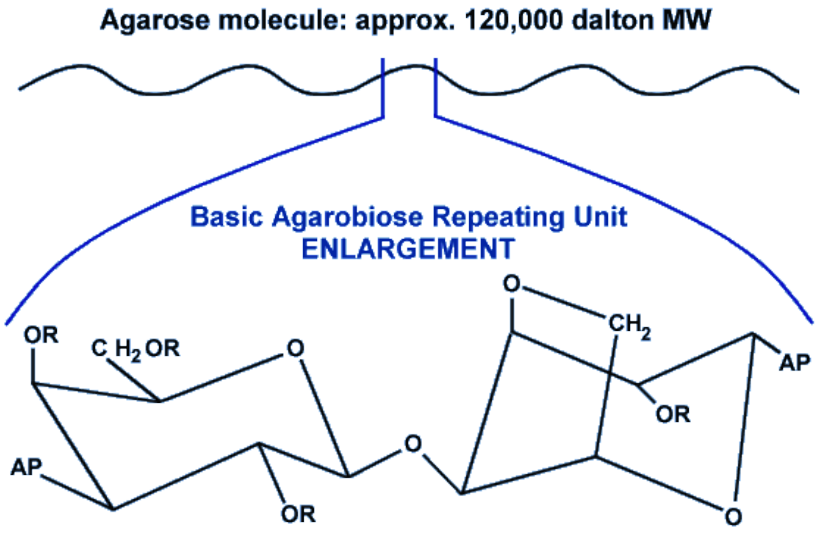

Figure 1.5*. Primary structure of agarose: The agarobiose (i.e. two sugars) unit represents the repeating 'monomer' in the agarose polymer. There are approximately 400 such repeating agarose units per polymer chain. The symbol 'AP' indicates the point of correction to the rest*

of the agarose polymer. The importance of the substituents on the 4 potentially free hydroxyl groups on each agarobiose unit: If R = H, then the hydroxyl group is 'free' to be derivatized (i.e. crosslinked or activated to attach ligands as in affinity chromatography). If any R = CH_3, then the coupling capacity of the agarose is reduced. If any R = SO_3 or pyruvate, then the coupling capacity is further reduced for either crosslinking or coupling activation (for affinity chromatography) (http://www.abtbeads.com).

1.5. Characterization techniques

The macroscopic properties (such as mechanical strength and permeability) of porous chromatographic adsorbents are directly influenced by the internal structure, with the pore size distribution playing a major role in bioseparation, beyond simply the mean pore size (Yao and Lenhoff 2004). In size exclusion chromatography the separation is based upon the relative sizes of pores and biopolymer coils whereas in liquid adsorption chromatography the size of pores determines the available surface area for biomolecule adsorption (Trathnigg *et al*. 2006). From the above it is rather clear that absolute control (where possible) and the ability to fully characterize the internal porous structure of adsorbents is essential to chromatographic applications. The importance of structural characterization is even greater for novel adsorbent systems.

There is a number of methods regarding the structural characterization of porous media. Some of the most common methods (e.g. mercury intrusion porosimetry, nitrogen sorption measurements) derive from classical adsorption science. Because these techniques require dewatering of the sample they cannot be used on hydrogels since upon drying the soft structure of the latter will collapse and information about pore size or internal surface area

is lost. These methods are well suited for rigid materials such as silica, glass and polymethacrylate beads where upon dewatering their structure is preserved (Stenekes 2000, Jungbauer 2005). Therefore, considering the delicate nature of hydrogels and agarose in particular, it is essential that the characterization method, besides being fast and reproducible, has a minimal effect upon the structure of the gel. Below, a review of techniques for characterization of agarose beads and/or slabs is presented, as well as methods used in this project and the reasons behind selecting the latter.

Inverse Size Exclusion Chromatography: A method for characterizing the porous structure of chromatographic adsorbents can be realized by the inverse application of size exclusion chromatography (SEC). Briefly, in SEC, biomolecules are separated according to their size. A mixture of biomolecules is applied from the top of the column. Entities larger than the exclusion limit of the adsorbent will not enter the pores of the gel and will quickly pass through the bed. Smaller molecules will diffuse in and out of the porous network thus will need more time to elute (Amersham Biosciences 2002). Consequently the mixture will separate in order of decreasing molecular size. By applying a mixture of molecular probes with defined size the pore size and pore size distribution of the adsorbent can be determined. ISEC analysis of the structure of the adsorbent requires *a priori* selection of a physical model that describes the molecular probe properties as well as the structural characteristics of the adsorbent (Yao and Lenhoff 2004). Therefore a drawback of the method is that the results obtained will depend on the selected probe and pore model (Hagel *et al*. 1996). ISEC has been applied for the structural characterization on a number of adsorbents such as composite polyacrylamide-agarose, dextran, polyacrylamide (Grimaud *et al*. 1978), silica, alumina (DePhillips and Lenhoff 2000), polystyrene, and controlled pore

glass (Knox and Ritchie 1987). Molecular probes used in ISEC include dextrans (Hagel *et al*. 1996), pullulan, ficol, proteins and DNA (Yao and Lenhoff 2004).

Gel Electrophoresis: This technique separates proteins according to their charge. When applied in a free solution (free electrophoresis), proteins will move at different speeds due to differences in charge densities and thus separate. In practice the separation usually takes place in a gel medium. The gel can act as an inert support for the electrophoresis buffer or actively participate in the separation thought its interaction with the proteins. In the latter, the protein-gel interaction is the actual separation factor, whereas the electrical field promotes the migration of proteins though the gel. Commonly used gels for electrophoresis include polyacrylamide and agarose (Laas 1998). Structure and transport of solutes in agarose gels have been widely studied with respect to this technique (Fatin-Rouge *et al*. 2004). Similarly to ISEC, by applying a mixture of predefined macromolecules, information on the structure of the gel can be obtained. Probes (molecular and particulate) used of studying the structure of agarose gels by electrophoretic means include proteins, dextrans, DNA molecular weight ladders (Pluen *et al*. 1999) and polymer beads in the size range 10-140nm (Pluen *et al*. 1999, Fatin-Rouge *et al*. 2004).

Microscopy: A significant number of attempts to characterize the structure of agarose gels and beads by microscopy means are available in the literature. Examples include: Transmission electron microscopy (TEM) of agarose beads (Amsterdam *et al.* 1975, Attwood 1988) and freeze-fractured (Waki *et al.* 1982) gel slabs (Griess *et al*. 1993), atomic force microscopy (AFM) of agarose gel surfaces (Pernodet *et al*. 1997, Maaloum *et al*. 1998) and scanning electron microscopy (SEM) of freeze-dried (Medin *et al*. 1995) slabs and critical

point-dried (Zhou *et al*. 2007) pellicular agarose-glass composite beads. Other microscopically characterized (SEM) adsorbents include dextran, polyacrylamide and polyacrylamide-agarose composite beads (Grimaud *et al*. 1978). A common drawback of microscopy is sample preparation. This is especially true when considering the sensitive nature of hydrogels. It is therefore essential to choose the least invasive sample preparation method in order to avoid distorting the gel network. Unfortunately it appears that the more invasive the sample preparation is, the better the quality of the images, irrelevantly as to whether information extracted from them is realistic. This unfavoured invasion-quality relationship is especially pronounced in Electron Microscopy (SEM, TEM etc.). For example, sample staining, buffer exchange and sample embedment in epoxy resin (Amsterdam *et al.* 1975, Attwood 1988, Griess *et al*. 1993) results into average quality images, freeze fracturing without freeze-drying improves the quality of images (Waki *et al.* 1982) but not to a significant degree, whereas freeze-fracturing followed by freeze-drying and gold staining produces images of excellent quality (Medin *et al*. 1995).

Templated Electrodeposition: A technique for characterizing thin agarose slabs (sheets) can be derived from templated electrodeposition of silver deposits (Hasse and Scholz 1996). The method has been used to control the size of silver crystals by applying agarose layers of defined concentration onto platinum electrodes with subsequent immersion into suitable solution and application of a reduction potential for a short period of time. Silver crystals are then grown in the pores of the gel. Agarose can be then removed by immersion of the electrode into boiling water. The grown silver crystals can be collected and examined under a suitable microscope (e.g. SEM or AFM) for the determination of their size distribution. The latter will correspond to the pore size distribution of the gel. This relatively simple and fast

method for characterizing the structure of agarose gels offers a significant advantage over other rapid characterization methods, such as microscopy, as it only provides information on pores that are accessible for molecular diffusion. Although this method cannot be used for the structural characterization of *beaded* agarose, an alternative can be realized through it: Agarose beads can be soaked into a UV-curable, heat-resistant epoxy resin. After separation of the beads from the bulk of the resin and subsequent UV-treatment, the gel beads can be dissolved/removed with boiling water. What is left behind is an imprint of the porous network of the gel. Following examination with a suitable microscope the size distribution of pores available for diffusion can be determined. This method may only be limited by the molecular size of the epoxy resin.

Nuclear Magnetic Resonance: NMR can provide non-destructive measurements on the structure of hydrogels without the need for gel drying. The technique is based on the interaction between water molecules and the solid surface of the pores of the gel. The relaxation rate of water molecules near the solid surface (termed *surface* water) is enhanced and the spin-lattice relaxation time[1] is shorter than that of bulk water (bulk water refers to the water molecules other that the ones coming in contact with the surface of the pores in the gel) Water in the large pores tends to relax slower than water in small pores because of the different relative amounts surface and bulk water. Thus the measured relaxation profile provides information on the pore size distribution of the gel or more precisely the volume to surface area distribution. The technique has being applied on agar, agarose and polyacrylamide gels slabs (Chui *et al.* 1995).

[1] Spin-lattice relaxation time characterizes the rate at which the longitudinal M_z component of the magnetization vector recovers. It is thus the time it takes for the signal to recover 63% [1-(1/e)] of its initial value before being flipped into the magnetic transverse plane (McRobbie 2003)

Other absorbance measurements: Small Angle Scattering (SAS) is a collective name given to the techniques of Small Angle Neutron Scattering (SANS), Light Scattering (SALS or LS) and X-ray scattering (SAXS). In each of these techniques radiation is elastically scattered by the sample of interest and the resulting scattering pattern is analysed to provide information about the size, shape and orientation of the microstructure of the sample (http://www.isis.rl.ac.uk/largescale/loq/documents/sans.htm). SANS has been used to study the evolution of agarose gelation (sol-gel transition) (Qualli 2001) and agar-gelatin complexes gelation (Singh *et al*. 2007). Besides agarose, SANS has been used to study the structures of activated carbon (Hoinkis and Ziehl 2003) and mesoporous silica (Connolly *et al*. 2004). SALS (Manno *et al*. 1999) and SAXS (Djabourov *et al*. 1989) have also been used to study the gelation of agarose. Finally, gelation of agarose has also been studied by light absorbance at the wavelength range of 700-800 nm (Narayanan *et al*. 2006).

Thermoporometry: Similarly to NRM, thermoporometry exploits the interactions between surface water, bulk water (defined above) and the surface of the pores. Surface water has different thermodynamic properties than bulk water, e.g. surface water crystallizes at temperatures considerably lower than 0° C (Higuchi and Iijima 1985). Thermoporometry is based on the principle of freezing (or melting) point depression of water, which is due to the strong curvature of the solid-liquid interface present within the pores (Cuperus *et al*. 1992). By subjecting the sample of interest to differential scanning calorimetry measurements the cooling traces of water crystallisation, can be transformed to porosity distribution (Faroongsarng and Peck 2003). Furthermore by selecting solvents with different polarities and thus different interactions with the gel, one can obtain more information on the structure of gel network (Nedelec *et al*. 2006). The method has been

applied on ultrafiltration membranes (Cuperus *et al*. 1992), polyvinyl alcohol membranes (Higuchi and Iijima 1985), croscarmellose starch sodium and sodium starch glycolate (Faroongsarng and Peck 2003), silica gels (Nedelec *et al.* 2006) and resorcinol-formaldehyde hydrogels (Yamamoto *et al*. 2005). Although recognized as a powerful tool for the study of hydrogels (Nedelec *et al.* 2006), Thermoporometry cannot be applied on beaded material since distinction between cooling traces of water around particles and cooling traces of water within particles (pores) is difficult (Stenekes *et al*. 2000).

In attempting to characterize the structure of existing or novel agarose formulations one has to consider that the results obtained will depend on the characterization method, in other words, different methods will produce different results. Additionally, different techniques will produce results of different importance and applicability. For example, in ISEC and (inverse) electrophoresis, where both methods rely on molecular diffusion, the information obtained on the porous structure of the support will depend upon the molecular probe used and the pore model assumed (Hagel *et al*. 1996). Consequently, different sets of probes and pore models will produce different results. Although these methods do not provide any information on pore geometry and pore connectivity, both important parameters in solute transport (Yao and Lenhoff 2004), they do provide information on pores only accessible to diffusion. This is of practical importance since it is directly relevant to the chromatographic applications. In the same context, information on the properties of the porous network extracted from images acquired with a suitable microscope will give a far more accurate and objective characterization, assuming minimal distortion from sample preparation. This is because dimensions of pores and fibres as well as distribution of pores will be directly measured, rather that derived (e.g ISEC). The latter may be useful for linking

the properties of the gel network with gelation kinetics, but will be of somewhat less practical importance in terms of the application of the adsorbent, since no distinction between pores available for diffusion and 'sealed' regions can be made using microscopy images. Nevertheless the importance of microscopy as a characterization is paramount since it is by far the least time consuming, reproducible, and in some cases can provide structural information on different parts of the adsorbent (e.g. surface, interior). The latter is especially significant as the accurately determined resulting properties can be directly linked to processing conditions during manufacturing and instances of under- or over-processing can be identified and eliminated.

For the above reasons two types microscopy (AFM and cryo-SEM) were initially used to characterize the structure of the agarose formulations tested in this work. AFM was chosen since sample preparation is very simple and samples can be viewed in aqueous conditions, similar to these of chromatographic applications. Because AFM provided information only on the pore size and pore size distribution of the particle surface (thin-sectioning of agarose beads using microtome resulted in artefacts on the gel structure, results not presented) cryo-SEM was utilized in order to obtain information on the internal structure of the adsorbent. The third technique used was Micromanipulation. This technique can be used for the determination of mechanical properties (e.g. elastic and shear moduli, compression strength at given deformations, rupture force, viscoelastic properties) of individual particles thus allowing manufacturing conditions to be linked with resulting mechanical properties of particles. Furthermore the measurement of the mechanical properties of individual particles allows the determination of mechanical loads that particles can be exposed to during functionalization and operation. Micromanipulation also offers an indirect method for

calculating the average pore size of the adsorbent by using equations derived from rubber elasticity theory (Stenekes *et al*. 2000).

Atomic Force Microscopy: AFM (Fig. 1.6) was invented by Binnig *et al*. in 1985 (Binnig *et al*. 1986). It was developed in order to overcome the fundamental drawback of Scanning Transmission Microscopy (STM). The latter can only produce images of conducting or semiconducting surfaces. AFM on the other hand, can produce images of almost any type of surface, including polymers, ceramics, composites, glass, and biological samples. (http://www.nanoscience.com/education/AFM.html, Colton *et al*. 1997). AFM operates by measuring the attractive or repulsive forces between a tip and the sample (Binnig *et al*. 1986). It is a light-lever technique in which a micro-fabricated cantilever interacts with the surface of interest, with the deflection of the cantilever monitored by a laser beam reflected from the cantilever onto a position-sensitive photodiode (Bowen 2005).

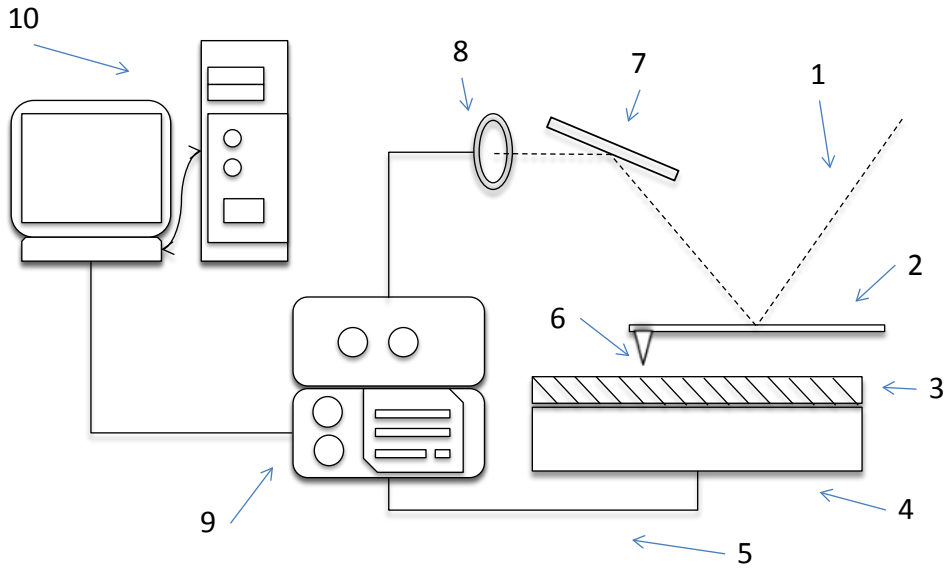

***Figure 1.6**. Schematic diagram of AFM: (1) laser beam, (2) cantilever, (3) sample, (4) piezoelectric translator, (5) feedback loop, (6) cantilever tip, (7) mirror, (8) photodiode, (9) controller, (10) user interface (redrawn from Bowen 2005).*

AFM generally uses two types of tip. The *normal tip* (Fig. 1.7a) is a 3 µm tall pyramid with about 30 nm end radius. The *electron-beam-deposited* (EBD) tip or *supertip* (Fig. 1.7b) improves on the former with an electron-beam-induced deposit of carbonaceous material made by pointing a normal tip straight into the electron beam of a scanning electron microscope (Baselt 1993).

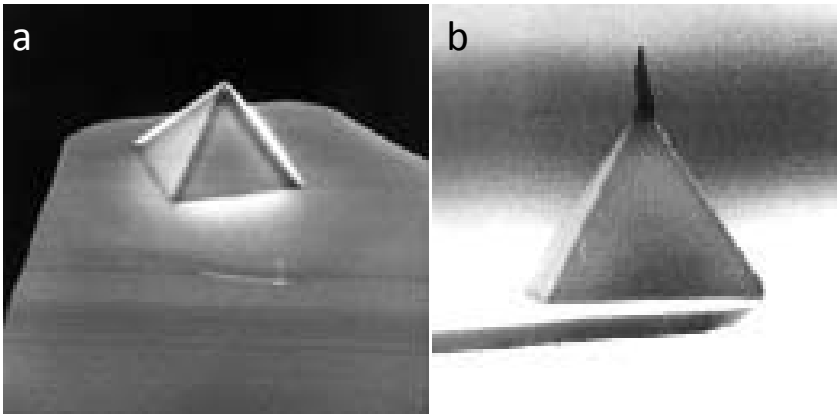

***Figure 1.7**. Two common types of AFM tip: (a) normal tip (3 µm tall), (b) super-tip (Baselt, 1993).*

AFM also operates in two modes: tapping and contact mode. In the latter, the cantilever tip is in direct contact with the surface and as the tip moves across the surface the change in cantilever deflection is monitored via the change in the position of the laser beam on the photodiode. A feedback control system is used to maintain the contact between the cantilever and the sample. In tapping mode the cantilever vibrates close to its resonance frequency at a short distance above the sample. If the tip and surface move relative to each other in a vertical direction, the tip can interact with the sample surface thus allowing adhesive and repulsive interaction forces between the tip and sample to be determined (Baselt 1993, Bowen 2005).

Scanning Electron Microscopy: The SEM (Fig.1.8) produces a highly magnified image by using electrons instead of light to form an image. A beam of electrons is produced at the top of the microscope by an electron gun. The electron beam follows a vertical path through the microscope, which is held within a vacuum. The beam travels through electromagnetic fields and lenses, which focus the beam down toward the sample. Once the beam hits the sample, electrons and X-rays are ejected from the sample. Detectors collect these X-rays,

backscattered electrons, and secondary electrons and convert them into a signal that is sent to a screen similar to a television screen. This produces the final image. (www.purdue.edu/REM/rs/sem.htm) A high energy (typically 10-50 keV) electron beam is scanned across the surface of the sample. Backscattered electrons can also give information on the surface topography and on the average atomic number of the area under the electron beam. (http://www.jeolusa.com/sem/docs/sem_guide/tbcontd.html)

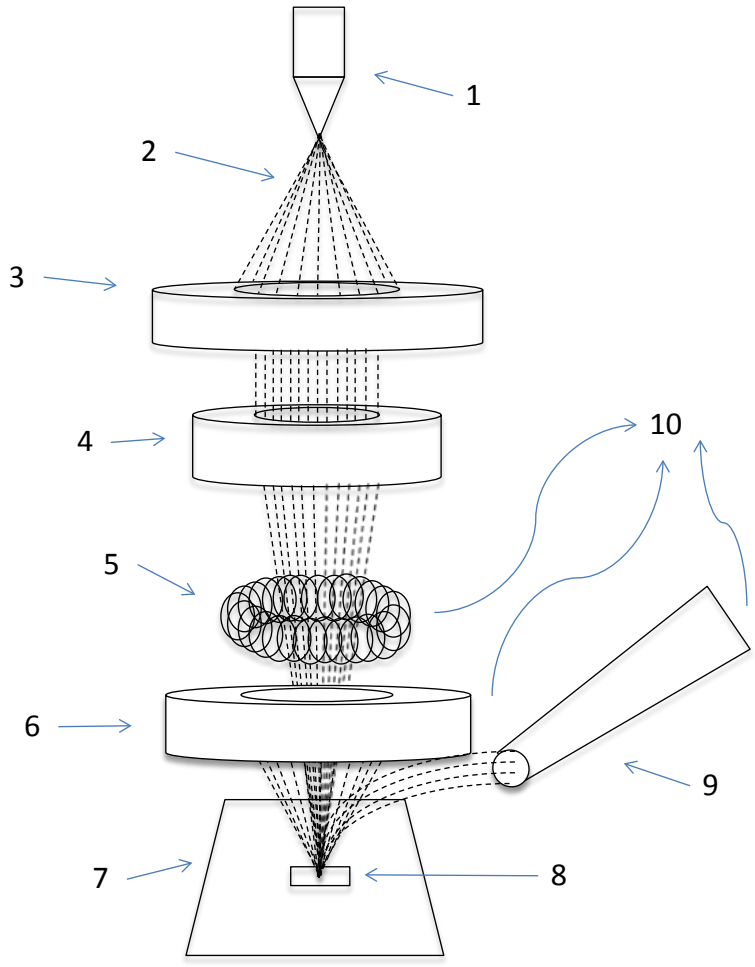

***Figure 1.8**. Schematic diagram of SEM: (1) electron gun, (2) electron beam, (3) anode, (4) magnetic lens, (5) scanning coils, (6) backscattered electron detector, (7) stage, (8) sample, (9) secondary electron detector, (10) to TV scanner (redrawn from www.purdue.edu/REM/rs/sem.htm).*

Micromanipulation: The mechanical stability of chromatographic columns is traditionally determined with the construction of pressure drop-flow rate curves. Extensive work on conventional compression of chromatographic beds has been reported (Stickel *et al*. 2001). This macroscopic approach for the determination of the mechanical stability of chromatographic adsorbents presents two issues: first, no information on the state (extent of deformation, recovery time, permanent deformation, crashing etc.) of individual particles can be obtained (Muller *et al.* 2005). Second, functionalization of chromatographic adsorbents is usually a high intensity, multistep process (vacuum washing, turbulent mixing, centrifugation etc.) (Mu *et al.* 2005) that exposes particles to mechanical loads and hydrodynamic pressures much higher than in chromatographic columns. It is therefore important to know what range of mechanical load individual particles can withstand without causing irreversible damage to their structure. Such information cannot be obtained from a pressure drop-flowrate curve.

The theoretical concept of measuring mechanical properties of individual particulate matter using micromanipulation was first introduced in 1987 (University College London) while the first practical rig was constructed at the University of Birmingham in 1990. The first set of experiments using the technique involved biological materials and the measurement of tensile forces as well as the strength of single fungal hyphae subjected to uniaxial extension. The outcome of these experiments was ultimately linked to the hydrodynamic forces imposed to fungal cells during fermentation and their mechanical damage as well as the loss of viability and productivity caused by the latter (Blewet 2000). The progression of the technique was realised with the compression of single mammalian cells (Zhang *et al*. 1991), yeast cells (Srinorakutara 1997, Mashmoushy *et al*. 1998) and tomato cells (Wang *et*

al. 2003), as well as non-biological materials such as dextran beads (Stenekes *et al.*, 2000), polymeric chromatographic adsorbents (Muller *et al.* 2005), agarose beads (Mu *et al.* 2005) and gelatin-rich micro-particles (Ding *et al.* 2007). Recently the application of the technique was taken one step further with the construction of a composite ESEM-nanomanipulation rig where the mechanical properties of single nanoparticles (800 nm in size) where measured (Liu *et al.* 2007).

Based on a simple concept, the micromanipulation technique relies on compressing single particles with a refined glass rod while a force transducer determines the compression force by measuring the deflection of a cantilever as voltage difference (Shiu 2000). From the raw data obtained (voltage-time tracer), force-deformation and force-time graphs can be extracted, thus allowing the determination of said properties of particulate materials at a wide range of deformations. A detailed description of the micromanipulation rig can be found in section *2.5*.

1.6. Methods and equipment for manufacturing agarose based chromatographic media

A small number of methods is available for the manufacturing of agarose particles. These include emulsification in a stirred vessel or high shear mixer (Jahanshahi *et al*. 2003, Mu *et al*. 2005, Yan *et al*. 2009), membrane emulsification (Zhou *et al*. 2007, Zhou *et al*. 2008, Zhou *et al.* 2009, Yan *et al*. 2009) and spray-gelation (Egorov et al. 1970). Irrespectively of method of choice, production of agarose beads usually involves the dispersion of an aqueous phase (agarose-containing phase) at elevated temperature into an organic phase followed by cooling below the gelation temperature of agarose to form solid particles.

The control of the following parameters is very important in the commercial manufacturing of agarose beads: particle size/size distribution, internal structure of the particles, throughput and yield. Additionally ease of scale-up is an important factor in minimizing manufacturing cost. In general, particle size/size distribution is *primarily* a function of energy input in the system. The structure of agarose (pore size, pore size distribution), is controlled by the physical and chemical composition of the gel and by the quenching temperature of the emulsion. The latter has been largely ignored in a number of publications concerning the manufacturing of agarose beads and the characterization of the resulting properties of the adsorbent. Throughput is an inherent property of the processing element as well as a function of the scale of the operation, while yield is essentially determined by the resulting particle size/size distribution.

The following review of the features of processing methods mentioned above, attempts to identify the ideal equipment of large-scale manufacturing of agarose particles intended for chromatographic applications.

Stirred vessels and high shear mixers (Fig1.9)**:** The choice of stirred vessels or high shear mixers is often due to scale-up from laboratory product development (Karbstein and Schubert 1995). As mentioned above, conventional emulsification by rotational shearing involves the dispersion of agarose into an oil phase at elevated temperature (usually around 80°-90° C) with subsequent cooling well below the gelling point of agarose. This process can be carried out in batch (stirred vessel or high shear mixer) or continuous (high shear mixer) mode. Batch systems are better suited for manufacturing relatively small quantities of various particle types (high flexibility) whereas continuous rigs are better suited for the

production of large volumes of single types of particles (less flexibility, higher productivity (Mu *et al*. 2005)). Continuously operating rigs have very narrow residence time distributions along with short mean residence times (Karbstein and Schubert 1995) resulting in high throughputs. Factors affecting the resulting particle size/size distribution in stirred vessels and high shear mixers are the input energy density, concentration and type of emulsifier, the physical properties of the dispersed and continuous phases (interfacial tension, viscosity) and drop coalescence. Cooling of the emulsion in the continuous setup is achieved by injection of cold oil at the outlet of the rotor-stator assembly. In batch systems, solid bead formation can be achieved by decreasing the temperature in the vessel containing the emulsion as well as by discharging the latter in a separate vessel containing a large volume of the continuous phase at low temperature (quenching). Quenching of the emulsion offers high degree of flexibility in terms of cooling rates achieved. Therefore a wide range of intraparticle structures can be produced by selecting the appropriate quenching temperature.

An inherent flaw of emulsification by rotational means is that a lot of the input energy is dissipated as heat when compared to e.g. membrane emulsification (Joscelyne and Tragardh 2000). This is especially true for stirred vessels that, despite the general opinion, are not necessarily the cheapest emulsifying machines (Karbstein and Schubert 1995). An issue commonly encountered with stirred vessels and high shear mixers is the broad size distribution of particles (Zhou *et al*. 2008). Typically, after emulsification sieving is employed for obtaining particles with a narrow size distribution but this leads to reduced yields and high manufacturing costs (Zhou *et al*. 2007).

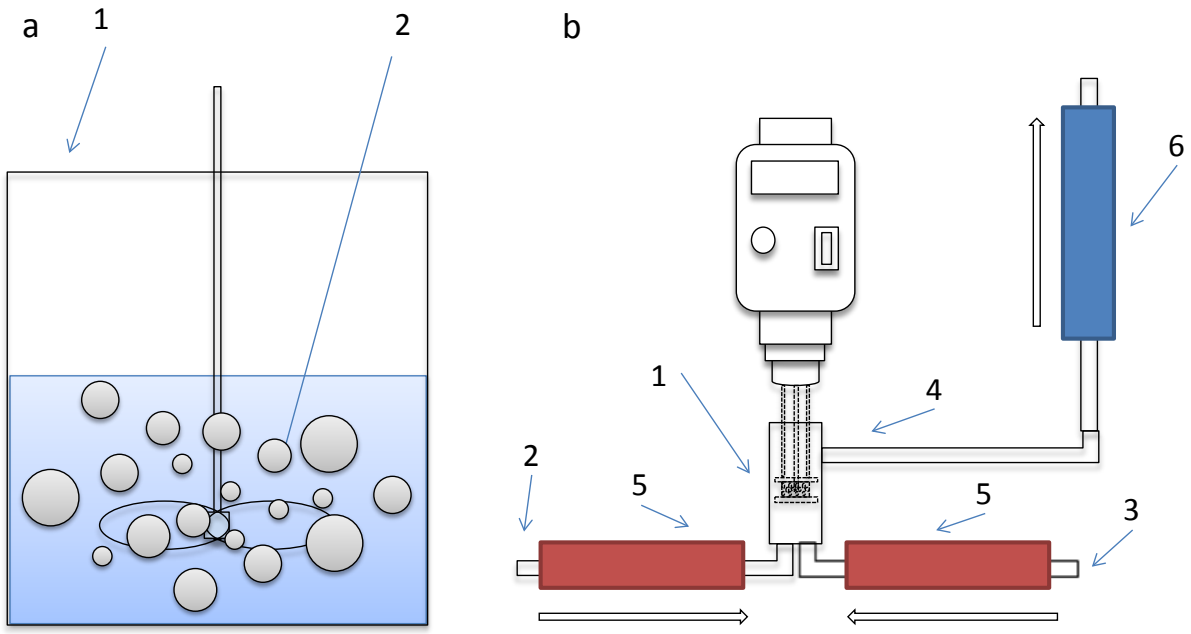

Figure 1.9. *(a) stirred vessel: (1) vessel, (2) impeller, (b) continuous high shear mixer rig, (1) rotor stator assembly, (2) dispersed phase tube, (3) continuous phase tube, (4) emulsion output tube, (5) heat exchangers for heating the two phases, (6) heat exchanger for cooling the emulsion, arrows show the direction of flows.*

Membrane emulsification (Fig. 1.10)**:** A number of recent publications concern the manufacturing of agarose beads using membrane emulsification technology (Zhou *et al*. 2007, Zhou *et al*. 2008, Zhou *et al.* 2009). In general membrane emulsification involves the dispersion of one phase into another by pressing the former through the pores of a membrane. A cross-flow stream of the continuous phase collects the newly formed particles in a bulk phase. The detachment of the droplets from the membrane surface results in an emulsion with a very narrow droplet size distribution (Lambrich and Schubert 1999). In the case of agarose emulsification particles can be collected and subsequently cooled to induce gelation of beads at conditions similar to that of a stirred vessel (Yan *et al*. 2009). Production

of emulsions with membranes requires that the dispersed phase does not wet the membrane. For this reason hydrophobic membranes should be used to prepare W/O emulsions and hydrophilic membrane for O/W emulsions (Joscelyne and Tragardh 2000). The narrow size distribution of particles obtained from membrane emulsification is particularly attractive to chromatographic applications as column performance and resolution improves with bead monodispersity (Amersham 2002, Sun *et al*. 2005). Additionally, narrow particle size distributions are economically favoured with respect to adsorbent manufacturing costs as there is no need for sieving of the particles (Zhou *et al*. 2009) and, hence, no material is wasted. In membrane emulsification, average particle size *primarily* depends on the average pore size of the membrane and it has been reported that a linear relationship exists between the two (Zhou *et al.* 2007). Other factors affecting particle size are membrane porosity, transmembrane pressure, concentration and type of surfactant, physical properties of the two phases, dispersed phase flux, velocity of the continuous phase and drop coalescence (Joscelyne and Tragardh 2000). A drawback of membrane emulsification is the low dispersed phase flux which is mainly restricted by the small pore size of the membrane and the viscosity of the dispersed phase (Zhou *et al.* 2008). A way to significantly increase trasmembrane flux is by premixing the emulsion (coarse emulsion), using conventional methods, before passing through the membrane (Vladisavljevic *et al.* 2004).

Although preparing economically favoured monodispersed agarose beads using membrane emulsification technology seems an attractive alternative to conventional emulsification techniques (stirred vessels, high shear mixers), a critical factor regarding the resulting structure of the adsorbent appears to have been overlooked: A general condition

for the preparation of monodispersed emulsions using membrane emulsification is that the interfacial tension between phases should be relatively high (Zhou *et al.* 2007). Specifically for the case of agarose, this suggests that the emulsification temperature should be kept low otherwise the lowering of interfacial tension due to the increase in temperature results in a polydisperse emulsion. Indeed in the number of recent publications (Zhou *et al*. 2007, Zhou *et al*. 2008, Zhou *et al.* 2009) process temperature was maintained between 55°-60° C while a range of agarose concentrations were used (4 %-14 % (w/w)). This temperature is very close to the gelation temperature of agarose (measured in this work 46°-52° C for 3 %-6 % (w/w), see section *3.2.3*). The latter observation suggests that the structure of agarose during droplet formation has transitioned and in fact is very close to gel state. This increases the possibility of large inhomogenities in the internal structure of the particles. Furthermore, there is no information on the structure of particles obtained by membrane emulsification at such low temperature. In the same context, high temperature emulsification using conventional methods appears to be advantageous in obtaining beaded agarose of higher product quality than membrane emulsification.

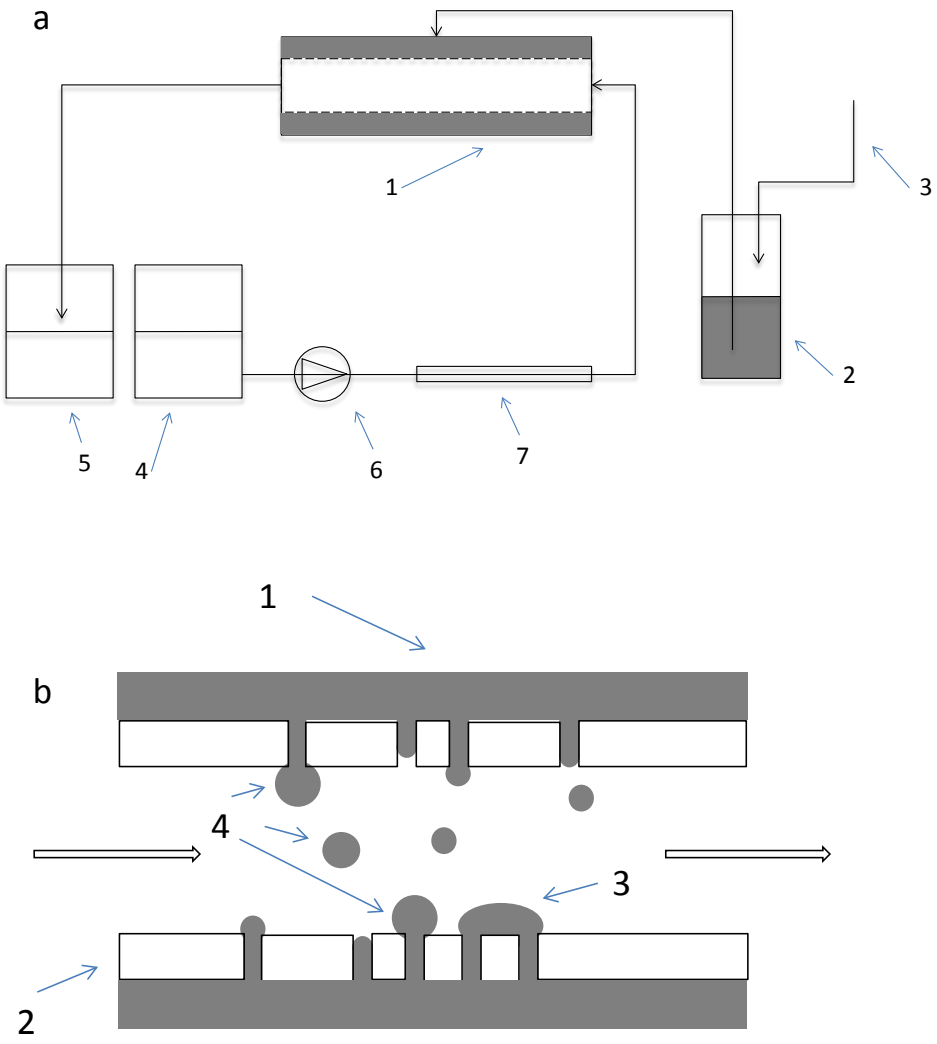

Figure 1.10. *(a) semicontinuous membrane emulsification rig: (1) membrane module, (2) disperse phase, (3) pressurized nitrogen, (4) continuous phase, (5) collection tank, (6) pump, (7) heat exchanger, (b) membrane module: (1) dispersed phase, (2) membrane, (3) drop coalescence, (4) drops, arrows show the direction of continuous phase flow (redrawn from Joscelyne and Tragardh 2000).*

Spray-gelation (Fig. 1.11)**:** A method for producing agarose beads by spraying a hot agarose solution through a nozzle with subsequent cooling (quenching) of the beads in water-ether was proposed by Philipson and Bengtsson in 1964 and modified by Egorov *et al.* (Egorov *et al.*1970). The device consists of a hermetically closed vessel containing the

agarose solution at elevated temperature. The lower outlet of the tank is connected to a sprayer with removable brass discs that have a conical orifice. Compressed nitrogen is fed in the tank with the melted agarose which is then squeezed through the sprayer. The atomized agarose enters a vessel containing a large volume of cold water-ether mixture continuously stirred to induce the gelation of agarose beads. Particle size is controlled by the diameter of the orifice, and the applied pressure, while optimum agarose solution concentrations are between 2-7 % (w/w). Although scalability of the process does not appear to be an issue (Egorov *et al.* 1970), the method has not attracted much attention in the industrial manufacturing of agarose beads.

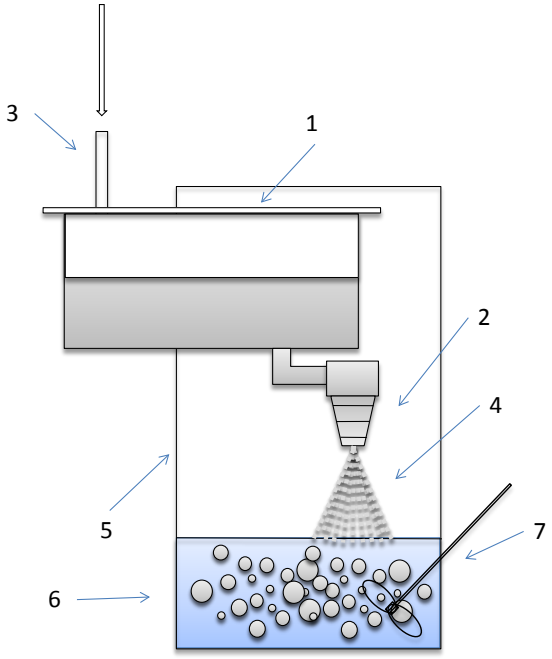

Figure 1.11. *Spray gelation for producing agarose beads: (1) hermetically closed vessel containing agarose solution at elevated temperature, (2) spray nozzle with removable discs, (3) compressed nitrogen inlet, (4) beaded agarose, (5) cooling vessel, (6) water- ether mixture, (7) stirrer.*

CHAPTER 2

-

EXPERIMENTAL SETUP AND MATERIALS & METHODS

2.1. Manufacturing of agarose beads

2.1.1 Experimental rig

Emulsification was carried out with a Silverson high-shear mixer (L4 series, Silverson, UK) (Fig. 2.1 (2)) Process temperature was controlled with a water-bath (model OLS 200, Grant Instruments, UK) (Fig. 2.1 (1)) connected to the heating jacket (Fig. 2.1 (13)) of a stainless steel vessel (I.D: 0.1 m, H: 0.15 m, V ≈ 1 L) (Fig. 2.1 (5)). The particular vessel does not incorporate baffles, the head is fitted eccentrically (Fig. 2.1 (18)). The stator used (D: 0.026 m, H: 0.017 m, voidage ε: 22.5 %, gap size: 0.175 mm) was the standard emulsor screen (Silverson manual) (Fig. 2.1 (18)). Cooling of the emulsion was achieved by discharging the hot emulsion, using compressed air (Fig. 2.1 (16)), into a separate glass vessel (I.D: 0.145 m, H: 0.28 m) (Fig. 2.1 (3)) containing 3.8 L of cold mineral oil at the desired quenching temperature. Mixing in the quenching vessel was achieved using an overhead mixer employing a six-blade 45° pitched blade impeller (D: 0.085 m, H: 0.025 m) (Fig. 2.1 (12)) fitted eccentrically. The quenching temperature was controlled with a second water-bath (Fig. 2.1 (4)) connected to the cooling jacket of the glass vessel (Fig. 2.1 (14)). Temperature was measured in both vessels using two separate J-type thermocouples (Radleys, UK) (Fig. 2.1 (15), (17) connected to the same digital display (in-house made) (Fig. 2.1 (10)).

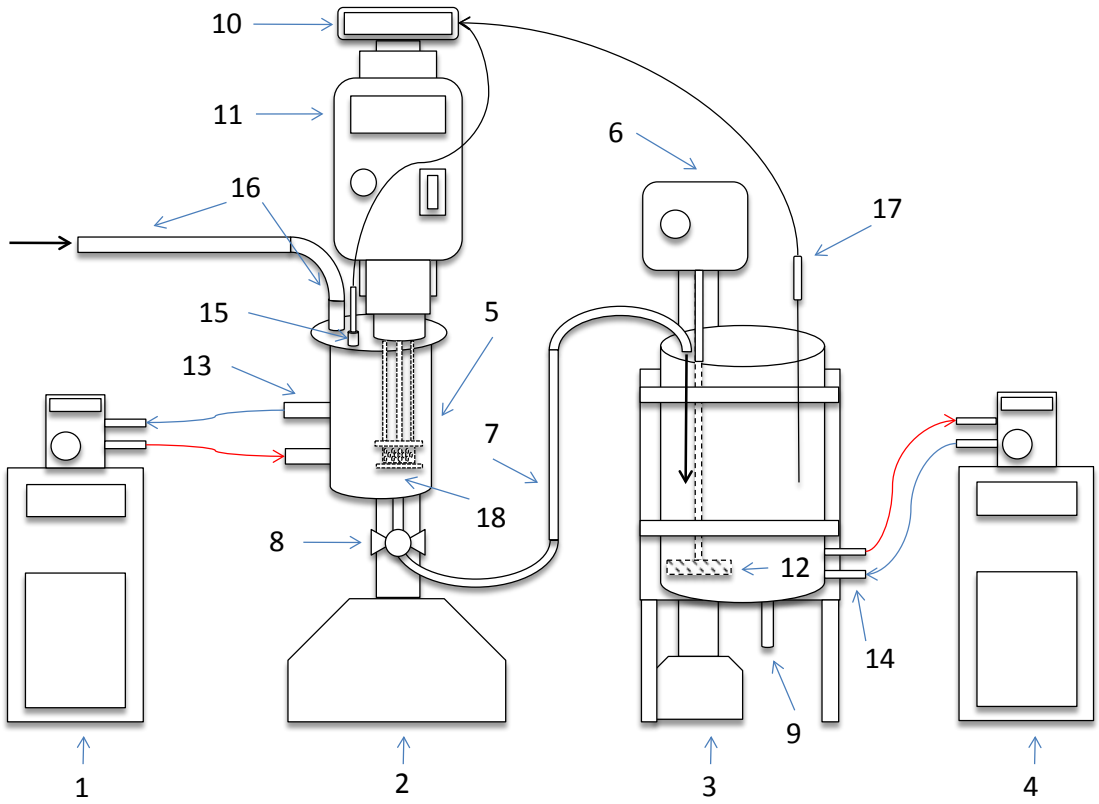

Figure 2.1. *Experimental rig for manufacturing agarose beads: (1) hot water-bath, (2) high-shear mixer, (3) quenching vessel, (4) cold water-bath, (5) emulsification vessel, (6) quenching stirrer, (7) emulsion discharging tube, (8) discharging valve, (9) quenching vessel outlet, (10) temperature LED display, (11) rotor speed LED display, (12) quenching impeller, (13) heating jacket inlet (red) - outlet (blue), (14) cooling jacket inlet (blue) - outlet (red), (15) mixer inlet and thermocouple, (16) compressed air tube and inlet, (17) thermocouple, (18) rotor-stator assembly.*

2.1.2 Materials

High-melting agarose D5 (M_r = 120 KDa, gelation temperature 46°-52° C, depending on concentration, composition and setting conditions, $\rho_{(dry)}$ = 1.64 g mL^{-1}) (supplied by Millipore, UK) was used as raw material for the manufacturing of the adsorbent. White mineral oil Marcol N82 ($\nu_{(90^\circ C)}$ = 3.5 mm^2s^{-1}, $\rho_{(90^\circ C)}$ = 812.3 kg m^{-3}) (ESSO, UK) was used as the continuous phase. Sodium chloride (Sigma Aldrich, UK) was used as a co-solute for controlling the pore size of the adsorbent. Oil-soluble surfactants Span 80 (sorbitan monoleate, HLB 4.3, $\rho_{(20^\circ C)}$ = 986 kg m^{-3}, M_r = 446.62 g mol^{-1}) and Span 85 (sorbitan trioleate, HLB 1.8, $\rho_{(20^\circ C)}$ = 956 kg m^{-3}, M_r = 975.51 g mol^{-1}) (Sigma Aldrich, UK) were used for controlling particle size.

2.1.3. Agarose solution preparation

Agarose powder at a concentration of 4 % (w/w) was dissolved in saline solutions of distilled water containing a certain amount of NaCl in a glass beaker. Distilled water was also added to account for water loss during subsequent heating. The mixture was then placed in a microwave oven for a total of 3 mins. To ensure complete dissolution of the agarose, the mixture was stirred by hand every 0.5 mins and for about 10 s. After obtaining a transparent solution the beaker was sealed and placed in a submersion water bath at 90° C where it was held for at least 30 mins to allow air bubbles to escape. Due to water evaporation a thick crust of dried agarose was formed on the surface of the solution. For this reason it was necessary to load the pre-heated syringe for the bottom of the beaker were the bulk concentration of the agarose solution remained constant. This was done by

penetrating the crust of dried agarose with the syringe and immersing it into the beaker until it touched the bottom. Considering the viscous nature of agarose solutions, later observation of agarose beads with the SEM confirmed the mixing procedure followed resulted in homogenous mixture as the internal structure of the particles appeared fairly uniform.

2.1.4. Emulsification

A volume of 800 mL (80 % (v/v), continuous phase) of mineral oil was loaded to the emulsification vessel. Oil soluble surfactant of desired type and concentration was added to the vessel from the top port using a syringe. The mixture was allowed to equilibrate to 90° C while stirring at 1000 rpm for about 30 mins. Then, 4 L of mineral oil were placed in a plastic bottle and stored in deep freezer (-70°C) for approximately 45 mins thus cooling the oil to -10°C. After cooling the bulk volume of oil, 3.8 L were loaded to the quenching vessel and allowed to equilibrate for 30 mins to the desired quenching temperature while stirring at 300 rpm. As soon as the two vessels were equilibrated to the desired temperatures and air bubbles had escaped from the agarose solution, the high shear mixer rotor was fixed at the desired speed. Then, using a preheated syringe, 200 mL (20 % (v/v), dispersed phase) of the agarose solution were injected in the high shear mixer from the top port. After 5 mins of shearing the emulsion was discharged in the cooling vessel using compressed air (0.5 bars). To ensure complete gelation of the agarose particles, the mixture was allowed to equilibrate to the final cooling temperature (20° C) for at least 15 mins while stirring at 300 rpm. This relatively low speed was chosen in order to avoid altering the resulting particle size distribution coming out of the high shear mixer.

The above concentrations and conditions were kept constant during the following experiments. To study the effect of ionic strength on pore size / size distribution and particle size / size distribution, NaCl was dissolved in the agarose solution at the following concentrations: 0, 0.01, 0.025, 0.05 and 0.1 molal. In this set of experiments the emulsion contained 0.1 % (v/v) Span 85, was emulsified at 30.7 W kg^{-1} (3500 rpm) and was quenched at 0° C.

To study the effect of quenching temperature on pore size / size distribution and particle size / size distribution the emulsion was quenched at three different temperatures: 0°, 10° and 20° C, and three concentrations of salt were used at each quenching temperature (0, 0.01, 0.05 m NaCl), 0.1 % (v/v) Span 80 was added as a surface active agent. In all three experiments, formulations were emulsified at 30.7 W kg^{-1} (3500 rpm).

To study the effect of surfactant concentration the resulting particle size / size distribution Span 85 was added to the continuous phase prior to emulsification at the following concentrations: 0, 0.1, 0.5, 1.0 and 1.35 % (v/v). The salt-free dispersion was emulsified at 2.87 W kg^{-1} (2000 rpm) and quenched at 0° C.

The effect of surfactant type on particle size was studied by preparing two separate emulsions. In the first, Span 80 at a concentration of 0.1 % (v/v) was added to the continuous phase. In the second emulsion, Span 85 was added at the same concentration (0.1 % (v/v)). No salt was used in this experiment while the dispersions were emulsified at 30.7 W kg^{-1} (3500 rpm) and quenched at 0° C.

Finally, to study the effect of rotor speed on the resulting particle size / size distribution two salt-free agarose solutions, each containing 0.1 % (v/v) Span 85, were emulsified at 2.87 (2000 rpm) and 30.7 W Kg^{-1} (3500 rpm) respectively , and quenched at 0° C.

2.1.5. Centrifugation

Following solid bead formation, the oil-particle mixture was transferred from the cooling vessel to the centrifuge (model Jouan C4 22, Thermo Fisher Scientific, UK). Centrifugation at 3000 rpm (1830 g) for 10 mins successfully separated the particles from the bulk volume of the oil as the liquid removed from the centrifuge bottles was transparent. A 25 % (v/v) aqueous ethanol solution was used to wash out the particles from the centrifuge bottles.

2.1.6. Washing

Prior to any characterization measurements particles where washed using the following procedure: A small volume of particles (~30 ml) was placed in a sintered glass funnel connected to a vacuum pump. Particles where then washed with 3 volumes of 25 % (v/v) aqueous ethanol, 3 volumes of 50 % (v/v) ethanol, 3 volumes of 75 % (v/v) ethanol, 30 volumes of ethanol, 3 volumes of 75 % (v/v) ethanol, 3 volumes of 50 % (v/v) ethanol and finally 3 volumes of 25 % (v/v) ethanol. The successive washing with increasing following decreasing concentration of ethanol aqueous solutions prevents particles from possible structural damage caused by the rapid dehydration when washing directly with pure ethanol

(Amsterdam *et al*. 1975). After washing, particles were kept in 25 % (v/v) aqueous ethanol solution to prevent bacterial contamination.

2.2. Particle sizing

Particle size distributions, mean diameters (D(0,1), D(0,5), D(0,9) and D(3,2)), and yield (obtained from undersize curve) were determined with the Mastersizer 2000 (Malvern, UK). Refractive index values of 1.58 and 1.33 (Malvern manual) were used for agarose particles and distilled water respectively. The 25 % (v/v) aqueous ethanol solution was exchanged with distilled water prior to sizing. A 10 % (v/v) dispersion of particles was slowly added to the dispersion unit using a pipette until laser obscuration reached 10 % of its total value. A stirrer speed of 2000 rpm was used in the measuring cell (loop) to ensure complete dispersion of particles. Three measurements were performed per sample and the results presented in *Chapter 3* are the average of said measurements.

2.3. Physical properties of agarose solution and mineral oil

2.3.1. Viscosity measurements

The rheological properties of all agarose formulations used in this project were determined using the AR 1000 rheometer (TA Instruments, UK). A cone-and-plate (cone specs: D: 40 mm, α: 4°) configuration was used for all the measurements (Fig. 2.2 (2), (3)). The stage of the rheometer was allowed to equilibrate to the desired temperature (90° C). Then, a certain quantity of agarose solution (~ 10 ml) was loaded using a pre-heated syringe

onto the centre of the hot plate. The cone was lowered to 'geometry height', determined by software for the particular setup, while pushing excess material on the side of the plate. The excess solution was removed using a spatula until a meniscus was formed (Fig. 2.2 (1)). A solvent trap was then placed on top of the cone to prevent solvent evaporation during measurements (Fig. 2.2 (4)).

The gelation temperature of agarose was determined by the crossover of the elastic (G') over the viscous modulus (G'') while cooling the gel from 90° to 35° C at 3°C min^{-1}. The gelation temperature was determined for 3, 4, 5 and 6 % (w/w) agarose solutions. Flow curves (viscosity vs. shear rate) were determined for increasing polymer concentration in the solution (3, 4, 5 and 6 % (w/w) agarose), increasing ionic strength in the solution (4 % (w/w) agarose (D5 type) with 0, 0.01, 0.025, 0.05, 0.1 m NaCl) and mineral oil at two temperatures (20° and 90° C). Measurements were performed with increasing shear in the range of 0.01-100 s^{-1}.

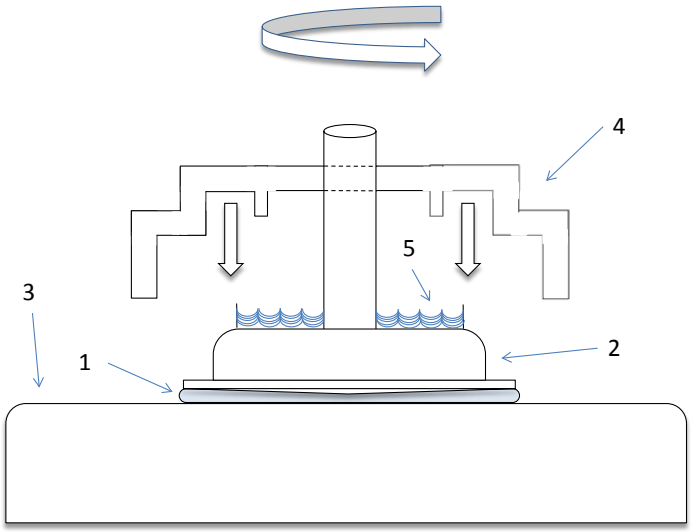

Figure 2.2. *Sample loading on rheometer plate: (1) agarose solution, (2) cone, (3) hot plate, (4) solvent trap, (5) water.*

2.3.2. Interfacial tension measurements

The interfacial tension of agarose and oil was measured using the pendant drop method (Arashiro and Demarquette 1999). The needle of a syringe containing the denser of the two phases (agarose solution) is vertically submerged into a beaker containing the less dense phase (mineral oil). A drop of agarose is generated by slowly pushing the plunger of the syringe. As soon as the weight of the drop, minus the buoyancy, is equal to the holding force the drop falls. The volume of the falling drop can be measured either by an image obtained with a suitable microscope (assuming the drop is spherical) (Fig. 2.3) or from the scaling of the syringe. Both ways were used in this work. Interfacial tension was then calculated from the following equation:

$$\sigma = \frac{g(\rho_1 - \rho_2)V}{2\pi r f_{HB}} \tag{2.1}$$

where: σ: interfacial tension (Nm^{-1})

g: gravitational acceleration (ms^{-2})

ρ_1, ρ_2: the density of the heavy and light phase respectively (kgm^{-3})

V: volume of the drop (m^3)

r: capillary (syringe) radius (m)

f_{HB}: correction factor

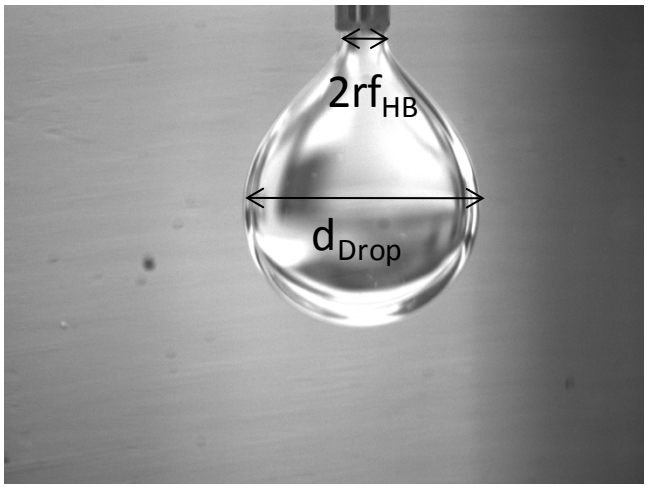

Figure 2.3. *Pendant drop method for calculating interfacial tension.*

Agarose solution and mineral oil were allowed to equilibrate to the desired temperature (90° C) prior to any measurements. Temperature control was not available during measurements but the duration of each measurement was no more than 2 mins therefore it can be assumed that no significant temperature changes occurred during this interval. Interfacial tension was determined for the following systems and concentrations: 4 % (w/w) agarose / oil, 4 % (w/w) agarose / oil / 0.1 % (v/v) Span 80 and 4 % (w/w) agarose /oil / 0.1 % (v/v) Span 80 / 0.05 m NaCl.

2.3.3. Density measurements

The density of agarose at 3, 4, 5 and 6 % (w/w) and mineral oil at 90° C as well as mineral oil at 20° C was measured with a 25 mL density bottle. The density bottle was weighted before and after loading. The weight difference was recorded as the mass of the 25 mL sample and density was obtained by dividing the mass of the sample by its volume (25 mL). Measurements were repeated in triplicate to ensure accuracy. For density measurements at 90° C the gravity bottle was submerged in a water-bath during loading.

2.4. Microscopy

2.4.1. AFM sample preparation

AFM images were acquired using a MultiMode AFM (Veeco, UK) housed on a vibration isolation table. Nanoscope v5.12 software (Veeco, UK) was used throughout for both real-time analysis and post-capture image processing. A drop of particle aqueous suspension (70 % (v/v)) from each sample was immobilized on a glass slide using double-side tape. The slide was rinsed with distilled water to remove excess amount of particles and large aggregates. Excess water was removed using paper tissue. All images were acquired while operating in Tapping Mode under ambient conditions, using rectangular 180 µm length pyramidal-tipped Si cantilevers (Veeco, UK) with nominal spring constants of 40 N m^{-1} and resonant frequencies in the range 250-350 kHz. The AFM piezoelectric tube scanner had a maximum

lateral range of 14 µm x 14 µm and a maximum vertical range of 1.9 µm when operating in Tapping Mode. All images were acquired at scan rates between 0.5-1.5 Hz, each image being composed of 512 x 512 pixels. Each sample was examined for up to 20 mins to ensure drying of the gel network did not occur. Later visual examination of the film confirmed that particles were still wet.

2.4.2. Cryo-SEM sample preparation

All samples were examined with a Philips XL 30 FEG ESEM microscope operating in SEM mode. A drop of particle aqueous suspension (70 % (v/v)) from each sample was placed on a brass stage mounted on a steel rod. The rod was immersed in nitrogen slush (-140° C) and then quickly transferred to the SEM preparation chamber. Samples were fractured using a metal rod accessing the preparation chamber. After freeze-fracturing the sample was sublimated (etched) at -90° C and 4 X 10^{-5} mbar of vacuum for 8 mins. After etching the temperature was lowered back to -140° C. Finally a platinum coating (1 min exposure, thickness 5 nm) was applied on the surface of the sample in order to prevent damage by the electron beam. After sample preparation the rod was transferred from the preparation chamber to the interconnected examination chamber. An electron beam of 8 keV was used at 4 X 10^{-5} mbar of vacuum and -140° C, for the examination of agarose particles.

2.4.3. Microscopy data interpretation

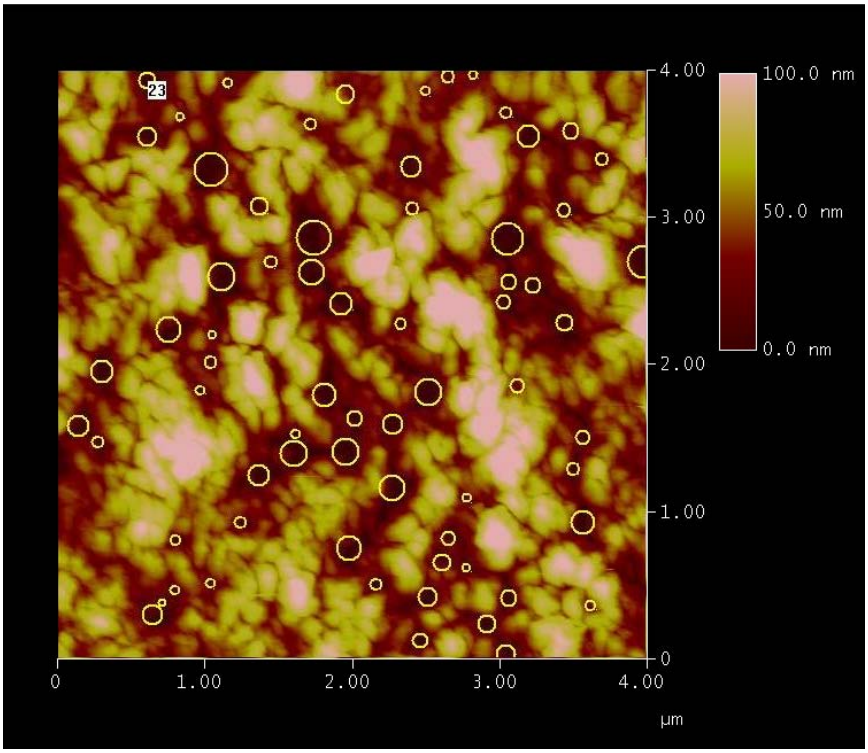

***Figure 2.4**. Example of pore size measurements using in-house image analysis software.*

AFM images exhibit the topological characteristics of the sample through height differences (Fig. 2.4). The height bar (Z-range) on the top right side of each image indicates the height differences of the surface of the sample as scanned by the tip of the AMF. Therefore, light yellow colour indicates peaks on the surface, while dark brown colour indicates valleys on the particle surface, i.e. entrance of pores. The Z-range is also an indication of sample surface roughness. The raw data extracted from the AFM and cryo-SEM images were interpreted in the following way: average pore size (arithmetic mean) and pore

size distributions were obtained using in-house image analysis software. Assuming circular pore geometry, superimposed circles were created on the image analyzed (yellow circles in Fig. 2.4) with a simple 'point and click' method of the software. The radii of these circles were recorded as number of pixels and the resulting pore size (diameter) and pore size distribution were derived using Excel spreadsheet. Ten images were acquired per sample while 200-500 pore size measurements were obtained in total for each sample. Although this method is a two-dimensional approach to a three-dimensional 'problem', it is consistent for determining the average distance between two neighbouring cross-links, i.e. the correlation length of the gel, or pore size, between samples.

2.5. Micromanipulation

2.5.1. Experimental rig and compression method

The micromanipulation rig used for the determination of the mechanical properties of agarose beads is shown in Fig. 2.5. A glass probe (length 15 mm) with a 150 μm in diameter flattened tip (Fig. 2.5 (1)) was placed on the 2 mm in diameter output tube (length 20 mm) of the force transducer (model 406A, Aurora Scientific, Canada) (Fig. 2.5 (2)). The glass probe was adjusted by hand to a parallel position with respect to the output tube. It was then fixed in place using super-glue. Parallel alignment of the glass probe was confirmed by drawing a square on the TV screen (Fig. 2.5 (11)) and by moving the probe downwards while ensuring the two vertical sides of the probe remained aligned within the square. Flattening of the glass probe was also confirmed in the same way.

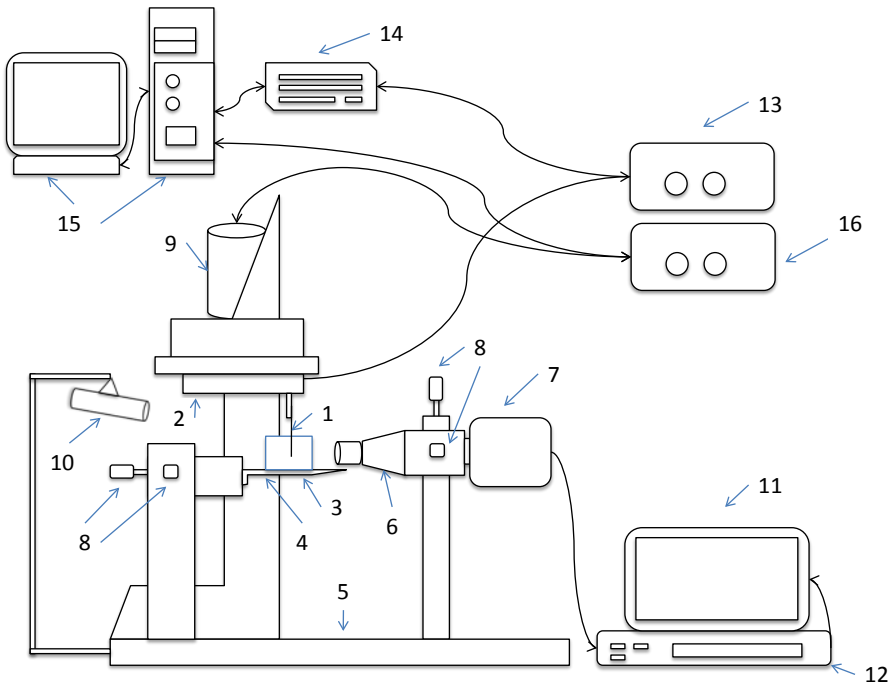

Figure 2.5. *Schematic diagram of Micromanipulation rig: (1) glass probe, (2) force transducer, (3) glass cell, (4) micromanipulator stage, (5) micromanipulator frame, (6) microscope, (7) camera, (8) manual plane adjusters, (9) stepper motor, (10) light source, (11) TV screen, (12) video, (13) transducer box, (14) data acquisition card, (15) user interface (PC), (16) stepper motor control box.*

Using a pipette, a drop of a dilute bead suspension was transferred in a glass cell (20 X 10 X 10 mm) (Fig. 2.5 (3)), resting on the micromanipulator stage (Fig. 2.5 (4)). The stage enabled the glass cell to move, through manual adjustment (Fig. 2.5 (8)), in two dimensions on the horizontal plane, thus allowing the positioning of individual agarose beads underneath the probe tip. The precise positioning of the probe directly above each particle was assisted by the horizontally mounted microscope (X 20 magnification) (Fig. 2.5 (6)). By adjusting the angle of the light source (Fig. 2.5 (10)) it was possible to produce a reflection of

the probe tip on the bottom of the glass cell, thus allowing the positioning of each particle in the centre of the ellipsoidal reflection (Fig. 2.6).

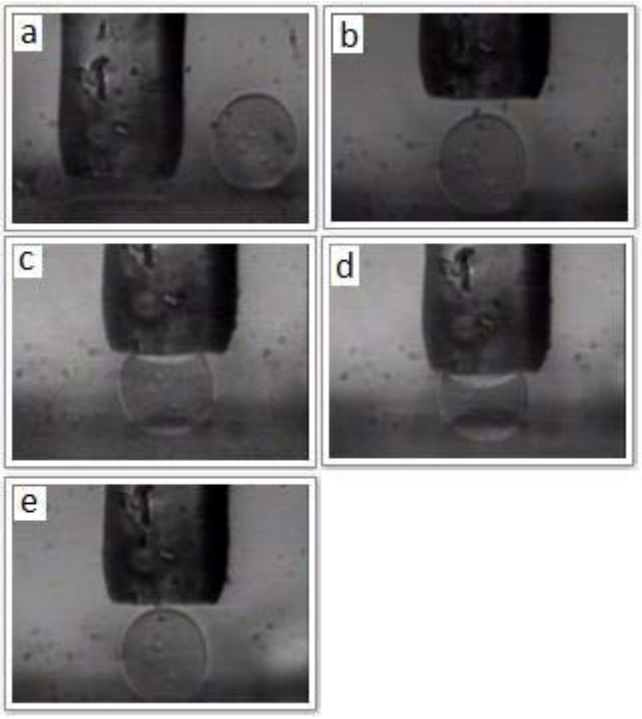

Figure 2.6. *Single particle compression at 30 % deformation: (a) probe-particle horizontal alignment, (b) probe-particle vertical alignment, (c) beginning of compression, (d) full compression, (e) decompression. Note: probe tip diameter 150 µm.*

As the density of particles is close to that of water, it was necessary to allow particles to settle for at least 10 mins prior to measurement. Particles were compressed for the determination of their mechanical properties in the following way:

From the video image, the size of a single particle was measured using a ruler superimposed on the screen. The glass probe was then lowered until it came in contact with the bottom of the glass cell. It was then raised to a known distance well above the diameter of the particle thus allowing the bead to be placed underneath the probe tip. The required

deformation (10 and 30 %) as well as the distance needed by the probe to travel in order to achieve this deformation, were calculated. The calibrated distance was then inserted in the micromanipulator software (in-house development) and particles were compressed by starting the stepper motor (Prior-Martock Ltd, UK) (Fig. 2.5 (9)) which drove the transducer at a pre-determined speed. The force transducer measured the force imposed on the probe tip which was recorded with a data acquisition card (model PC30F, Amplicon Liveline, UK) (Fig. 2.5 (14)) connected to a user interface (PC) (Fig. 2.5 (15)). Speed (20 µm s^{-1}) of the glass probe and data acquisition frequency (100 Hertz) was controlled by the micromanipulator software. At least ten particles were compressed from each sample in order to obtain statistically representative results.

2.5.2. Probe manufacturing:

A 350 µm in diameter glass rod was made by heating two pieces of glass until red hot and pulling them fast apart. From this rod, a length of about 30 mm was removed and mounted on the device (model PB -7, Narashige, Japan) shown in Fig. 2.7. The particular device consists of a top fixed end, a small heating coil and bottom mobile end, in vertical alignment. The glass rod is inserted from the top end and fixed (Fig. 2.7a). The coil heats up the rod (Fig. 2.7b) and seconds later the bottom mobile end free-falls, thus thinning the middle section of the rod to about 30 µm (Fig. 2.7c). At this point, by breaking this rod, two 15 mm glass probes with un-flattened ends were produced, ranging from 30 to 50 µm in diameter. Finally, the glass rod was mounted on a grinding apparatus (model EG-40, Narashige, Japan)

(Fig. 2.8) where it was flattened for about 120 mins producing a glass probe with a tip of 150 µm in diameter (Fig. 2.9).

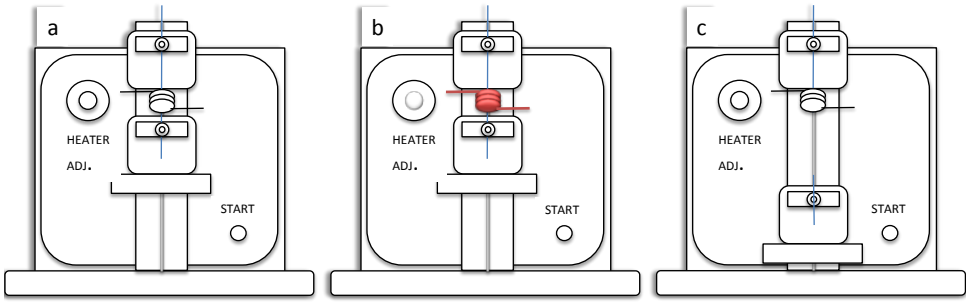

Figure 2.7. *Device for glass probe thinning: (a) probe positioning, (b) coil heat-up, (c) bottom end free-fall and probe thinning.*

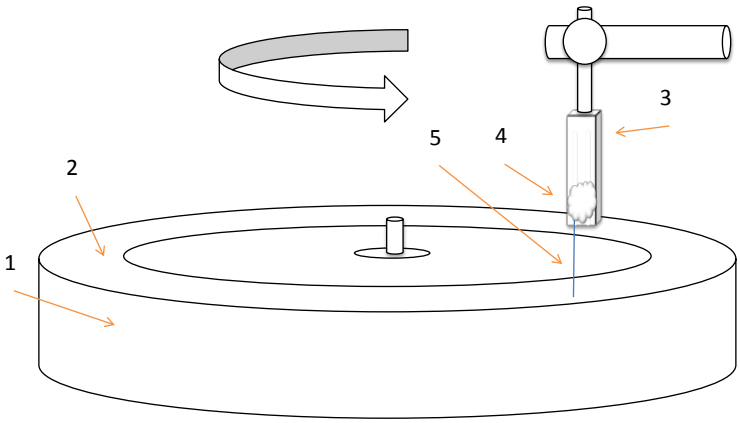

Figure 2.8. *Grinding apparatus: (1) rotating disc, (2) fine sand-paper, (3) capillary tube holder, (4) blu-tack, (5) glass probe.*

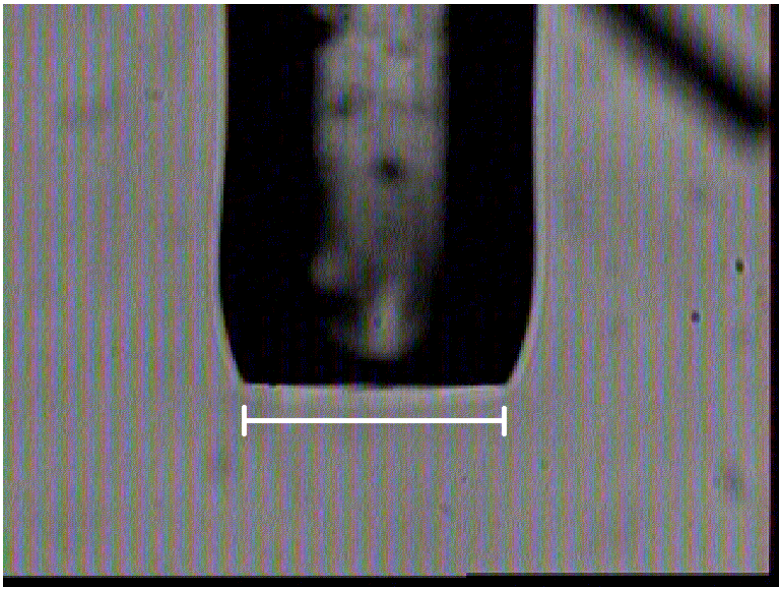

Figure 2.9. *Glass probe, scale bar: 150 µm.*

2.5.3. Screen and stepper motor calibration

A 100 µm graticule was placed on the micromanipulator stage while microscope magnification was fixed to X 20. As soon as the graticule ruler appeared on the TV screen the full length of the graticule lines was measured with the superimposed ruler, thus giving a calibration of 100 µm ≡ 62 mm. Stepper motor (software)-screen calibration was performed by instructing the micromanipulation probe to travel a distance of 100 µm while the superimposed ruler was fixed on the screen in a vertical position, thus giving a calibration of 100 µm ≡ 55 mm. Both calibrated values were used for determining the distance travelled by the probe in order to reach the required deformation (10 and 30 %) for each particle compressed. Stepper motor speed (Table 2.1) was determined by raising the probe to a distance of 300 µm and by measuring the time needed to cover this distance.

Table 2.1. *Stepper motor (probe speed) calibration.*

Measurement	Distance	Time	Speed
(-)	(μm)	(sec)	(μm/s)
1	300.00	13.65	19.49
2	300.00	13.10	20.31
3	300.00	13.00	20.47
4	300.00	13.10	20.31
5	300.00	12.80	20.79
Actual distance:	266.10		
Average:	266.10	13.13	20.27

2.5.4. Force transducer calibration

The 0.5 g transducer (maximum weight given by supplier) was calibrated in the following way (Table 2.2): five pieces of blu-tack of increasing size were separated and their weight was recorded. The transducer was then placed on a surface facing up-side down with the probe in a vertical position. Each pre-weighted piece of blu-tack was placed on top of the glass probe and the corresponding voltage tracer was recorded. Finally, the base-line voltage of the transducer (no weight) was also recorded. The above procedure yielded a six-point force vs. voltage graph that allowed the accurate calculation of the transducer sensitivity.

Table 2.2*. Force transducer calibration.*

Weight	Force	Voltage	Normalized voltage	Force
(g)	(mN)	(V)	(V)	(mN)
-	-	-0.46	-	-
0.0497	0.49	-1.33	0.87	0.49
0.1216	1.19	-2.56	2.10	1.19
0.2082	2.04	-4.11	3.65	2.04
0.3069	3.01	-6.24	5.78	3.01
0.4184	4.10	-9.10	8.63	4.10

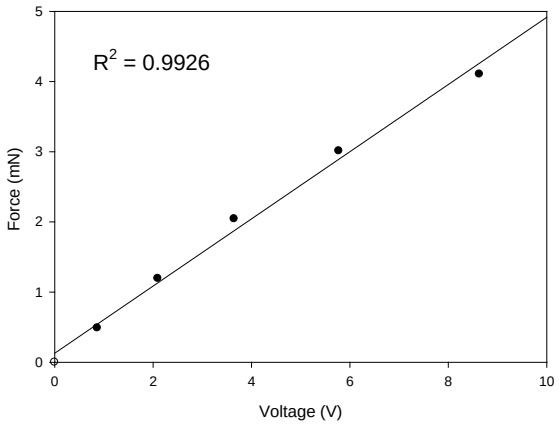

Figure 2.10. *Results and linear regression of transducer sensitivity.*

From the graph above:

$$slope\ m = \frac{y_2 - y_1}{x_2 - x_1} = 0.465\ \frac{mN}{V} \tag{2.2}$$

$$0.465\left(\frac{mN}{V}\right) \times g\left(\frac{m}{s^2}\right) = 0.0475\frac{g}{V} \tag{2.3}$$

where: g = gravitational acceleration (9.81 m s^{-2})

The calculated transducer sensitivity was in rather good agreement with the manufacturer's suggested value of 0.05 g V^{-1}. Slight changes in the sensitivity of the transducer are expected due to ageing and usage of the device.

2.5.5. Force transducer compliance

The force transducer operates by measuring cantilever beam deflection and then converts it to an electrical signal (Fig. 2.11). This deflection is known as compliance. Displacement, i.e. the distance travelled by the probe during compression, is calculated by multiplying the speed of the probe by the time taken for compression. This calculation though does not represent true displacement since it accounts for compliance as well. Therefore calculation of true displacement requires the determination of compliance and the subtraction of this value from the original value of displacement.

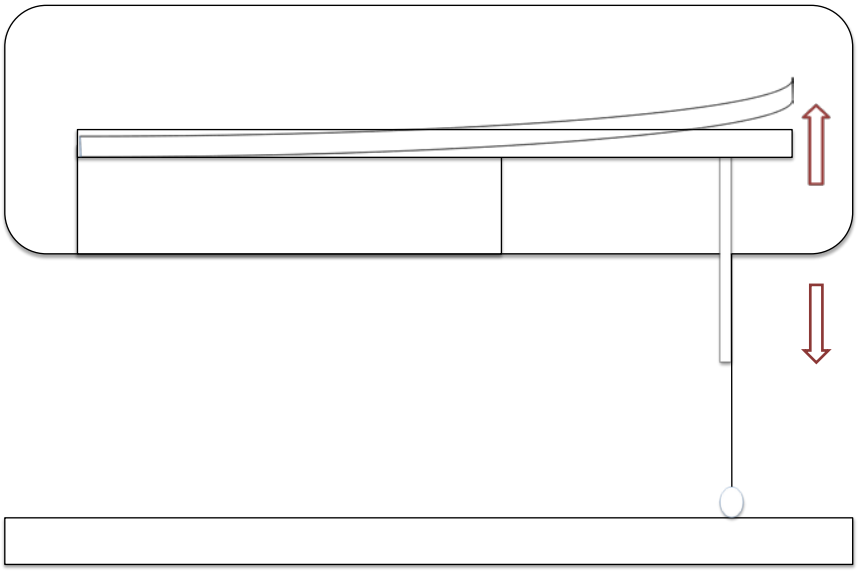

Figure 2.11. *Transducer compliance during compression. Downward arrow: transducer movement direction, upward arrow: compliance of cantilever beam.*

Compliance can be determined by pressing the glass probe against the bottom of the glass cell and recording the voltage-time trace of the probe (Table 2.3), (Fig. 2.12).

Table 2.3. *Compliance calculation results.*

Measurement	speed (μm/s)	slope	*	μm/V	Trans. sensitivity (mN/V)	Compliance μm/mN
1	20.27	-375.6	-37.56	-0.54	0.465	-1.1606
2	20.27	-542.7	-54.27	-0.374	0.465	-0.8032
3	20.27	-451.3	-45.13	-0.449	0.465	-0.9659
Average:						-0.9766

* *normalized by amplifier intensity (X 10)*

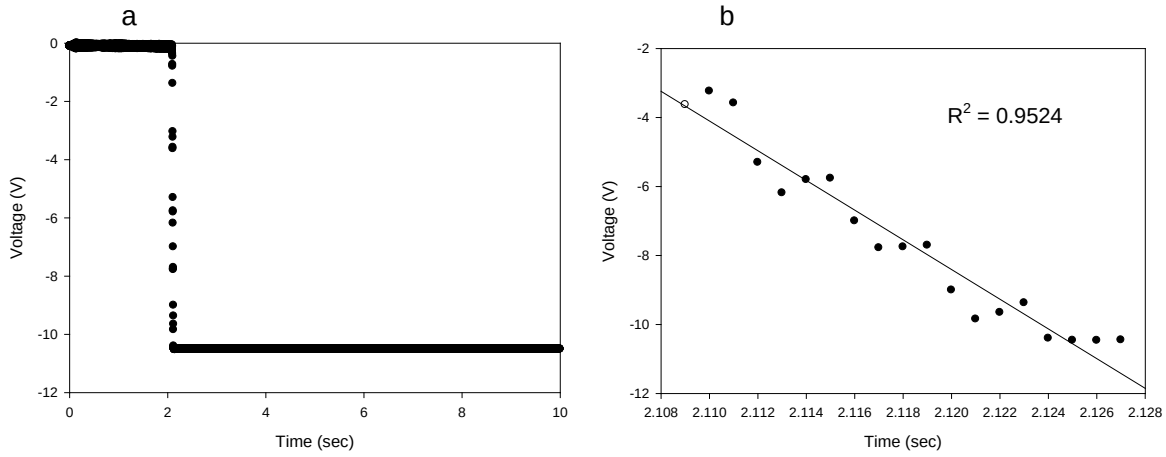

Figure 2.12. *Compliance calculation: (a) voltage-time tracer, (b) linear regression of vertical line of (a) (voltage-time tracer).*

From the linear regression graph in Fig. 2.12:

$$U\ (\mu m\ s^{-1}) \times \Delta t = D\ (\mu m) \quad (2.4)$$

$$D\ (\mu m) \div \Delta V = (\mu m\ V^{-1}) \quad (2.5)$$

$$(\mu m\ V^{-1}) \div S\ (mN\ V^{-1}) = C\ (\mu m\ mN^{-1}) \quad (2.6)$$

where U: probe speed ($\mu m\ s^{-1}$)

D: distance travelled by the probe (μm)

S: transducer sensitivity (mN V^{-1})

C: compliance (µm mN^{-1})

$\Delta t \div \Delta V$: slope (s V^{-1})

Therefore:

20.27 (µm s^{-1}) X 45.13 (s V^{-1}) = 0.449 (µm V^{-1}) (2.7)

0.449 (µm V^{-1}) ÷ 0.466 (mN V^{-1}) = 0.9642 (µm mN^{-1}) (2.8)

The above procedure was repeated three times and the final value of compliance obtained (C = 0.9766 (µm mV^{-1})) was in good agreement with the transducer's manufacturer suggested value (C = 1 (µm mV^{-1})).

2.5.6 Raw micromanipulation data interpretation

The pseudostress-displacement graphs were obtained from the raw micromanipulation data (voltage vs. time tracer) with the conversion of voltage (V) in to force (mN) by multiplying by the calibrated transducer sensitivity (mN V^{-1}). Total displacement of the probe was determined by multiplying the raw time data (sec) with the calibrated probe speed (µm s^{-1}) while subtracting the calculated compliance. Lastly, pseudo-stress (MPa) was determined by dividing the calculated force (N) data with the cross-sectional area (m^2) each particle thus eliminating the factor of particle size from the data obtained. Dimensionless deformation was determined by dividing the displacement of the probe (µm) from the moment it came in contact with the particle until the end of compression, with the particle diameter (µm). The

resulting curve for each sample is the total pseudostress of all particles divided by the number of particles compressed.

CHAPTER 3

-

MANUFACTURING AND MACROSCOPIC CHARACTERIZATION OF AGAROSE BEADS

3.1. Manufacturing and macroscopic characterization

The effect of surfactant concentration and type and energy dissipation rate on particle size / size distribution as well as process yield was investigated. Additionally, as ionic strength of the agarose solution and quenching temperature of the emulsion were used to control the pore structure of the adsorbent, the effect of these two process parameters on particle size was also investigated. Particle size / size distribution and process yield were determined with the Mastersizer 2000 (Malvern, UK) using refractive index values and conditions described in section *2.2.* The physical properties of the dispersed and continuous phase, such as flow curves, gelation temperature of agarose at different polymer concentrations, density and interfacial tension of agarose solution and oil were also determined, as described in *Chapter 2.*

In the manufacturing of chromatographic adsorbents, 'process yield' depends upon size specification and application, i.e. batches can be prepared for analytical or preparative applications. In analytical applications, small particle size and narrow size distributions will result in high resolution but high pressure drop and long processing times, whereas in preparative applications large particle size is desired for large throughput (Jungbauer 2005). Generally, the most popular intervals are: 20-50 μm, 20-90 μm, 50-150 μm and 250-350 μm, with the 50-150 μm interval being extensively used in preparative applications of affinity, ion

exchange and size exclusion chromatography (www.bioscience-beads.com, www1.gelifesciences.com). Since particles manufactured in this work are designated for industrial preparative applications, 'process yield' is considered the volume fraction of particles in the 50-150 μm interval. However, it should be noted that the purpose of the following experiments was not to identify the ideal process conditions (energy dissipation rate, surfactant concentration and type, ionic strength and quenching temperature) that result in the highest process yield, but rather to establish the effect of these parameters on the macroscopic properties of the resulting particles. For this reason, in the results presented below, process yield values do not always represent batches with the most desirable particle properties (average particle size / size distribution). For example, in the case of samples with Span 80 and Span 85, the latter is characterized by a size distribution with a standard deviation smaller than the former (40 μm for 0.1 % (v/v)) Span 85 over 100 μm for 0.1 % (v/v) Span 80) but also, based on the above 'process yield' definition, resulted in smaller process yield (42 % for 0.1 % (v/v) Span 85 over 46 % for 0.1 % (v/v) Span 80). Therefore the resulting yield values are not discussed but only indicated at the end of *Chapter 3* (see Table 3.3).

Furthermore it should be noted that the results below are based on experiments run in a Silverson high shear mixer operated in batch mode. A similar apparatus can be used in a continuous setup (see section *1.6*). Although the hydrodynamic conditions developed by the two setups are meant to be very similar, the issue of scaling-up, as well as moving from batch to continuous production, still remains.

3.1.1. Effect of surfactant concentration and type on particle size / size distribution

One of the initial objectives of this work was the manufacturing of agarose-based chromatographic adsorbents without the use of any surfactants. This is especially desirable for large scale production as the continuous phase (mineral oil), which is otherwise discharged as waste, can be reused (Millipore 2006). Preliminary experiments (results not presented) indicated that manufacturing without the use of surfactants using mechanical agitation is not feasible since the size distribution of the resulting particles was very wide (10-3000 μm), resulting in less than 5 % process yield, even at the highest energy dissipation rate (367 W kg^{-1}, 8000 rpm). Additionally, different emulsification screens as well as different ports of agarose injections into the oil were tested, but due to the instability of the system results were irreproducible and hence no conclusions could be drawn from those experiments.

To study the effect of surfactant concentration on the macroscopic properties of the adsorbent, oil-soluble non-ionic Span 85 (sorbitan trioleate, HLB value 1.8, molecular weight 975.51 g mol^{-1}) (Fig. 3.1a, c) was used at four different concentrations (0.1, 0.5, 1.0, 1.35 % (v/v)) (Fig. 3.2a). For examining the effect of hydrophobic tail group, oil-soluble non-ionic Span 80 (sorbitan monoleate, HLB value 4.3, molecular weight 446.62 g mol^{-1}) (Fig. 3.1b, d) was used at a concentration of 0.1 % (v/v) (Fig. 3.2b). Selecting oil-soluble surfactants ensures that a minimum amount of impurities will be present in the aqueous phase, thus a product of higher purity is obtained. Non-ionic surfactants have the advantage of electrical neutrality. Therefore they are less sensitive to the presence of electrolytes in the dispersed phase compared to ionic surfactants (Padron 2005, Giribabu and Ghosh 2007). Furthermore,

these surfactants are currently used by major manufacturers in the production of agarose-based chromatographic adsorbents (Millipore 2006) and therefore are FDA-approved.

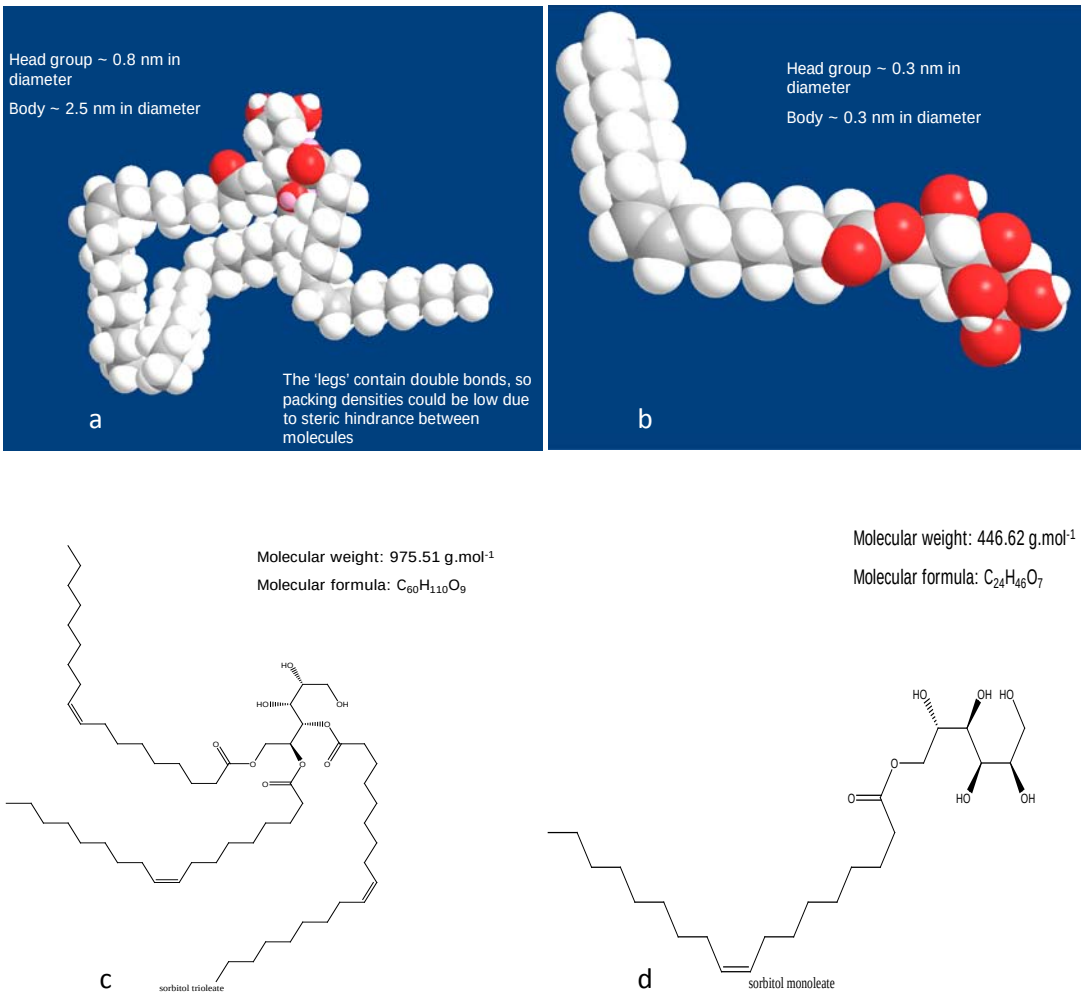

Figure 3.1. *(a) Span 85, (b) Span 80, (c) stereo-chemical structure of Span 85 and (d) Span 80, note: The dimensions and images of molecules where acquired using ChemDraw.*

Particles in the following experiments were manufactured as described in section *2.1.4*. In brief, an arbitrary energy dissipation rate (2.87 W kg^{-1}, 2000 rpm) was used in order to determine the effect of surfactant concentration of particle size / size distribution. The emulsions were quenched at 0° C. No salt was added in the agarose solution. At 0.1 % (v/v)

Span 85 (Fig. 3.2a) average particle size was reduced to 236 μm with a standard deviation of 225 μm and at 0.5 % (v/v) Span 85 particle size was reduced to 74 μm with a standard deviation of 116 μm. The corresponding values at 1.0 % (v/v) and 1.35 % (v/v) were 50 μm, 55 μm, and 50 μm standard deviation for both. D(0,1) at 0.1 % (v/v) was 37 μm while for the rest of concentrations (0.5, 1.0 and 1.35 % (v/v)) it remained constant between 22-23 μm. D(0,9) followed a decrease similar to that of D(0,5) while the decrease of D(3,2) was not as sensitive (Fig. 3.2c). As 2.87 W kg^{-1} (2000 rpm) is a relatively low value for a high shear mixer an energy dissipation rate experiment (results discussed later in this chapter) was carried out in order to take advantage of the high energy dissipation rate of the Silverson mixer while at the same time reducing the amount of surfactant added to the system. At 30.7 W kg^{-1} (3500 rpm) and 0.1 % (v/v) Span 85 average particle size /size distribution and process yield were very similar to 2.87 W kg^{-1} (2000 rpm) and 1.0 % (v/v) Span 85 conditions (Fig. 3.5a and Fig. 3.2a). The effect of surfactant hydrophobic tail group was then tested at 30.7 W kg^{-1} (3500 rpm) and 0.1 % (v/v) surfactant (Fig. 3.2b). The emulsion was quenched at the same temperature as before (0° C) and no salt was added to the agarose solution. 0.1 % (v/v) Span 85 reduced the particle size to 48 μm with 75 μm standard deviation while the respective values for the same concentration of Span 80 were 87 μm and 100 μm, characterized by pseudo-bimodal size distribution.

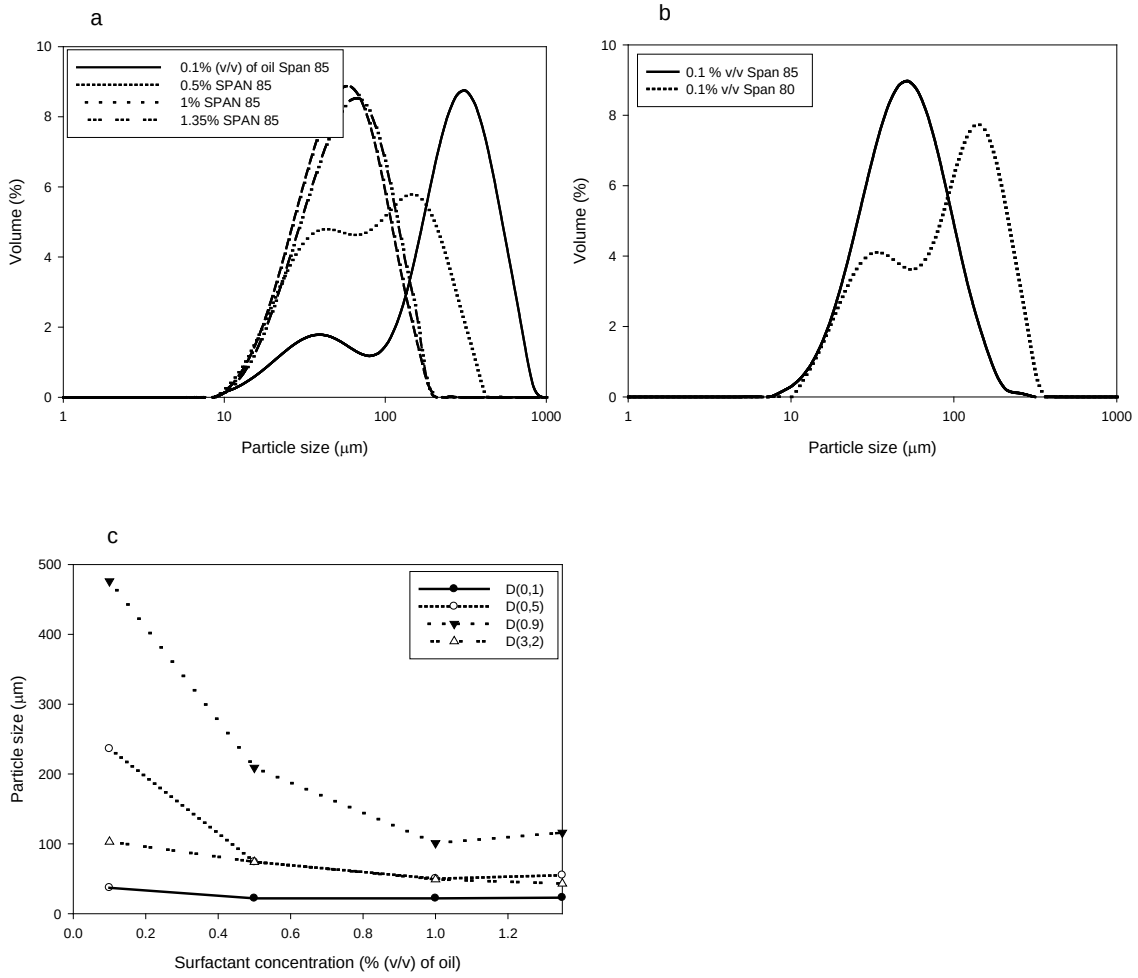

Figure 3.2. *Particle size distribution (a) for increasing concentration of Span 85 at 2.87 W kg^{-1} (2000 rpm), (b) for different types of surfactant Span 85 and Span 80, at 30.7 W Kg^{-1} (3500 rpm), (c) mean diameters for increasing concentration of Span 85.*

Results from increasing surfactant concentration in the continuous phase clearly show that the use of surfactants greatly contributes to the control of particle size / size distribution as well as dramatically increases process yield (see Table 3.3 for yield values). The lowest surfactant concentration used (0.1 % (v/v)) resulted in a rather broad pseudo-bimodal size distribution of particles (standard deviation 225 μm) characterized by a large peak in the range of 100-1000 μm and a smaller peak in the range of 10-100 μm. At

moderate surfactant concentration (0.5 % (v/v)) the standard deviation of the distribution reduced (115 μm), while the two peaks of the distribution tend to equate in size. At high surfactant concentrations (1.0 and 1.35 % (v/v)) the size distribution of particles significantly reduced (standard deviation 50 μm for both concentrations) while it is characterized by a mono-modal shape in the region of 10-100 μm. For a given energy dissipation rate and rotor speed the transition of the particle size distributions in Fig. 3.2a is directly related to the adsorption of surfactant molecules in the liquid-liquid interface of the dispersion.

The two fundamental processes occurring during emulsification are drop rupture and drop coalescence (Lobo and Svereika 2003, Vankova *et al.* 2007). These two processes occur concurrently and their relative rates determine the final drop size (Lobo and Svereika 2003, Vankova *et al.* 2007, Jafari *et al.* 2008) as well as the shape of the size distribution. Surfactants, once adsorbed on the liquid-liquid interface, affect both of these processes by (a) reducing the interfacial tension and interfacial energy, thereby promoting rupture, and (b) reducing coalescence via interactions between the adsorbed layers on two colliding drops (Opawale and Burgess 1998, Lobo and Svereika 2003). For ionic surfactants, the repulsive force is of double layer type, whereas for non-ionic surfactants, the repulsion is of entropic origin (i.e., steric repulsion) (Giribabu and Ghosh 2007).

There have been a number of attempts to try to understand drop break-up in the presence of surfactants. Lucassen-Reynders and Kuijpers (Lucessen-Reynders and Kuijpers 1992) concluded that at moderate surfactant concentrations interfacial viscoelasticity is important. The authors also accounted for the diffusional effects on the interfacial tension, in terms of the characteristic adsorption parameters of the surfactant. Leal *et al.,* (Stone *et*

al. 1990, Milliken *et al*. 1993, Milliken *et al.* 1994) developed drop break-up models in the presence of soluble and insoluble surfactants concluding that the shape of deformed drops depends on the type of surfactant used. Agterof *et al.* (Agterof *et al*. 1994) developed visual techniques to monitor rupture of single drops in the presence of surfactants under different flow fields. They concluded that the mode of rupture is determined by the shear rate and the surfactant concentration.

Recoalescence in the presence of surfactants has been studied to a lesser extent than drop breakage (Lobo *et al.* 2002). Taisne *et al.* (Taisne *et al*. 1996) developed a technique to measure recoalescence in O / W dispersions in a high-pressure homogenizer by preparing two different emulsions, one of which was brominated in order to alter its refractive index. The emulsions were then mixed and passed through the homogenizer. The extent of coalescence was measured by determining the refractive index of the resulting drops. Authors concluded that the extent of coalescence depends on the coverage of droplets by the surfactant molecules. A similar attempt to determine the extent that coalescence affects final drop size of O / W dispersions in rotor-stator systems and high pressure homogenizers was done by using a florescent probe (Lobo and Svereika 2003). Authors concluded that in stirred tanks coalescence can be arrested by the use of surfactants below saturation level, whereas increasing the volume of the dispersed phase at this surfactant level (or higher) does not affect drop size since coalescence rate is essentially zero.

In general, not all droplet collisions result in recoalescence. The continuous phase film between droplets should first drain, as drops approach each other (Mohan and Narsimhan 1997). Between new droplet formation and its subsequent encounter with surrounding

droplets, surfactants adsorb onto the newly created interface and prevent recoalescence. If the timescale of surfactant absorption is longer than the timescale of collision, the fresh interface will not be completely covered and leads to re-coalescence (Karbstein and Schubert 1995, Jafari *et al.* 2008) Based on the above as well as on the emulsification experiments without any surfactants (mentioned earlier) it is clear that recoalescence of droplets sets a fundamental limitation on the efficiency of the emulsification; it is pointless to apply high fragmentation power unless sufficient surfactant is present to counteract coalescence (Taisne *et al*. 1996).

During emulsification there is a maximum area that can be covered by the surfactant molecules. As emulsification proceeds, the surface area of the dispersed phase increases substantially. Below a certain particle size or a surfactant concentration there is not enough surfactant to fully cover the newly created interface of the dispersed phase and therefore droplets tend to coalesce (Jafari *et al.* 2008). The minimum particle size during emulsification is then determined by surfactant concentration and type (McClements 2005):

$$d_{min} = \frac{6\Gamma_{\text{sat}}\,\varphi}{C_s} \tag{3.1}$$

where d_{min}: minimum drop size

Γ_{sat}: surface excess concentration of surfactant at saturation

φ: dispersed phase volume

C_s: initial surfactant concentration in the emulsion

It has been shown experimentally (Narshimhan and Goel 2001, Lobo and Svereika 2003, Tcholakova *et al.* 2004) that two surfactant concentration regimes exist. In the surfactant-rich regime particle size is independent of surfactant concentration and depends on interfacial tension (which is surfactant-characteristic (Jafari et al., 2008)) and the energy dissipation rate (recoalescence probability of droplets is essentially zero (Vankova *et al.* 2007)). In the surfactant-poor regime particle size depends on the initial surfactant concentration C_s (Eq. 3.1).

Results presented in Fig. 3.2a suggest that at low and moderate surfactant concentrations (0.1 % and 0.5 % (v/v)) the liquid-liquid system is in the surfactant-poor regime since particle size / size distributions strongly depend on the initial concentration of Span 85. At these concentrations the shape transitions of the particle size distribution essentially reflects the binary mode of action of surfactants. At 0.1 % (v/v) Span 85, the large peak in the range of 100-1000 µm results from large unbroken particles due to high interfacial tension and from smaller particles that have collided, both due to the insufficient coverage by the surfactant molecules. The presence of a smaller peak in the range of 10-100 µm indicates that only a small portion of the distribution was produced and maintained at this size range therefore has had full coverage by the surfactant molecules. At 0.5 % (v/v) the two peaks tend to equate in size indicating greater coverage of agarose droplets by the surfactant and therefore smaller particle size. At high surfactant concentrations (1.0 and 1.35 % (v/v)) the two peaks have merged and the single peak in the range of 10-100 µm indicates further coverage of the entire population of particles with further reduction in particle size. For these concentrations, the liquid-liquid system appears to be in the surfactant-rich regime as particle size / size distributions do not appear to depend on the initial concentration of Span

85. In fact, the values of D(0,5) and D(0,9) for 1.35 % (v/v) Span 85 are of the order of 10 % and 15 % respectively higher compared to those for 1.0 % (v/v) Span 85. These concentrations are well above the critical micelle concentration of Span 85 which has been reported to be in the range of 0.1-0.2 % (v/v) (Ogawa *et al*. 1972, Opawale and Burgess 1998) although this range may be extended depending on temperature. At concentrations above c.m.c and saturation of the interface further deposition of surfactant may involve the adsorption of monomers and / or micelles as well as intermolecular interactions, molecular rearrangement and multilayer adsorption (Opawale and Burgess 1998) which has been found to result in increase of particle size (Jahanshahi 2003) and instability of emulsions (Gafonova and Yarranton 2001).

In order to determine the extent to which the surfactant concentrations provided surface coverage of droplets sufficient to prevent coalescence the surface coverage θ can be calculated from (Tcholakova *et al*. 2004):

$$\theta = \frac{\Gamma}{\Gamma_{sat}} \tag{3.2}$$

where θ*:* surface coverage

Γ: surface excess concentration of surfactant

Γ_{sat}: surface excess concentration of surfactant at saturation

For non-ionic surfactants, the Gibbs adsorption equation can be used to estimate (Γ) (Peltonen *et al*. 2001, Giribabu and Ghosh 2007):

$$\Gamma = -\frac{1}{RT}\frac{d\,\sigma}{d\,ln\,c} \tag{3.3}$$

where σ: interfacial tension

c: surfactant concentration in the bulk

R: gas constant

T: temperature

(Γ_{sat}) can be obtained by fitting σ vs. c curve.

Once the value of (Γ_{sat}) is obtained the minimum area occupied per molecule (A_{min}) can be calculated by:

$$A_{min} = \frac{1}{\Gamma_{sat}\,N} \tag{3.4}$$

where N: Avogadro's number

Since interfacial tension in this work has only been measured for one concentration of surfactant as well as for the surfactant-free system, values for (Γ) and (Γ_{sat}) cannot be obtained. Instead, a crude estimate of surfactant molecules potentially available for surface coverage of the emulsion droplets can be realized by comparing the specific surface area of the dispersion with the specific surface area of the surfactant (assuming monolayer arrangement). The specific surface area of the surfactant molecules per unit volume of dispersion, forming a mono-layer, at each concentration can be calculated if the dimensions of surfactant molecule are known (Fig. 3.1a-b, Table 3.1a). Since the oil-soluble surfactants used in this work are incorporated in a W / O emulsion, the specific surface area of the

hydrophilic head group should correspond to the specific surface area of the emulsion droplets at saturation and hence the dimensions of the hydrophilic head group should be used in surface area calculations. However, in the case of Span 85 (Fig 3.1a) the steric hindrance arising from the three double bonds in the fatty acid chains results in lower packing densities than that of Span 80, which only has one fatty acid chain (Ma *et al*. 2005). Therefore, for the calculation of the total specific surface area corresponding to the Span 85 concentrations used, the diameter of the hydrophobic tail group has been used. From the diameter of the hydrophobic head group the cross sectional area of the molecule can be estimated. The specific surface area of the emulsion droplets can be calculated if the Sauter mean diameter of the droplets is known. The Sauter mean diameter (obtained with the Masterisizer) is related to the specific surface area of the dispersed phase by (Gafonova and Yarranton 2001, Padron 2005):

$$d_{32} = \frac{6\varphi}{A_s} \tag{3.5}$$

where d_{32}: Sauter mean diameter

φ: volume fraction of dispersed phase

A_s: specific surface area of dispersed phase

Table 3.1a. *Surfactant molecular dimensions.*

Surfactant	**M_r**	**Density**	**Head diameter**	**Tail diameter**	**Area**
(type)	(g mol^{-1})	(g mL^{-1})	(m)	(m)	(m^2)
Span 85	975.51	0.956	8.00E-10	2.50E-09	4.91E-18
Span 80	446.62	0.986	3.00E-10	3.00E-10	7.07E-20
Note: Avogadro's no.	*6.022E+23*				

Table 3.1b*. Surfactant specific surface area.*

Surfactant (concentration and type)	**Volume** (mL)	**Mass** (g)	**Mass** (mol)	**Number of molecules** -	**Total area per concentration** (m^2)	**Specific surface area of surfactant** (m^2 / m^3)
0.1 % (v/v) Span 85	0.8	0.76	7.84E-04	5E+20	2.32E+03	**2.32E+06**
0.5 % (v/v) Span 85	4.0	3.82	3.92E-03	2E+21	1.16E+04	**1.16E+07**
1.0 % (v/v) Span 85	8.0	7.65	7.84E-03	5E+21	2.32E+04	**2.32E+07**
1.35 % (v/v) Span 85	10.8	10.32	1.06E-02	6E+21	3.13E+04	**3.13E+07**
0.1 % (v/v) Span 80	0.8	0.79	1.77E-03	1E+21	7.52E+01	**7.52E+04**

Table 3.1c*. Dispersed phase specific surface area.*

Sample -	**D(3,2)** (m)	**Volume fraction of dispersed phase** (-)	**Specific surface area of dispersed phase** A_s (m^2 / m^3)
2000 rpm 0.1 % (v/v) Span 85	1.03E-04	0.2	**1.165E+04**
2000 rpm 0.5 %(v/v) Span 85	4.90E-05	0.2	**2.449E+04**
2000 rpm 1.0 % (v/v) Span 85	4.00E-05	0.2	**3.000E+04**
2000 rpm 1.35 % (v/v) Span 85	4.40E-05	0.2	**2.727E+04**
3500 rpm 0.1 % (v/v) Span 85	3.70E-05	0.2	**3.243E+04**
3500 rpm 0.1 % (v/v) Span 80	5.20E-05	0.2	**2.308E+04**

Tables 3.1a-c show the results of the specific surface area calculations of surfactant and emulsion droplets, as well as the dimensions of the two surfactant molecules used. As can be seen in Table 3.1b, the specific surface area of 0.1 % (v/v) Span 85 is of the order of 10^6 (m^2 / m^3) whereas for the rest of concentrations of Span 85 the specific surface area is of the order of 10^7 (m^2 / m^3). The corresponding droplet specific surface areas of all the resulting emulsions using Span 85 are of the order of 10^4 (m^2 / m^3). These differences indicate that each surfactant concentration could potentially provide around 2-3 orders of magnitude more surface coverage (assuming monolayer adsorption) than the actual surface area of the corresponding resulting emulsions. On the other hand, results presented in Fig. 3.2a clearly show that the resulting particle size strongly depends on the initial surfactant concentration, suggesting that the surface of the agarose droplets was not saturated by surfactant molecules until the 1.0 % (v/v) Span 85 concentration where a cessation in particle size reduction was observed (C.m.c of a surfactant solution can be determined from the concentration of surfactant at which the value of interfacial tension 'levels-out' (Opawale and Burgess 1998). Since c.m.c is observed at or above interface saturation with cessation of the reduction in interfacial tension the same can be argued for emulsification and particle size. A cessation in the reduction of particles size with increasing concentration of surfactant indicates constant interfacial tension therefore interface saturation and c.m.c). The difference between the specific surface area of surfactant molecules potentially available for droplet coverage and the specific surface area of the resulting droplets suggests that most of the surfactant introduced in the system was not utilized for surface coverage of the emulsion droplets. This can be explained by considering the change in solubility of surfactants with temperature in combination with the relative high temperature of the

process (90° C). As temperature increases the solubility of the oil-soluble non-ionic surfactant reduces due to the breakdown of non-polar interactions between the hydrophobic part of the surfactant and the hydrocarbon chains of the oil (Overbeek *et al*. 1984, van Os 1997), undergoing an apparent increase in its HLB value (Shinoda and Kunieda 1986) and favouring micelle conformation and aggregation (Zana and Kaler 2007). This continues until a certain temperature is reached where the surfactant separates from the solvent, creating a finely dispersed phase which turns the solution cloudy (van Os 1997, Padron 2005). This temperature is known as the cloud point. The latter can be determined by slowly heating a solution of surfactant and recording the temperature at which the solution turns cloudy. After heating, the solution is slowly cooled and the temperature where the solution becomes clear is recorded. The average of the two temperatures is the cloud point of the particular surfactant (Sulthana *et al*. 1996).

Hence, based on the specific surface area calculations presented in Tables 3.1a-c, although relatively high concentrations of surfactant (≥ c.m.c) have been introduced into the continuous phase, only a small portion of the former has been utilized (monomer adsorption) for surface coverage of the resulting droplets while the rest of the surfactant is in the form of micelles, or otherwise 'oiled-out', due to the high temperature of emulsification. Therefore, micelles are present in the system before surface saturation, instead of the opposite. Theoretically, for a given energy dissipation rate, the same particle size / size distribution could be achieved using a smaller quantity of surfactant at a lower emulsification temperature, well below the cloud point of the surfactant, but practically this is clearly restricted by the gelling temperature of the agarose solution.

As previously mentioned, one of the initial objectives of this work was the production of agarose-based chromatographic adsorbents without using surfactants with the ultimate scope of recycling the continuous phase which is otherwise discharged as waste. Preliminary experiments suggested that this is practically impossible since the resulting particle size distribution was very wide leading to less than 5 % process yield.

The oil-phase is discharged because after emulsification an unknown amount of surfactant has been removed from the system along with the gelled agarose phase. Therefore emulsification using the same oil cannot be done since the resulting particle size / size distribution will progressively become larger with every recycling of the oil due to the cumulative reduction in surfactant concentration.

One way of overcoming this can be realized by determining the equilibrium concentration of the surfactant in the oil phase after emulsification and subsequently adding the 'missing' amount of surfactant in the continuous phase. This can be achieved by exploiting a specific physical property of the surfactant and the continuous phase, such as boiling point. Besides the surface coverage ϑ, the surfactant mass surface coverage can be determined, which is the total mass of the surfactant adsorbed in the interface divided by the total area of the dispersed phase (Gafonova and Yarranton 2001).

$$\Gamma_s = \frac{m_{s,i}}{A_d} = \frac{m_{s,i} d_{32}}{6 V_d} \tag{3.6}$$

where Γ_s: surfactant mass surface coverage

$m_{s,i}$: mass of surfactant adsorbed in the interface

Since the surfactant used in this work is soluble in the continuous phase, $m_{s,i}$ can be determined from the change of surfactant concentration in the continuous phase upon emulsification.

$$m_{s,i} = m_{s,t}\left(1 - \frac{C_A^{eq}}{C_A^0}\right) \tag{3.7}$$

where $m_{s,t}$: total mass of surfactant in the emulsion

C_A^0: initial concentration of surfactant in continuous phase prior emulsification

C_A^{eq}: equilibrium concentration of surfactant in the continuous phase after emulsification

Substituting Eq. (3.6) into Eq. (3.7) gives an expression for surfactant mass surface coverage in terms of measurable quantities.

$$\Gamma_s = \frac{m_{s,i} d_{32}}{6V_d}\left(1 - \frac{C_A^{eq}}{C_A^0}\right) \tag{3.8}$$

The above method of calculating surface coverage, via the estimation of the surfactant equilibrium concentration in the continuous phase after emulsification, was used by Gafonova and Yarranton (Gafonova and Yarranton 2001) with asphaltenes as surfactant and a mixture of toluene / heptane as the continuous phase. The authors estimated the equilibrium concentration of asphaltenes by evaporating a known volume of the continuous phase in a rotary evaporator and by weighing the residual asphaltenes reporting more than 95 % accuracy in their measurements. Considering the boiling points of Span 85 and mineral

oil (around 100° C and 210-640° C respectively) the same method could be exploited for the industrial manufacturing of agarose beads without having to discharge the continuous phase after every batch.

The equilibrium concentration of surfactant in the continuous phase can also be obtained from the relationship between concentration and equilibrium surface tension. Using an adsorption isotherm as a surface tension / concentration calibration curve, the concentration of a given surfactant solution can be evaluated by measuring its equilibrium surface tension (Padron 2005).

Clearly, although the above methods can prove to be fairly accurate in determining the surfactant equilibrium concentration in the continuous phase, the issue of cumulative error sill remains. Therefore repeated measurements may be needed over the span of certain number of batches.

Results of varying the surfactant hydrophobic tail group show that Span 85 is more efficient in producing small particles with a narrow single-modal size distribution than Span 80, when used at the same volumetric concentration (Fig. 3.2b). Since the hydrophilic head group of both molecules is very similar (Ma *et al*. 2005) (the production of Span 80 and 85 involves the esterification of 1.4-sorbitan, with one and three oleic acids respectively (Tadros 2005)), the difference in results clearly originates from the different structure of the hydrophobic tail group. It has being shown experimentally (Opawale and Burgess 1998) that Span 80 reduces the interfacial tension of oil/water interfaces to a larger magnitude than Span 85, at room temperature. This was explained by the fact that Span 85 has three fatty acid groups and a higher solubility in oil (lower HLB value) that essentially hinders interfacial

adsorption and molecular interaction. For the same reason, Span 80 was found to have high interfacial viscoelasticity compared to Span 85 that had exhibited very low interfacial elasticity. Consequently, Span 80 tended to form stronger interfacial films that resulted in long term stability of W / O emulsions. However, as previously mentioned, with an increase in temperature, the solubility of non-ionic oil-soluble surfactants reduces due to the interruption of the non polar interactions of the fatty acid chains with the hydrocarbon coils of the oil phase. This reduction in solubility favours micelle aggregation in the bulk before the interface of the emulsion is saturated. Considering again the structural differences of the two molecules, for the same temperature increase, a larger portion of Span 80 will adopt micelle conformation and subsequently phase separate compared to Span 85. This is because the amount of energy in the form of heat required for the breakdown of the non-polar interactions of one fatty acid chain will be less compared to the amount required for the three fatty acid chains of the Span 85. This behaviour is also reflected in the HLB value of the two surfactants. The more hydrophilic Span 80 (HLB value 4.3) will become even more hydrophilic for the same increase in temperature when compared to Span 85 (HLB value 1.8). Additionally from the specific surface area calculations in Tables 3.1b-c it can be seen that for the same volumetric concentration of the two surfactants, the specific surface area obtained from 0.1 % (v/v) Span 80 is of the same order as the specific surface of the resulting droplets (10^4 m^2 / m^3), whereas the respective specific surface area of Span 85 is 2 orders of magnitude larger than the resulting specific surface area of the agarose droplets, owing to the larger cross-sectional area of the sorbitan trioleate molecule. This indicates that in an ideal situation were molecules where arranged side by side to form a two-dimensional lattice, the total area of the lattice formed by Span 85 would be 2 orders of magnitude larger

than one formed by Span 80. In practice, where it was previously shown (see above: *Effect of surfactant concentration*) that 0.1 % (v/v) surfactant is well below surface saturation, this means that the surfactant layer formed on the agarose droplets by Span 80 will be less dense than of that of Span 85 (larger A_{min} for Span 80 in Eq. 3.4) (Ma *et al*. 2005), thus providing an smaller barrier to coalescence of droplets. The latter, in combination with the larger extend of micellization of the Span 80 due to the high temperature of emulsification, indicates that the surface coverage at 90° C will be more effective for Span 85 (smaller A_{min} for Span 85 in Eq. 3.4), therefore explain the ability to produce smaller particles, characterized by single-modal size distribution, than Span 80.

3.1.2. Effect of ionic strength of dispersed phase on particle size / size distribution

As the ionic strength of the agarose solution was used for controlling the pore size/ size distribution of the adsorbent, its effect on particle size/ size distribution was investigated in order to establish its impact on the macroscopic properties of the agarose beads. Salt was added at various concentrations (0, 0.01, 0.025, 0.05, 0.1 m NaCl) in the agarose solution preparation stage. The solution was then emulsified at 30.7 W Kg^{-1} (3500 rpm) with 0.1 % (v/v) Span 85 added to the oil phase. The emulsion was quenched at 0° C. Increasing the ionic strength of the agarose solution does not appear to have a significant effect on the resulting median diameters of the particles except on D(0,9) which in turn affects the standard deviation of the resulting distributions. D(0,1) remain constant between 19-21 μm, D(0,5) between 42-48 μm, and D(0,9) and D(3,2) between 83-106 μm and 37-39 μm

respectively. Standard deviation of the particle size distribution was 40 μm for 0 m, 50 μm for 0.01 m, 45 μm for 0.025 m, 75 μm for 0.05 m and 40 μm for 0.1 m (Fig. 3.3a-b).

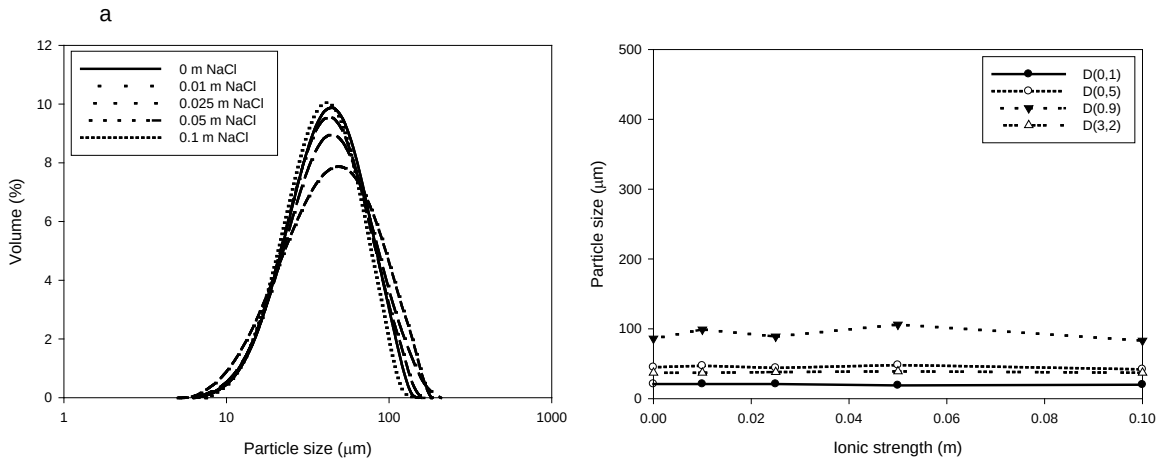

Figure 3.3. *Effect of ionic strength of agarose solution on (a) particle size distribution and (b) median diameter.*

Results from increasing the ionic strength of the agarose solution do not exhibit any specific trend, in particular all median diameters appear to remain constant with small deviation except D(0,9) which seems to fluctuate between 83-106 μm, again without following any particular trend.

It is well known that the addition of an electrolyte to the aqueous phase of surfactant-free W / O emulsions promotes instability and recoalescence through diminishing the electrostatic repulsion between droplets (Taisne *et al*. 1997). Additionally it has been shown experimentally (Taisne *et al.* 1997, Lobo and Svereika 2003) that this effect is suppressed by the presence of anionic surfactants at moderate or high concentrations due to the electrostatic repulsions arising from the adsorbed surfactant layer. It has also been shown (Opawale and Burgess 1998) that high salt concentrations (0.1-1 M) affect the stability of W

/ O emulsion containing low concentrations of non-ionic Span 80. This was explained by considering the preferential hydration of Na^+ and Cl^- ions over the surfactant molecules leading to the 'salting-out' of the hydrophilic head group of the surfactant from the water phase. Generally, the addition of an electrolyte in the aqueous phase of W / O emulsions, containing oil-soluble, non-ionic surfactants, works in the same direction as increasing the emulsification temperature (Overbeek *et al*. 1984).

With moderate concentration (0.1 % (v/v)) of surfactant been used, the ionic strength (0-0.1 m) was not high enough to affect the interfacial properties of the former, although no explanation can be given for the fluctuation of D(0,9). Consequently, although some degree of salting out of the hydrophilic head may be occurring, the concentration of surfactant on the interface remains sufficient to prevent recoalescence of drops. However it is possible that if higher ionic strengths were to be used (0.1-1 m) in the agarose solution in combination with very low surfactant concentrations (0.001-0.01 % (v/v)) and high energy dissipation rates (367 W kg^{-1}, 8000 rpm), this effect may become very obvious on the resulting particle size / size distributions, therefore adjustment of process conditions (surfactant concentration and rotational speed) may be needed to reproduce particle size / size distribution.

3.1.3. Effect of quenching temperature of the emulsion on particle size / size distribution

Since quenching temperature of the emulsion was also used to control the pore size /size distribution of the agarose gel, its effect on the resulting particle size / size distribution was examined. Agarose was emulsified at 30.7 W kg^{-1} (3500 rpm) using 0.1 % (v/v) Span 80 and no salt. Emulsions were then quenched by discharging the hot emulsion into a large volume of cold mineral oil at 0, 10 and 20° C.

Decreasing the quenching temperature of the emulsion appears to have practically no effect on the mean diameters (Fig. 3.4b) of the samples as well as on the particle size distributions (Fig. 3.4a). Average particle size (D(0,5)) was between 85-90 µm, D(0,1) was between 22-23 µm, D(0,9) between 191-192 µm and D(3,2) between 52-54 µm for all three quenching temperatures. Similarly unaffected, the standard deviation of the particle size distributions was 100 µm at all quenching temperatures.

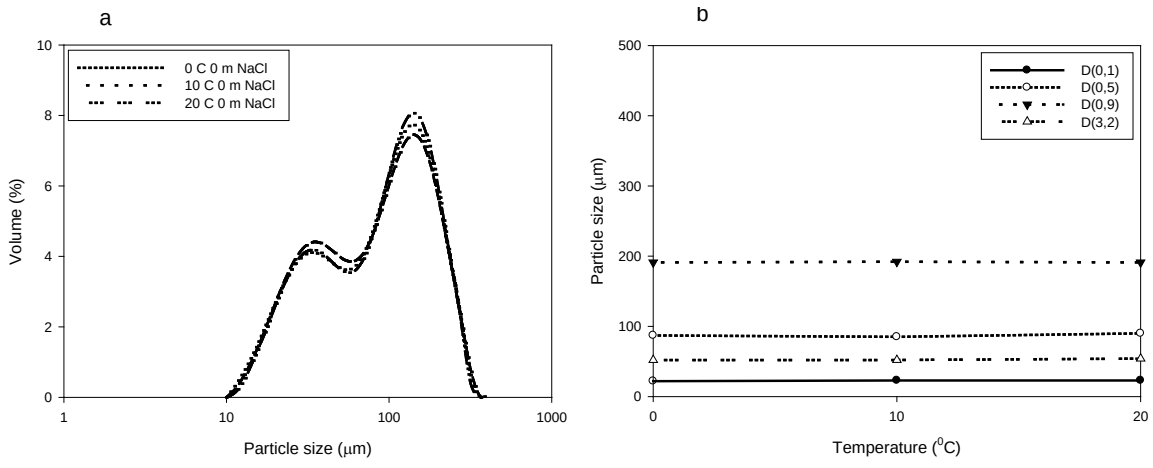

Figure 3.4. *Effect of quenching temperature on (a) particle size distribution (b) mean diameters.*

By increasing the quenching temperature of the emulsion (slower cooling), the time needed for the agarose droplets to reach gelation temperature is also increased. One could argue that increasing the particular time interval increases recoalescence probability of the liquid agarose droplets, especially in the absence or low concentrations of surface active agents. Since surfactants are present in the system, the complete absence of any effect of the quenching temperature on the resulting properties of the adsorbent can be attributed to the prevention of recoalescence by the surfactant molecules.

3.1.4. Effect of impeller speed and energy dissipation rate on particle size / size distribution

The effect of impeller speed and energy dissipation rate on particle size / size distribution was investigated at two different speeds (Fig. 3.5a-b). Particles were emulsified at 2.87 W Kg $^{-1}$ (2000 rpm) and 30.7 W kg^{-1} (3500 rpm) with 0.1 % (v/v) Span 85 and without salt (0 m NaCl). Rest of processing conditions was as before. At 2.87 W kg $^{-1}$ (2000 rpm), D(0,1) was 37 μm, D(0,5) 236 μm D(0,9) 476 μm and D(3,2) 103 μm. The respective values for 30.7 W kg^{-1} (3500 rpm) were 21, 45, 86 and 37 μm. The standard deviation of the particle size distributions was 225 μm for 2.87 W kg $^{-1}$ (2000 rpm) and 40 μm for 30.7 W kg^{-1} (3500 rpm).

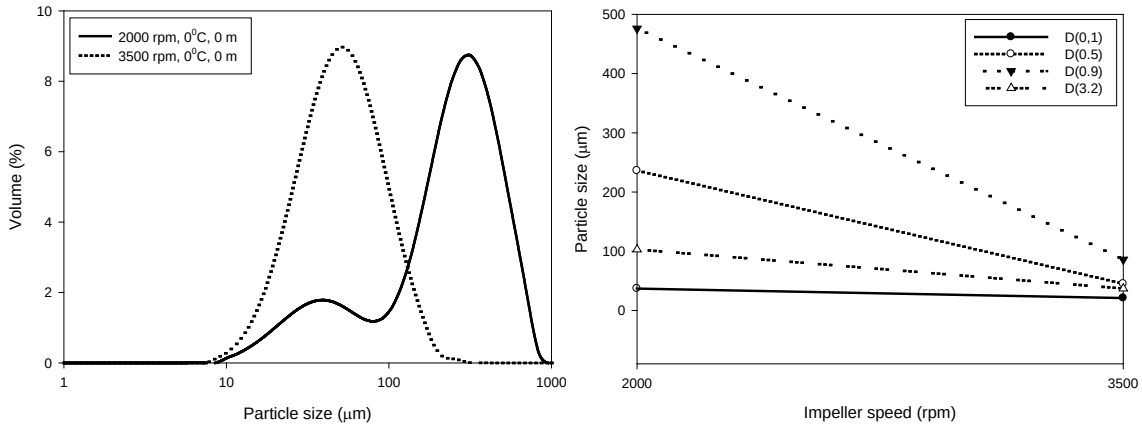

Figure 3.5*. Effect of impeller speed on (a) particle size distribution and (b) median diameter.*

Results presented in Fig. 3.5a clearly show that increasing impeller speed and energy dissipation rate has a pronounced effect on particle size / size distribution of the emulsion. During emulsification droplets are disrupted when the capillary pressure (p_c) is exceeded locally by the deforming stress (σ) ($\sigma > p_c$) and the deformation time (t_{br}) exceeds a critical breakage time ($t_{br,\,cr}$) ($t_{br} > t_{br,\,cr}$) (Walstra 1993, Karbstein and Schubert 1995).

In laminar flow the predominant deforming stress is the shear stress (τ). The ratio between shear stress and capillary pressure is given by the Weber number (*We*) and it essentially expresses the ratio of deforming to restoring forces of the droplet (Peters 1992):

$$We_l = \frac{\mu_c \, \dot{\gamma} \, d_{max}}{\sigma} \tag{3.9}$$

where μ_c: the viscosity of the continuous phase

γ: shear rate

d_{max}: maximum droplet diameter

σ: interfacial tension

Drops are deformed in laminar flow when the Weber number exceeds a critical value, (We_{cr}), which is a function of the viscosity ratio (λ) of the dispersed and continuous phase (Janssen *et al.* 1994). For simple shear flow the critical Weber number is minimal for $0.1 < \lambda < 1$ and increases rapidly for $\lambda > 5$. For this reason it is difficult to produce emulsions of high viscosity ratio in emulsification devices with simple shear flow in the dispersing zone (Karbstein and Schubert 1995).

In turbulent flow, two different regimes exist. In the inertial sub-range, drops are larger in size than the smallest turbulent eddies, whereas in the turbulent viscous regime drop size is smaller than the size of the smallest eddies. In the inertial sub-range, the maximum diameter of the stable drops is determined by the balance between the fluctuations of hydrodynamic pressure of the continuous phase, and the drop capillary pressure, which resists drop deformation. In the viscous sub-range, the maximum diameter of the stable drops is determined by the balance between the viscous stresses of the continuous phase acting on the drop surface and the capillary pressure of the drop (Vankova *et al*. 2007).

For turbulent flows the Weber number becomes (Karbstein and Schubert 1995):

$$We_t = \frac{C\,\rho_c^{1/3}\,d^{2/3}\,\varepsilon^{2/3}}{4\sigma/d} \tag{3.10}$$

where *C:* constant

ρ_c: density of continuous phase

d: droplet diameter

ε: energy dissipation rate (energy input per unit mass)

Power draw (Padron 2001, Meyrs *et al*. 2001, Doucet *et al*. 2005) and drop break-up (Calabrese *et al*. 2000, Padron 2005) in high-shear mixers has being studied to certain extent. Padron (Padron 2001) introduced several definitions of Reynolds number when constructing power curves. The first one is the commonly used definition for stirred tanks:

$$Re = \frac{\rho_c \, N \, D^2}{\mu_c} \tag{3.11}$$

where ρ_c: density of the continuous phase

N: rotational speed

D: impeller diameter

μ_c: viscosity of the continuous phase

The second definition introduces the rotor-stator gap width and the tip speed because the energy dissipation in the gap could be related to the planar shear (Doucet *et al*. 2005):

$$Re = \frac{\rho_c \, V_{tip} \, \delta_{gap}}{\mu_c} \tag{3.12}$$

where V_{tip}: tip speed

δ_{gap}: rotor stator gap width

A third definition was proposed, which uses for the characteristic length the hydraulic radius of the stator defined as the area of the slot over its wetted perimeter:

$$Re = \frac{4 \, \rho_c V_{tip} \, R_h}{\mu_c} \tag{3.13}$$

where R_h: characteristic length of hydraulic radius

Padron (Padron 2001) and Calabrese *et al.* (Calabrese *et al*. 2000) concluded that the main source of energy dissipation is not the viscous shear developed in the rotor-stator gap but rather the break-up of drops occurs due to the inertial sub-range eddies of the turbulent jets or the viscous stresses in the viscous sub-range, therefore suggesting that Reynolds number should be used in its classical form (Eq. 3.11). The same observation about the turbulent jets was reported by Pacek *et al*. (Pacek *et al.* 2008) where, with the aid of CFD, flow patterns produced in the rotor-stator assembly where visualized. Using the former, the same group investigated the effect of the stator geometry concluding that narrower holes on the stator can be correlated with narrower resulting particle size distributions (Utomo *et al.* 2009).

Table 3.2*. Reynolds number, Power number and energy dissipation rate at two impeller speeds.*

speed (rpm)	N (rps)	Re	Po	ε_t (Wkg^{-1})
2000	33.3	5450	0.9	2.87
3500	58.3	9500	1.8	30.7

Note: Power numbers are from Padron (Padron 2001)

In this set of experiments, flow was in the transitional regime (Table 3.2) and the information on drop break-up in this regime is very limited (Mu *et al*. 2005), especially in the presence of surfactants. Therefore the prediction and correlation of drop sizes is somewhat difficult in this case.

The shape of the curves in Fig. 3.5a indicates the relative rates of drop breakage and drop coalescence. In section *3.1.1* where the effect of surfactant concentration on particle size / size distribution was examined, the shape of the curves in Fig. 3.2a indicated that with increasing concentration of surfactant the breakage rate of droplets increases while coalescence rate reduces, with both processes being related to the adsorption of surfactant molecules in the liquid-liquid interface. In this experiment, where the surfactant concentration was the same in both samples, particles size reduces with increasing rotor speed and energy dissipation rate. This indicates that at 30.7 W kg^{-1} (3500 rpm) the rate of drop breakage is clearly increased due to the increased energy dissipation rate, compared to 2.87 W kg^{-1} (2000 rpm), while coalescence in the system is either the same or negligible due to the increase in the surface area of the emulsion with impeller speed (In Table 3.1c the specific surface area of the sample emulsified at 30.7 W kg^{-1} (3500 rpm) sample is approximately 2.8 times the specific surface area of the 2.87 W kg^{-1} (2000 rpm) sample).

***Table 3.3**. Summary results from emulsification experiments.*

Speed	Surfactant		Ionic strength	T	D(0,1)	D(0,5)	D(0,9)	D(3,2)	D(3,2) / D(0,9)	S.D.	Yield
(rpm)	(% (v/v))	(type)	(m)	(°C)	(μm)	(μm)	(μm)	(μm)		(μm)	(%)
2000	0.1	S 85	-	0.0	37	**236**	476	**103**	0.22	**225**	**15**
2000	0.5	S 85	-	0.0	22	**74**	209	**74**	0.35	**115**	**40**
2000	1.0	S 85	-	0.0	22	**50**	101	**49**	0.49	**50**	**50**
2000	1.35	S 85	-	0.0	23	**55**	116	**43**	0.37	**50**	**50**
3500	0.1	S 85	-	0.0	21	**45**	86	**37**	0.43	**40**	**42**
3500	0.1	S 85	0.01	0.0	21	**47**	99	**37**	0.37	**50**	**43**
3500	0.1	S 85	0.025	0.0	21	**44**	89	**38**	0.43	**45**	**41**
3500	0.1	S 85	0.05	0.0	19	**48**	106	**39**	0.37	**75**	**45**
3500	0.1	S 85	0.1	0.0	20	**42**	83	**37**	0.45	**40**	**36**
3500	0.1	S 80	-	0.0	22	**87**	191	**52**	0.27	**100**	**46**
3500	0.1	S 80	-	10.0	23	**85**	192	**52**	0.27	**100**	**45**
3500	0.1	S 80	-	20.0	23	**90**	191	**54**	0.28	**100**	**47**

3.2. Physical properties of agarose solution and mineral oil

The physical, rheological and interfacial properties of agarose solution and mineral oil were determined as described in *Chapter 2*.

3.2.1. Density of agarose solution and mineral oil

***Table 3.4.** Density measurements of agarose solution and mineral oil.*

Material	T	Conc.	Bottle + mass	Mass	Density	Density
	(°C)	(% w/w)	(g)	(g)	(g mL^{-1})	(kg m^{-3})
Mineral oil	20.0	-	43.3	21.4	0.9	**856.8**
	90.0-95.0	-	42.1	20.3	0.8	**812.3**
Agarose solution	90.0-95.0	3.0	46.9	25.0	1.0	**1001.2**
		4.0	46.9	25.1	1.0	**1003.9**
		5.0	47.0	25.2	1.0	**1008.1**
		6.0	47.1	25.3	1.0	**1011.7**
Bottle weight (g)	21.8					
Bottle volume (mL)	25.0					

3.2.2. Interfacial tension of agarose solution and mineral oil

The interfacial tension was determined for the following systems using the pendant drop method as described in section *2.3.2*: agarose / oil, agarose oil / surfactant and agarose / oil / surfactant / salt. Experiments were performed in duplicate. Table 3.5 shows the results of the interfacial tension of said systems.

Table 3.5*. Interfacial tension measurements.*

System	**Surfactant concentration**	**Ionic strength**	**Interfacial tension**
-	(% (v/v))	(m)	(N/m)
w / o	-	-	**6.3E-02**
w / o / s	0.1	-	**7.0E-04**
w /o / s / s	0.1	0.05	**7.8E-04**

3.2.3. Rheological properties of agarose solution mineral oil

3.2.3.1. Gelation temperature of 3, 4, 5 and 6 % (w/w) agarose solutions

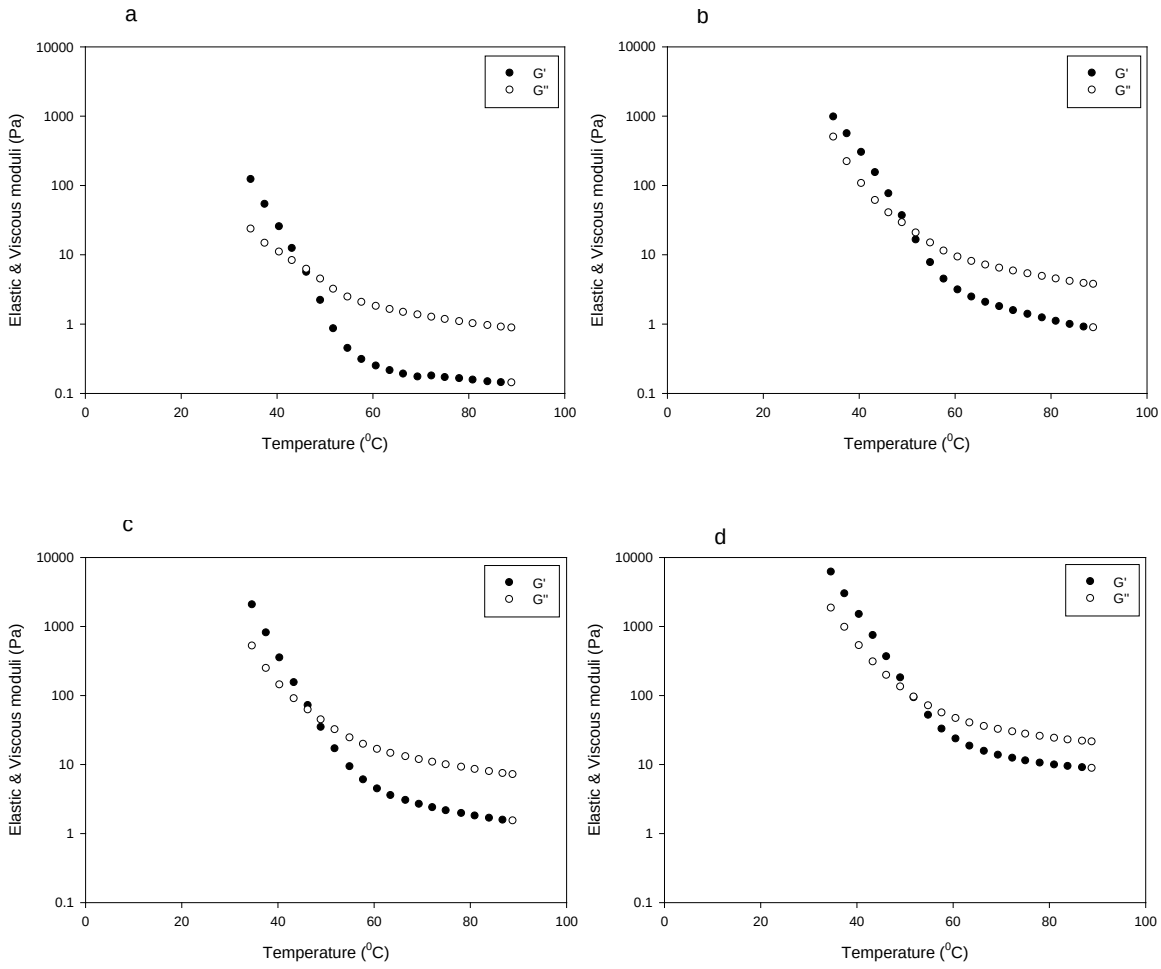

Figure 3.6. *Gelation temperature of (a) 3% (w/w), (b) 4% (w/w), (c) 5% (w/w) and (d) 6% (w/w).*

Table 3.6. *Gelation temperature of agarose solutions of increasing polymer concentration.*

Concentration (% (w/w))	**Gelation temperature** (^{0}C)
3	**46.0**
4	**50.0**
5	**48.5**
6	**52.0**

Note: agarose type: D3

Increasing the amount of agarose appears to raise the gelation temperature of the solution. The gelation temperature was measured by determining the point (Fig. 3.6a-d) at which the contribution of the elastic modulus overcame that of the viscous. Gelation of agarose involves a shift from a random coil in solution to a double helix in the initial stages of gelation, and then to bundles of double helices in the final stage (Quali 2001). In addition, agarose gelation exhibits a hysteresis between melting and setting temperature. Depending on conditions, setting of the gel occurs in a broad range of temperature (40°-10°C), while melting occurs around 70°-80°C. This hysteresis originates from the aggregation of double helices. The melting transition has been proposed to be the true equilibrium process of helix-aggregate conversion to coil, while setting is a nucleation-controlled process in which the limiting step is the helix-helix aggregation (Aymard *et al*. 2001). Since the two quantities, the elastic and viscous moduli, represent the solid and liquid nature of the material respectively (or the amount of stored energy and energy dissipated as heat), the cross-over of the elastic modulus over the viscous is an indication of double helix aggregation and polymer network formation. Upon increasing the amount of polymer in the gel, gelation

temperature increases. This is because more polymer chains per unit volume of the gel will result into a larger number of helix aggregate-nucleation sites that will in turn create a more stable structure at higher temperature.

3.2.3.2. Flow curves for 3, 4, 5, 6 % (w/w), 0, 0.01, 0.025, 0.05, 0.1 m (4 % (w/w)) agarose solutions and mineral oil

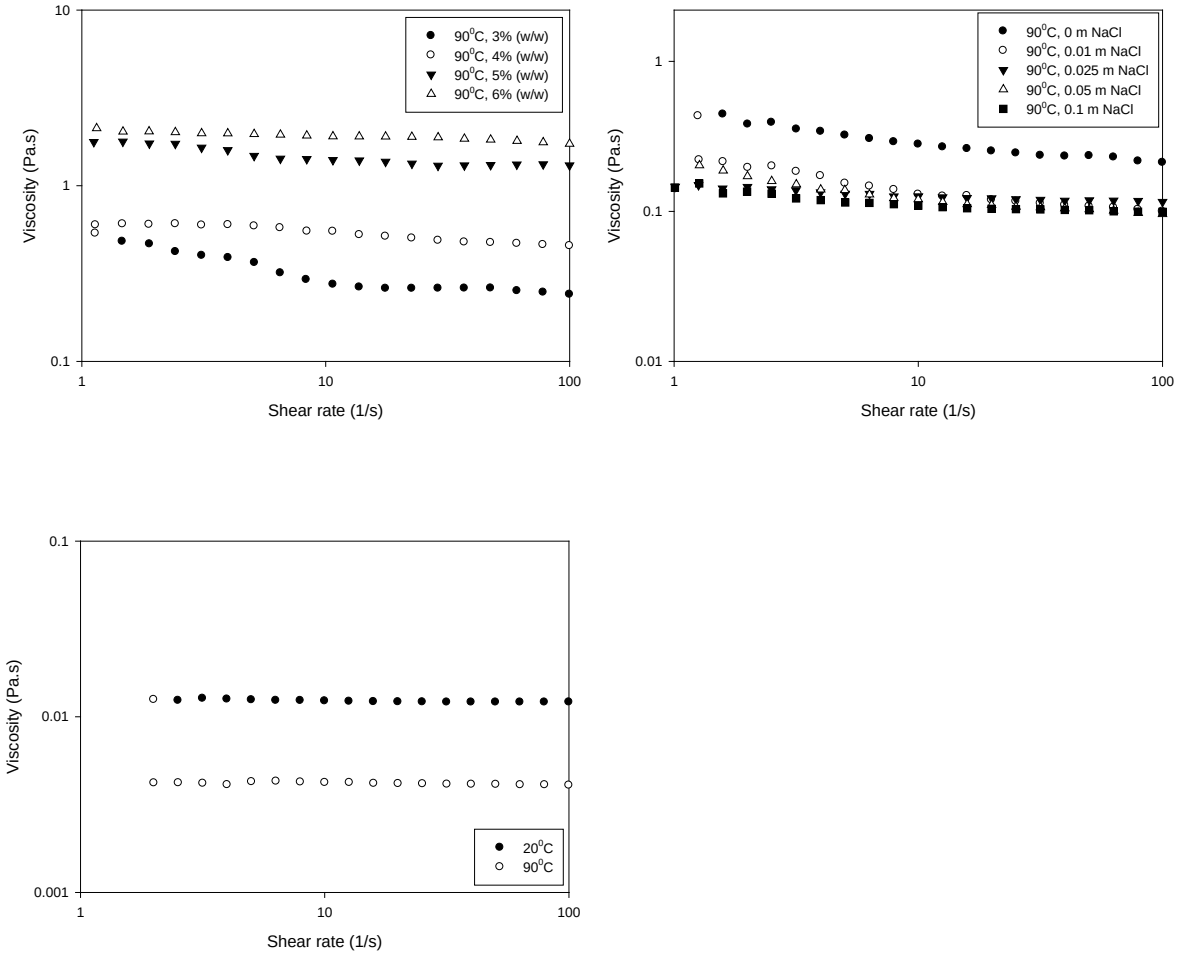

Figure 3.7. *Flow curves for (a) increasing polymer concentration at 90° C, (b) increasing ionic strength at 4% (w/w) agarose at 90° C and (c) mineral oil.*

Mineral oil was found to be Newtonian at both measured temperatures. Agarose solutions of increasing polymer and salt concentration were found to be weakly non-Newtonian (shear thinning), except the 3 % (w/w) solution which is non-Newtonian at low shear (up to 10 s^{-1}). The viscosities of solutions can be correlated as a function of shear rate by power law model (Barigou, 2003):

$$\eta = K\,\dot{\gamma}^{n-1} \qquad (3.14)$$

where η: apparent viscosity (Pa s)

K: consistency index (N $s^n m^{-2}$)

n: flow behaviour index (-)

$\dot{\gamma}$: shear rate (s^{-1})

Table 3.7 shows the consistency (*K*) and flow behaviour (*n*) indexes for solutions of agarose solutions. For engineering calculations solutions can be treated as Newtonian.

Table 3.7*. Consistency and flow behaviour indexes for solutions of increasing polymer concentration.*

Agarose type	**Agarose concentration**	**Ionic strength**	**Consistency index (K)**	**Flow behaviour index (n)**
-	(% (w/w))	(m)	(N $s^n m^{-2}$)	-
D3	3.0	-	0.4886	0.8199
D3	4.0	-	0.6274	0.9318
D3	5.0	-	1.7734	0.9192
D3	6.0	-	2.0918	0.9634
D5	4.0	-	0.4416	0.8233
D5	4.0	0.01	0.2379	0.7621
D5	4.0	0.025	0.1495	0.9357
D5	4.0	0.05	0.2001	0.8068
D5	4.0	0.1	0.1437	0.9004

CHAPTER 4

-

ATOMIC FORCE AND CRYO-SCANNING ELECTRON MICROSCOPY CHARACTERIZATION OF BEADED AGAROSE STRUCTURE

4.1. Pore size of agarose beads by AFM

Three sets of samples were examined with the AFM: the first set consisted of five samples of 4 % (w/w) agarose and increasing amount of salt (0, 0.01, 0.025, 0.05 and 0.1 m NaCl, quenched at 0° C) and it was manufactured in order to investigate the effect of ionic strength on the conformation of agarose fibres in the gel network and on the resulting pore size / size distribution of the adsorbent.

The second set included samples of 4 % (w/w) agarose quenched at three different temperatures (0°, 10° and 20° C) and three different salt contents (0, 0.01, 0.05 m NaCl) were used at each quenching temperature. This set was manufactured in order to investigate the combined effect of temperature and ionic strength on said properties of the agarose gel network.

The last set included Sepharose 4B and Sepharose CL 4B, commercial products extensively used in analytical laboratory applications. Sepharose 4B was examined in order to compare the structure of a benchmark product with the structure of agarose beads prepared in this work. Sepharose CL 4B was examined in order to test the assumption that cross-linking does not change the porosity of the gel, owning to the fact that the short cross-links only occur in the agarose double helices and junction zones at the boundaries of the gel pores

(www.bioscience-beads.com/stdspec.htm), and therefore verify that agarose beads manufactured in this work can be chemically cross-linked to any degree to produce chemically and mechanically superior gels while maintaining their original structural properties in terms of pore size / size distribution. The summary of all measurements with the AFM as well as with the cryo-SEM can be seen in Table 4.1.

4.1.1. Effect of ionic strength of agarose solution on pore size / size distribution

Ionic strength is defined by (Solomon 2001):

$$I = {}^{1}/_{2} \sum m_i z_i^2 \qquad (4.1)$$

where: m_i the ionic concentration (molality or mol kg^{-1})

z_i the number of charges on the ion

According to the Eq. 4.1 for an electrolyte consisting of univalent ions, such as NaCl, its ionic strength is equal to the molal concentration of the electrolyte, therefore, in the following results, the ionic strength of the agarose solution is also expressed by the molal concentration of NaCl.

Fig. 4.1a-e shows the effect of increasing ionic strength on the structure of agarose particles. Fig. 4.2a-b shows the measured average pore size and pore size distribution respectively. As mentioned in section *2.4.3,* 'pores' were considered the darker spots on the AFM images. These spots are roughly circular and their diameter appears to increase with ionic strength especially for the highest salt contents. In Fig. 4.1a, (image size is 1 µm X 1µm)

individual agarose chains are clearly visible. No differences in pore size were observed between pure agarose (0 m) and 0.01 m (38 nm and 40 nm respectively) (Fig. 4.1a-b). At 0.025 m pore size of agarose gels increased to 67 nm (Fig. 4.1c), at 0.05 m increased to 128 nm (Fig. 4.1d) and finally at 0.1 m increased to 190 nm (Fig. 4.1e), a five-fold increase of the original value for pure agarose. Since agarose concentration in the gel was the same for all samples the results suggest that increase in pore size is caused by changes in the conformational arrangement of the agarose fibres. It is worth noting that apart from an increase in average pore size with ionic strength, a significant increase in the standard deviation of the pore size distribution was also observed (Fig. 4.2b). In particular, standard deviation was 41 nm for 0 m, 45 nm for 0.01 m, 60 nm for 0.025 m, 74 nm for 0.05 m and 105 nm for 0.1 m. The effect of salt on the agarose structure appears to be especially pronounced for larger fibres, since the increase in the standard deviation of the pore size distribution is toward the large size. Roughness of the beads (Z-range) was not found to vary significantly with ionic strength. Samples were quite uniform with 20 nm vertical displacement for the pure agarose sample and 30 nm for the rest of the samples. The differences in sample roughness will be discussed after the second set of samples (effect of quenching temperature) is analysed.

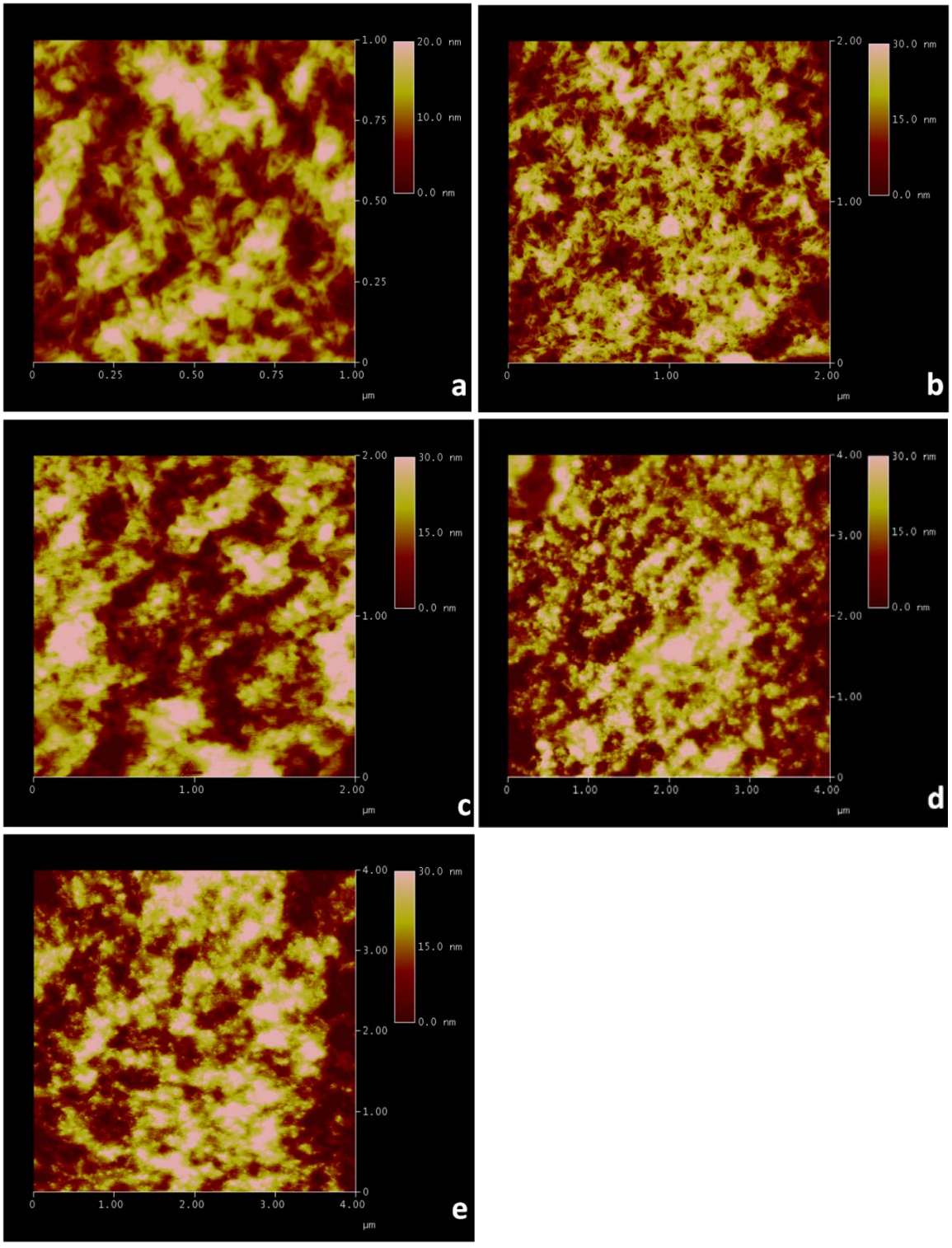

***Figure 4.1**. Effect of ionic strength on the pore structure of agarose beads (quenched at 0° C) (a) 0 m (XY: 1 µm, Z: 20 nm), (b) 0.01 m (XY: 2 µm, Z: 30 nm), (c) 0.025 m (XY: 2 µm, Z: 30 nm), (d) 0.05 m (XY: 4 µm, Z: 30 nm), (e) 0.1 m (XY: 4 µm, Z: 30 nm), note: X and Y are the horizontal and lateral distances of the scan respectively, therefore indicating the scale of the image.*

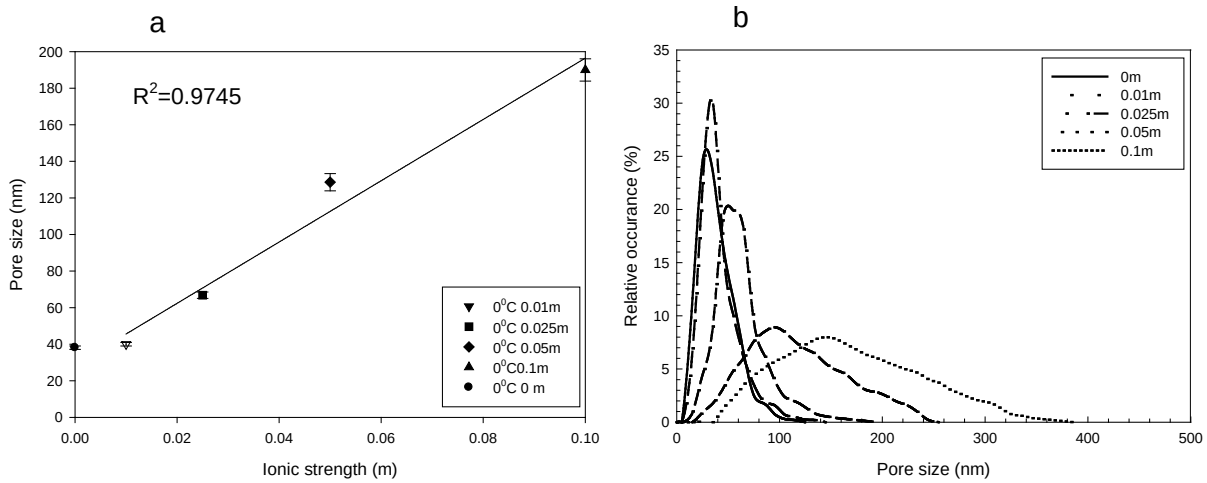

Figure 4.2. *(a) Average pore size for increasing ionic strength, (b) pore size distribution for increasing ionic strength, quenching temperature: 0° C.*

Despite different concentrations of solutes and co-solutes, gel casting/setting conditions and characterization methods, similar results on the effect of ionic strength on pore size of agarose gels have been reported in the literature. On the other hand, this is the first account in the open literature of examining this effect on the pore properties of *micron-sized agarose beads*. Maaloum *et al*. (Maaloum *et al.* 1998) studied the effect of concentration of TBE buffer on agarose gel slabs using AFM obtained images of similar quality and interpreted data in the same way as in this work (diameter-based measurements of circular dark spots on the AFM images). They reported increase in pore size and in the standard deviation of the pore size distribution with ionic strength of the agarose solution. Serwer and Griess (Serwer and Griess 1991) studied the effect of various buffers on the structure of agarose slabs designated for electrophoresis and reported an increase in average pore size with ionic strength. Waki *et al*. (*Waki et al.* 1982), studied agarose gels formed in the presence of TBE buffer using electron microscopy of freeze dried samples. Although the quality of their

images was not good they concluded that agarose fibres tend to aggregate in the presence of salts thus producing gels with large pore size and wide size distribution. In these studies researchers confirmed their results with electrophoretic measurements concluding that the relative migration rates of DNA plasmids substantially increased when salt was present in the gel. The increase in pore size / size distribution of the gel when adding salts as co-solutes is caused by the indirect interaction of neutral solute and co-solute (agarose and NaCl) in addition to the conformational change that agarose molecules undergo during gelation.

For an interpretation of the effect of ionic strength, it is necessary to briefly consider the gelation mechanism of agarose, a more detailed explanation will be given in the next set of results were the effect of cooling rate is examined. As mentioned before, agarose gelation involves a shift from a random coil in solution to a double helix in the initial stages of gelation, and then to bundles of double helices in the final stage (Quali 2001). The gel is formed when an infinite three-dimensional network of agarose fibres (consisting of helices) develops (Normand *et al*. 2000). Since the gel state is characterized by polymer-rich regions (agarose fibres) and solvent-rich regions (pores of water) (Emanuele *et al*. 1991) the gelation of agarose can be interpreted as a phase separation (Pines and Prins 1973, Narayanan *et al*. 2006) between the solvent and solute.

In general, when a polymer or biopolymer is dissolved in an aqueous solution, water molecules tend to create a hydration envelope caused by solvent-solute hydrogen bonding, around the dissolved chains. The formation of this envelope prevents the polymer chains, from aggregating through inter-chain hydrogen bonds and Van der Waals forces, as they would do in the solid state. However, any factor that tends to reduce the hydration of the

polymer molecules will reduce the size of the envelope, thus bringing the chains closer together. If the polymer solution is concentrated enough, cooling causes the formation of a continuous network of precipitating chains attached to one another through the aforementioned bonds and forces (Troy and Beringer 2005).

Besides lowering the temperature of the polymer solution, another way for reducing the size of the hydration envelope around the polymer molecules is the addition of salts. In general the effects of salts on an aqueous polymer or biopolymer solution may originate from their interaction with the polymer chain, i.e. the direct interaction of ions with the chain polar groups, and /or the hydrogen-binding ability of water (Suwa *et al*. 1998). It is a matter of current dispute as to whether the effect of salts on macromolecules through the interaction of ions with water is restricted only to the first hydration layer of the macromolecule (hydration envelope) or whether it is extended to the bulk volume of water through long-range structure-forming or structure-breaking effects on the hydrogen bonding network (Zhang and Cremer 2006, Nucci and Vanderkooi 2008).

In this work, where the biopolymer is a non-ionic polysaccharide, it is assumed that the effect of ionic strength on the conformation of the agarose chains is only through the interaction of salt ions and water molecules and not through the interaction of ions with agarose molecules. Furthermore the interpretation of the results presented above is based only on the interaction between the ions and the first hydration layer of the polymer. The possible long-range contributions of ions in the bulk volume of water were not addressed.

As salt binds part of the water in solution in order to become more hydrated, agarose molecules tend to dehydrate. This salt-induced dehydration promotes chain-chain

interaction and ultimately chain aggregation through hydrogen bonding and van der Waals forces, thus leading to a more pronounced phase separation during gel setting (Troy and Beringer 2005, Perreur *et al*. 2006). The result is a gel with richer polymer-rich regions (thicker agarose fibres) and richer solvent-rich regions (larger pores holding water) than that of pure agarose (Fig. 4.1, a-e). The phenomenon is known as *salting-out* and it is often used for precipitating proteins from dilute solutions with the most commonly used salt being ammonium sulphate due to its high solubility into water and low cost (Amersham Biosciences 2000). Salting-out of proteins can be reversed by dilution of the system with water.

The interpretation of the results presented above, with the salting-out effect, not only explains the increase in average pore size of the gel, it also accounts for the increase in standard deviation of the distribution of the agarose pores. In Fig. 4.2b, the width of distribution of pores is increased toward the large size of the graph with increasing ionic strength. Assuming a Gaussian distribution of the molecular weight of the agarose molecules (Normand *et al.* 2000) this observation suggests that larger agarose fibres have grown in size to a greater extent than smaller ones. This behaviour is expected since the enhanced-by - salting-out effect of inter-chain hydrogen bonds and attractive van der Waal forces during chain aggregation is greater for larger chains.

The effectiveness of electrolytes (such as NaCl) to cause salting-out effects on macromolecules depends upon the extent of hydration. The *Hofmeister* or *lyotropic series* arranges ions in order of increasing hydration and increasing effectiveness in salting-out

hydrophilic colloids (Troy and Beringer 2005). The series for typical monovalent and divalent ions are shown in Fig. 4.3:

a) $Cs^+ < Rb^+ < NH_4^+ < K^+ < Na^+ < Li^+ < Ba^{2+} < Sr^{2+} < Ca^{2+} < Mg^{2+}$

---

b) $F^- >$ citrate$^{3-} > HPO_4^{2-} >$ tartrate$^{2-} > SO_4^{2-} >$ acetate$^- > Cl^- > NO_3^- > ClO_3^- > Br^- > ClO_4^- > I^- >$ CNS^-

Figure 4.3. *The Hofmeister series for typical (a) cations and (b) anions.*

As it can be seeing from Fig. 4.3 the series move from monovalent to multivalent ions for both anions and cations, in term of increasing effectiveness to precipitate macromolecules. In other words, the 'salting-out' effect increases with the multivalency of ions and on the contrary, decreases with growth of the ionic radius (Perreur *et al.* 2006). The valency of ions can be related to ionic strength as shown in Eq. 4.1. An example illustrating this is the comparison between sodium chloride (NaCl) and ammonium sulphate ($(NH4)_2SO_2$) (Dennison 2003):

From Eq. 4.1 for 1 m NaCl:

$$\mathrm{I} = \frac{1}{2}[(1 \cdot 1^2) + (1 \cdot 1^2)] = 1\mathrm{m} \qquad (4.2)$$

Similarly, for 1 m $(NH4)_2SO_2$

$$\mathrm{I} = \frac{1}{2}[(2 \cdot 1^2) + (1 \cdot 2^2)] = 3\ \mathrm{m} \qquad (4.3)$$

From the above it can be deduced that ionic strength of solution determines the degree of salting-out (Park 1993). As a consequence, the solubility of polymer chains can be reduced by using a cation at a certain concentration (and ionic strength), while the same effect can be created by a different cation at a lower concentration (same ionic strength as above) placed further to the right on the cationic lyotropic series. Considering Na^+ and Cl^- ions, the smaller the ion (ionic radii 0.95 Å and 1.18 Å respectively, (Anslyn and Dougherty 2006)), the greater the hydration energy (energy released when a mol of the ion dissolves in water, -98 kcal mol^{-1}, -82 kcal mol^{-1} respectively (Anslyn and Dougherty 2006)). This trend is an indication of a largely electrostatic effect. Considering ions as spheres of charge, a smaller monovalent ion has the same charge as a large monovalent ion distributed over a smaller surface, which results into a higher charge per unit area and makes Coulomb interactions stronger (Anslyn and Dougherty 2006, Nucci and Vanderkooi 2008). Consequently, Na^+ cations contribute to a larger extent to the salting-out effect of the agarose molecules than Cl^- anions since the former are better hydrated as illustrated in Fig. 4.4. As can be seen, in an aqueous solution Na^+ cations attract six molecules of water whereas Cl^- anions attract five:

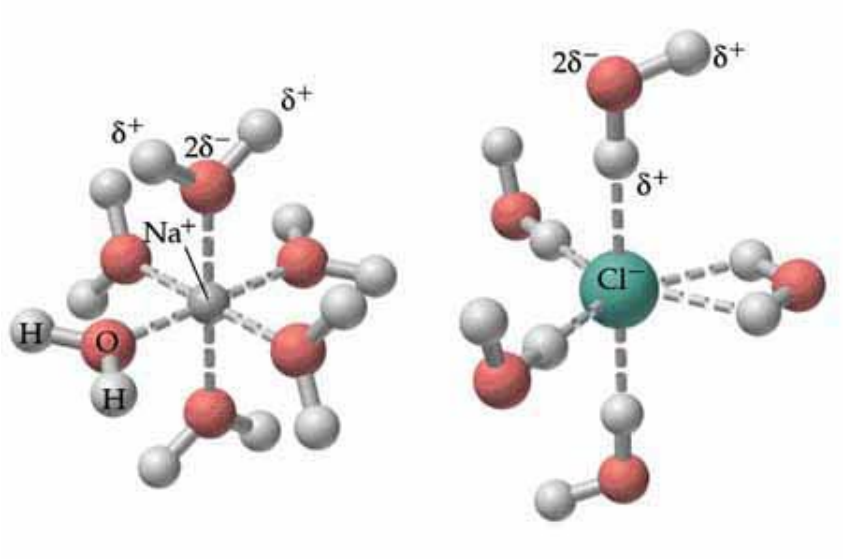

***Figure 4.4**. Hydration of Na^+ and Cl^- ions in aqueous solution (Image from http://wps.prenhall.com).*

It can be concluded therefore that the salting-out effect indeed depends on the ionic strength of the surrounding medium and not on the type of salt used. Similarly it has been reported (Waki *et al.* 1982) that Tris-borate buffer and potassium cations, (when used at the same ionic strength) had the same effect of the agarose gel structure. This finding supports the hypothesis that the addition of NaCl leads to only the reduction of the hydrating envelope and not to the direct interaction of the salt ions with the agarose chains, since the nature of composition of Tris-borate buffer is complex and very different of that of potassium ions.

4.1.2. Effect of quenching temperature of the emulsion on pore size / size distribution

Fig. 4.5a-c, 4.7a-c, and 4.9a-c, show the combined effect of ionic strength and quenching temperature on the structure of the agarose particles. Fig. 4.6, 4.8 and 4.10 show the pore size distribution of these samples. Fig. 4.11 shows the average pore size for nine different combinations of quenching temperature and ionic strength. Average pore size (Fig. 4.11) increases with increasing quenching temperature (slower cooling) for all three ionic strengths used. For pure agarose pore size increased from 38 nm (quenching temperature 0° C) to 101 nm (10° C) and 150 nm (20° C). For 0.01 m average pore size increased from 40 nm (0° C), to 109 nm (10° C) and 169 nm (20° C). The respective values for 0.05 m, the highest ionic strength used in this set, were 129 nm (0° C), 172 nm (10° C) and 195 nm (20° C). This result suggests that quenching temperature has a significant effect on the conformation of the agarose fibres. With slow cooling an increase in the standard deviation of the distribution of pores is also observed. In fact, the resemblance between the pore size distributions in Fig. 4.3b and Fig. 4.6, 4.8 and 4.10 indicates a similarity between the effect of quenching temperature and ionic strength on the structure of agarose. For pure agarose standard deviation increased from 41 nm (0° C) to 85 nm (10° C) and 126 nm (20° C). For 0.01 m standard deviation increased from 45 nm (0° C) to 105 nm (10° C) and 140 nm (20° C), while for 0.05 m the respective values were 74 nm (0° C), 120 nm (10° C) and 137 nm (20° C). The regression lines for 0 m and 0.01 m in Fig. 4.11 suggest that cooling rate is a predominant factor in changing the conformation of the agarose fibres in the gel, compared to ionic strength. There is no difference in pore size for fast cooling (0° C), whereas with increasing quenching temperature (10 and 20° C) the difference in pore size between the two samples becomes more significant. A phenomenon that was not observed with

increasing ionic strength for the lowest quenching temperature (first set of samples), was the increase of the roughness of the sample surface with increasing quenching temperature. In particular, samples quenched at 0° C had an average surface roughness of 30 nm where as the respective value for samples quenched at higher temperatures (10° and 20° C) was between 50 and 100 nm, again indicating the predominance of the effect of cooling rate over effect of ionic strength on the agarose structure.

In a simplistic way, one could argue that slow cooling allows more time to the gel network to develop. Thus fast cooling will result into a gel network that is closer to the solution state of agarose, whereas slow cooling rate results into well developed network with thicker agarose fibres and larger pores holding water. This is also indicated by the difference in roughness (Z-range in the AFM images) between samples manufactured at different cooling rates. Assuming that the roughness of the agarose droplets at 90°C (solution state during emulsification step) is 0 nm one observes an increase with slow cooling (20-30 nm at 0° C and 50-100 nm for 10 and 20° C). This increase indeed indicates that slow cooling shifts the agarose molecules from a solution state toward a well developed network consisting of thick fibres and large pores.

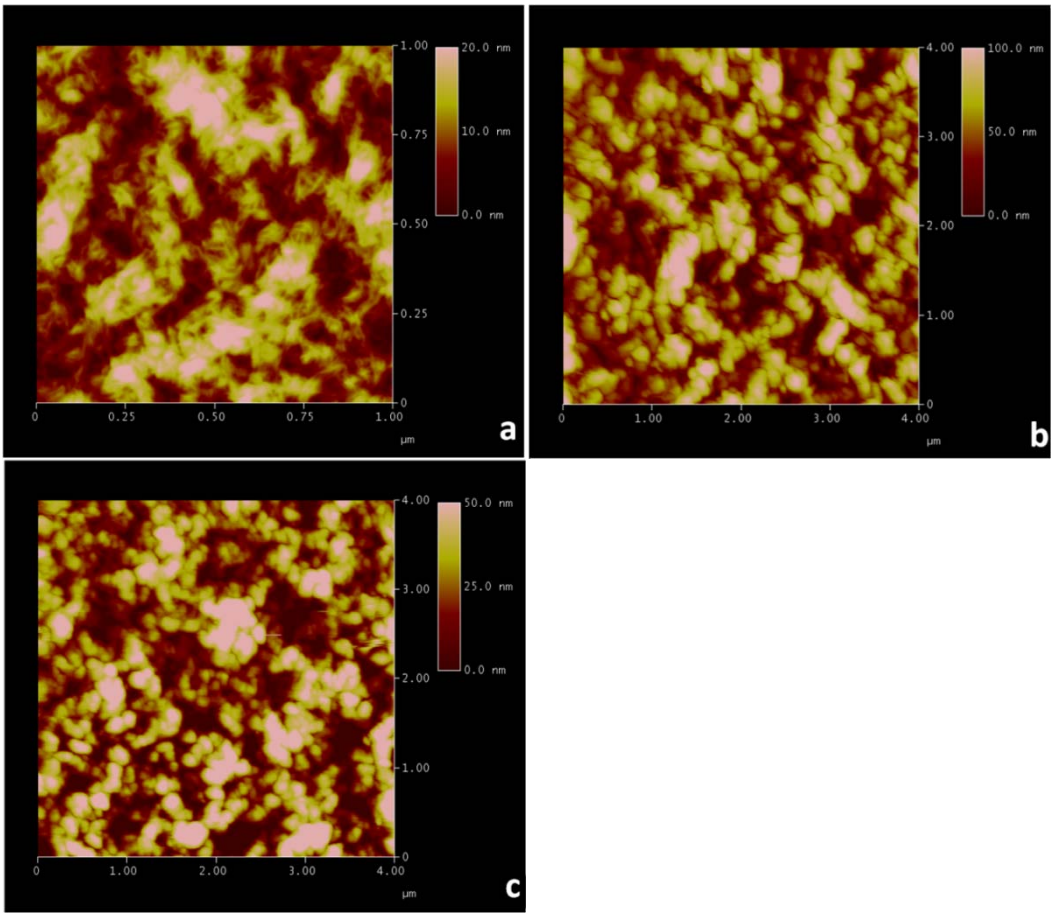

***Figure 4.5**. Effect of quenching temperature on pore structure (ionic strength: 0 m) (a) 0° C (XY: 1µm, Z: 20 nm), (b) 10° C (XY: 4 µm, Z: 100 nm), (c) 20° C (XY: 4 µm, Z: 50 nm).*

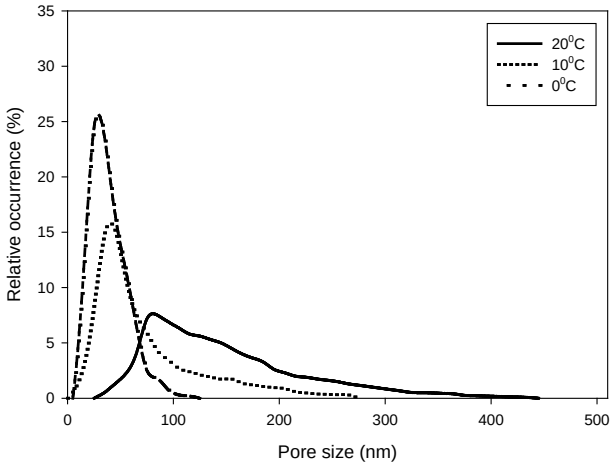

***Figure 4.6**. Pore size distribution for three quenching temperatures (ionic strength: 0 m).*

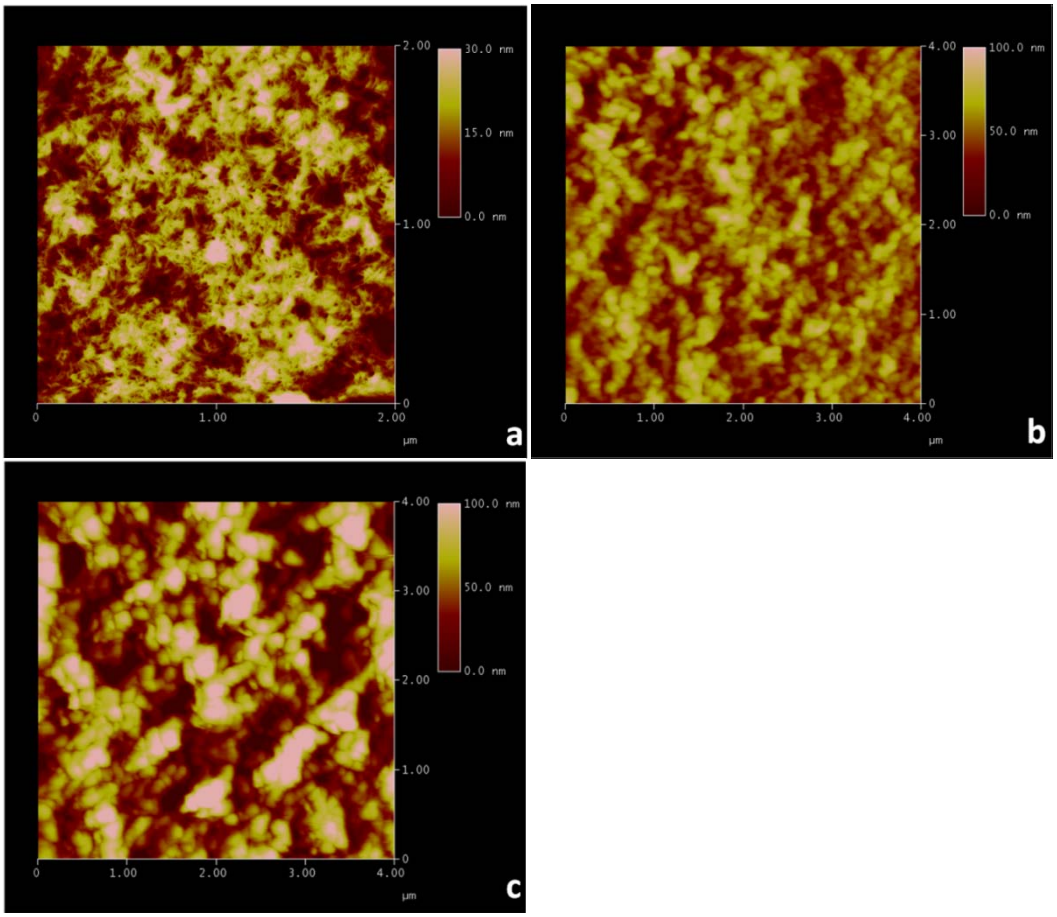

Figure 4.7. *Effect of quenching temperature on pore structure (ionic strength: 0.01 m): (a) 0° C (XY: 2 µm, Z: 30 nm), (b) 10° C (XY: 4 µm, Z: 100 nm), (c) 20° C (XY: 4 µm, Z: 100 nm).*

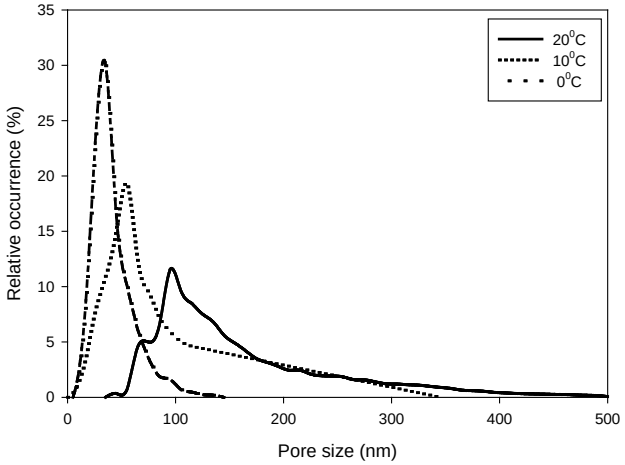

Figure 4.8. *Pore size distribution for three quenching temperatures (ionic strength: 0.01 m).*

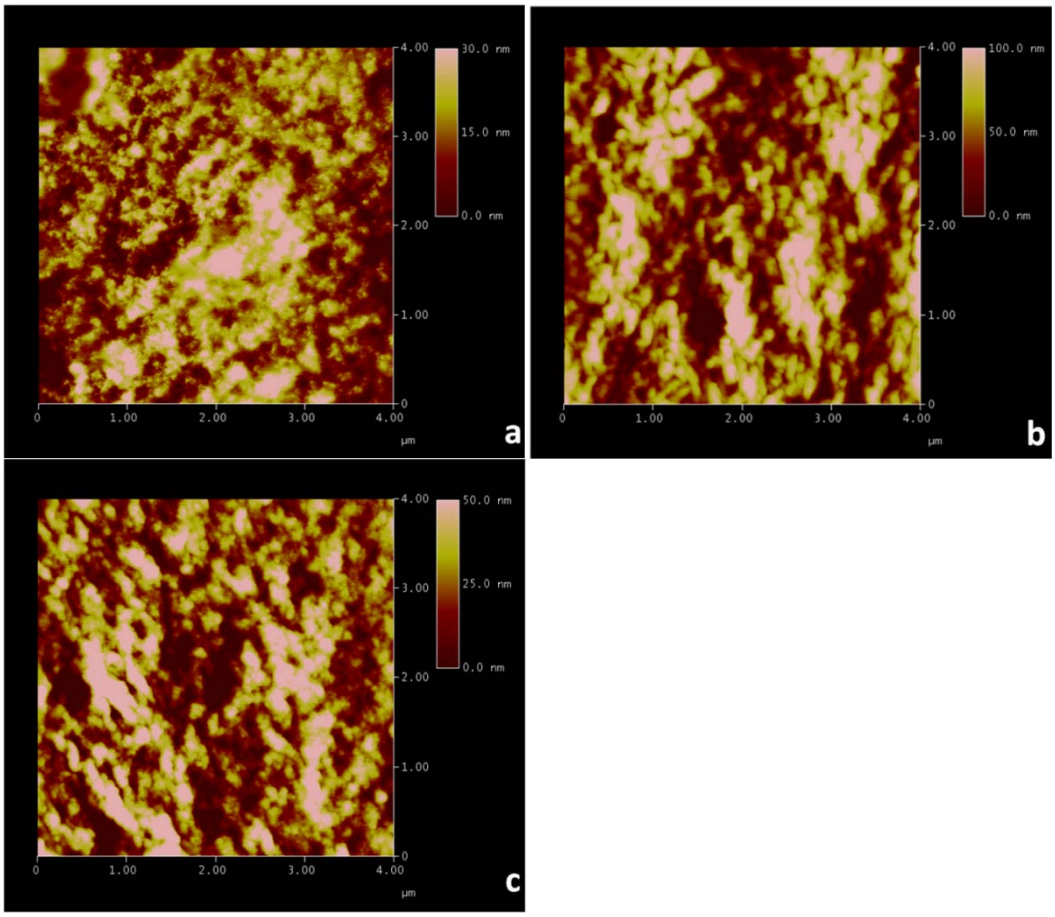

***Figure 4.9**. Effect of quenching temperature on pore structure (ionic strength: 0.05 m) (a) 0° C (XY: 4 µm, Z: 30 nm), (b) 10°C (XY: 4 µm, Z: 100 nm), (c) 20° C (XY: 4 µm, Z: 50 nm).*

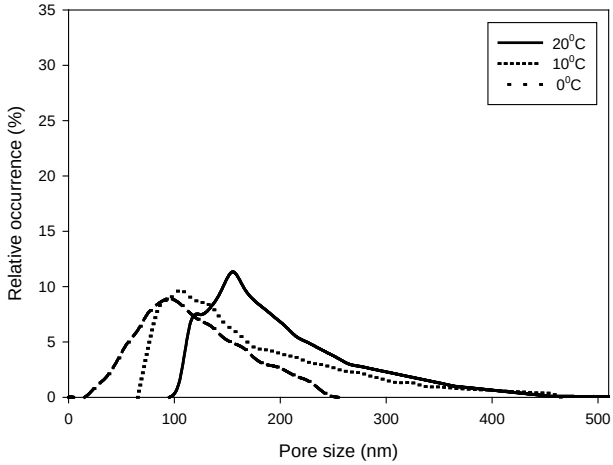

***Figure 4.10**. Pore size distribution for three quenching temperatures (ionic strength: 0.05 m).*

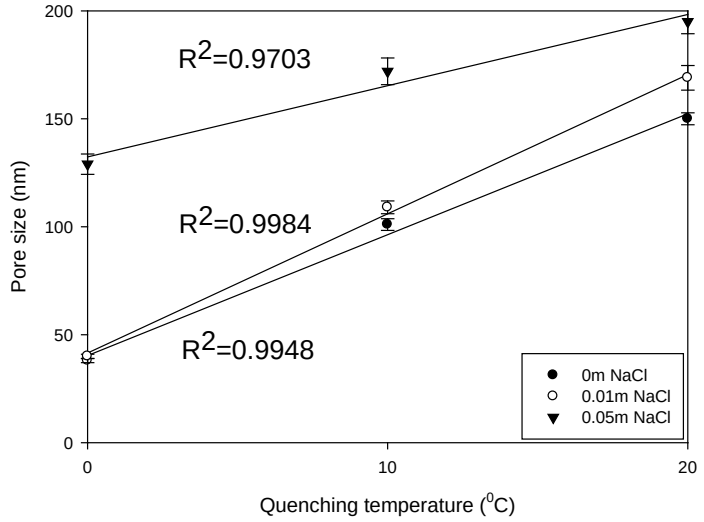

***Figure 4.11**. Average pore size for three quenching temperatures at three ionic strengths.*

The increase in pore size and standard deviation of the pore size distribution of agarose gels with quenching temperature found in this work are in good agreement with the literature. The effect of cooling temperature on the structure of agarose gels has been previously studied on centimetre-sized gel slabs using a variety of techniques including small angle neutron scattering (Quali 2001), absorbance measurements (Narayanan *et al*. 2006) and electrophoresis (Kusukawa *et al*. 1999). Despite that, this is the first account in the literature relating cooling conditions to the pore size of micron-sized agarose beads. All of the above researchers reported increase in average pore size of agarose gels with slow cooling, while the last (Kusukawa *et al*. 1999) also reported increase in the standard deviation of the distribution of pores as well as differences in the melting profiles (measured by differential scanning calorimetry) of gels cooled at different final temperatures.

Pore size of agarose gel increases with slow cooling because of the different conformation that agarose chains adopt when cooled at different temperatures. At the molecular level, it

has been proposed (Tako and Nakamura 1988) that, as temperature decreases, an intramolecular hydrogen-bonding between OH-4 of the D-galactopyranose residue and the adjacent hemiacetal oxygen atom of the anhydro-cY-L-galactopyranose residue (dashed line in Fig. 4.12a) is responsible for the transition of the random coil to a rod-like structure. The anhydro-a-L-galactosyl residue is a cage-like residue that contributes to the rigidity of the molecular chain of agarose, and stabilizes the intramolecular hydrogen bonding. With further decrease in temperature, an intermolecular hydrogen-bonding between the ring O-3,6 atom and OH-2, which has an axial orientation (dashed lines in Fig. 4.12b) is responsible for the ordered coil to double-helix transition. As a given polysaccharide chain can participate in many double helices (Malmqvist 1977) the same intramolecular hydrogen bond is responsible for helix-helix aggregation. This intermolecular bonding results from the cage effect of the anhydro-cZ-L-galactosyl residue, which may adopt a tetrahedral distribution and, therefore, may attract not only each other, but also water molecules with hydrogen bonding. When slow cooling is applied, the characteristic interval for each stage of gelation (random coil -> rod-like structure -> double helix -> helix aggregates) increases, thus a greater number of intermolecular hydrogen bonding events between double helices will occur. This produces longer and thicker helix aggregates which in turn result into a gel with large pore size. The same is observed when changing the ionic strength of the agarose solution. The addition of salt ions promotes helix-helix aggregation thus producing gels with larger pore size than pure agarose.

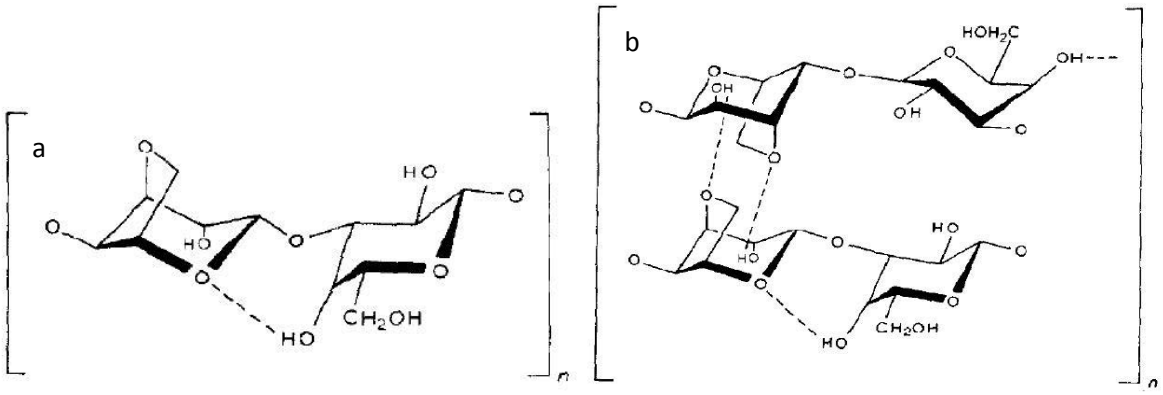

Figure 4.12. *(a) Intramolecular hydrogen bonding in agarose repeating unit, (b) intermolecular hydrogen bonding between the repeating units of two agarose molecules (redrawn from Tako and Nakamura 1988).*

The increase in helix-length with slow cooling has been also been confirmed by rheological measurments. Gelation of agarose is achieved when the contribution of the elastic or storage modulus (G') (solid-like nature of fluid) overcomes that of the viscous or loss modulus (liquid-like nature of the fluid). It has been shown experimentally (Mohammed *et al*. 1998, Aymard *et al*. 2001) that when the quenching temperature of the gel is increased, the temperature at which the elastic contribution overcomes that of the viscous increases. In addition, the melting temperature also increases (Mohammed *et al*. 1998, Kusukawa *et al*. 1999). It was suggested that the helix-length required for stable association increases with increasing gelation temperature with consequent increase in melting temperature (Mohammed *et al*. 1998, Kusukawa *et al*. 1999). The same holds true for increasing ionic strength of solution (Tako and Nakamura 1988). Fast cooling therefore promotes the aggregation of short helices whereas slow cooling promotes the aggregation of longer helices (Mohammed *et al*. 1998). Longer helices will promote helix-helix aggregation as more sites for intermolecular entanglement (Fig. 4.12b) will be available on a

longer helix; therefore a gel with large average pore size is obtained. Similarly as discussed in the case of the effect of ionic strength, the different conformation that agarose fibres adopt when cooled at different temperatures also accounts for the increase in the standard deviation toward the right-hand side of the pore size distribution. Large agarose fibres will tend to grow to a larger extent than smaller ones, since the net effect of inter-fibre hydrogen bonds and attractive van der Waal forces during fibre aggregation is greater for larger fibres.

4.1.3. Examination of Sepharose 4B and Sepharose CL-4B

Sepharose 4B and Sepharose CL 4B were also examined with the AFM. The number before the letter B represents the weight concentration of agarose in the gel, where as the 'CL' indicates that the gel is chemically cross-linked. Fig. 4.13, a-b show the surface of Sepharose beads as scanned by the AFM. Fig. 4.14 shows the pore size distribution of these two gels. Average pore size for Sepharose 4B was 51 nm whereas for Sepharose CL-4B the respective value was 42 nm. The standard deviation of the pore size distribution for the two gels was practically the same (38 nm for Sepharose 4B, 39 nm for Sepharose CL-4B). Given the fact that no information is available about the manufacturing conditions of Sepharose (propertiery method) no connection between the latter and the gel network properties can be made. Despite that, upon comparing pore size and pore size distributions of these gels with samples manufactured in this work (same polymer concentration in all samples), the resemblance between these and the 0 m or 0.01 m quenched at 0° C is striking. The only difference between Sepharose and the latter is sample roughness, with Sepharose having a Z-range of about 100 nm (30 nm for samples in this work).

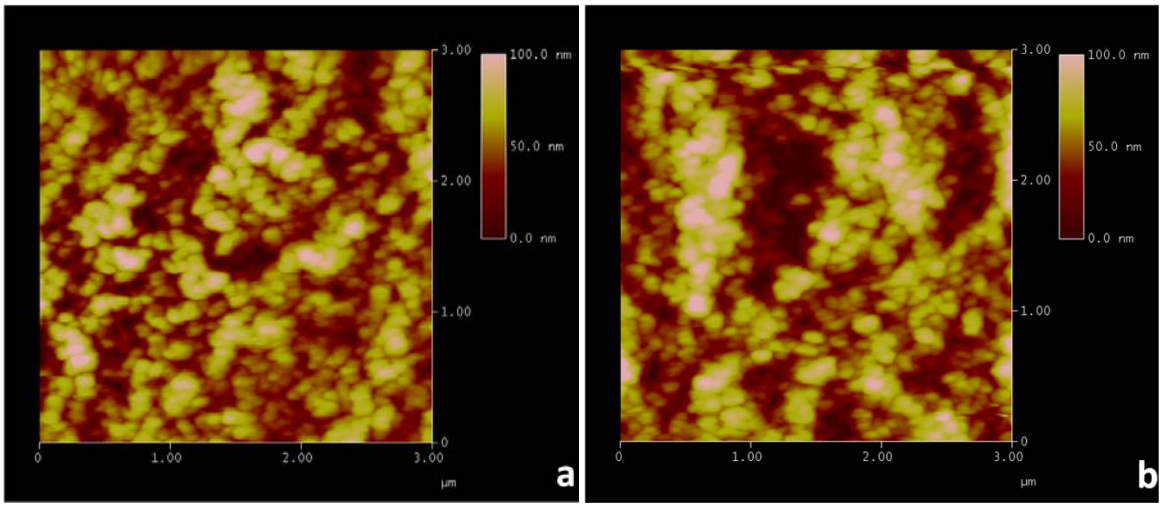

***Figure 4.13**. (a) Sepharose 4B (b) Sepharose CL-4B (XY: 3 µm, Z: 100 nm).*

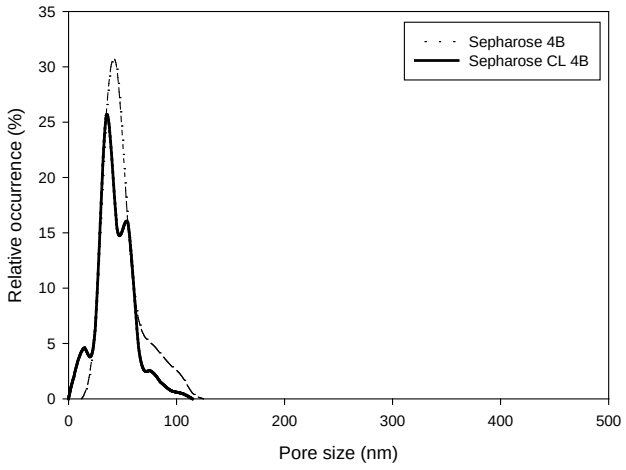

***Figure 4.14.** Pore size distribution for Sepharose 4B and Sepharose CL-4B.*

Nevertheless, obtaining information on pore size and pore size distribution of a commercial product is a useful piece of information as areas for improvement on the gel structure and resulting properties may be identified. For example, the resulting structural properties of beads manufactured in this work with slow cooling and high ionic strength (up 200 nm average pore size and 500 nm maximum pore size) give an indication about the extent the agarose structure can be manipulated to produce a tailored adsorbent that can

reversibly accommodate large bioproducts, in its interior, rather to its exterior, therefore increasing the surface area available for adsorption (see section *i*). Furthermore, the assumption that cross-linking does not change the pore size / size distribution of the adsorbent appears to be valid as pore properties of Sepharose 4B and Sepharose CL-4B are virtually the same. Therefore particles manufactured in this study can be chemically cross-linked to various degrees producing gels of superior mechanical and chemical stability compared to pure agarose while maintaining their original porous properties.

4.2. Pore size of agarose beads by cryo-SEM

4.2.1. Effect of ionic strength of agarose solution on pore size / size distribution

Fig. 4.15 shows the effect of ionic strength on the structure of agarose beads. Four of the five manufactured samples of this set produced good quality images. In last sample, 0.1 m, images were not of good quality as samples with high ionic strength interact with the electron beam and the microscope cannot be focused. Fig. 4.16a-b show the average pore size and pore size distribution respectively, for this set. Average pore size and pore size distributions were calculated with the same procedure as with the AFM images. A value of 15 nm was subtracted during the calculation of average pore size in order to account for the gold coating. Average pore size ranged from 167 nm for 0 m, 84 nm for 0.01 m, 110 nm for 0.025 m to 80 nm for 0.05 m. The average pore size calculated from the SEM images decreases with ionic strength of solution. Similarly, the standard deviation of pore size distribution decreases with ionic strength (Fig. 4.16b).

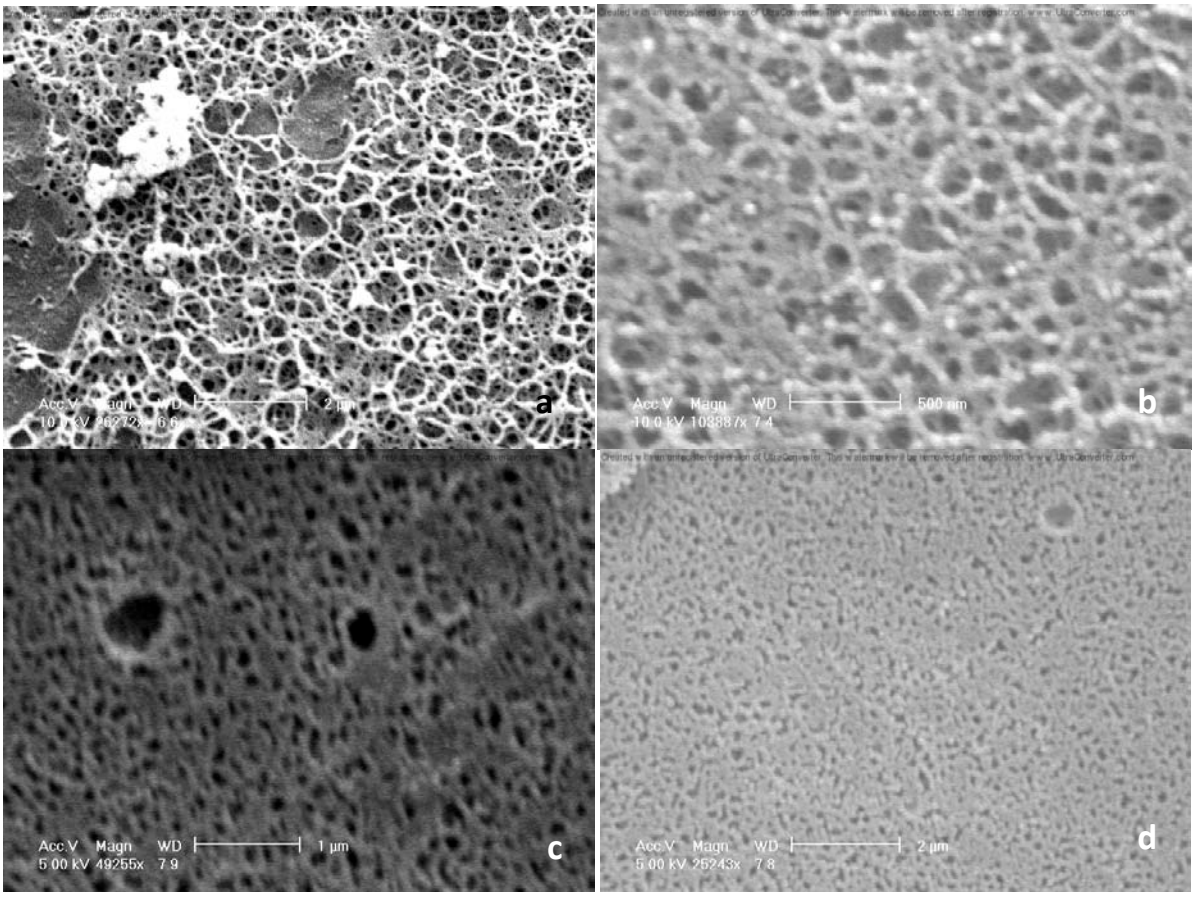

Figure 4.15. *Effect of ionic strength on pore structure: (a) 0 m (scale bar: 2 µm), (b) 0.01 m (scale bar: 500 nm), (c) 0.025 m (scale bar: 1 µm) and (d) 0.05 m (scale bar: 2 µm).*

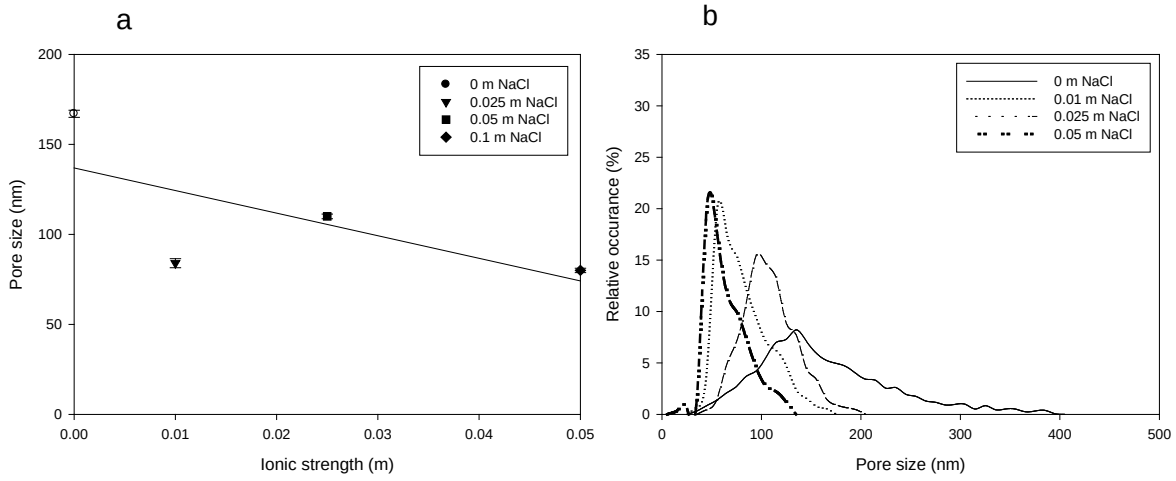

Figure 4.16. *(a) Average pore size for increasing ionic strength, (b) pore size distribution for increasing ionic strength, quenched at 0°C.*

The results obtained from this set of samples contradict what was found for the same set with the AFM (Fig. 4.2a-b), as well as what is reported in the literature (Waki *et al*. 1982, Serwer *et al*. 1991, Maaloum *et al*. 1998). Average pore size appears to decrease rather than increase with ionic strength. Similarly, the standard deviation of the pore size distribution was also reduced. This can be explained by considering sample preparation for cryo-SEM in combination with sensitive nature of salt-containing hydrogels. It has being suggested (Tako and Nakamura 1988, Saito *et al*. 1990) that the cavity in the double-stranded helix of agarose is occupied by water molecules, the arrangement of which are very nearly tetrahedral, in a manner similar to that of the anhydro-a-L-galactosyl residues in the aqueous solution, thus contributing to the stability of the helix by hydrogen bonding. In fact, the mass fraction of internally bound water has been reported to be 0.375 of the total double helix mass (Johnson *et al*. 1995). This suggests that agarose gels formed in the presence of ions will contain a moderate amount of salt along with water molecules in and between the agarose fibres. In order to examine samples under cryogenic conditions with the SEM samples are submerged in nitrogen slush at -140° C, then etched at -90° C in order for some surface water to evaporate and the structure of the particles to become visible. During this etching therefore any inter- and intra-fibre salt will precipitate on the agarose fibres thus making pores appear smaller and with narrower size distribution. In fact, the higher the salt concentration the smaller the pore size appears to be.

4.2.2. Effect of quenching temperature of the emulsion on pore size / size distribution

Fig. 4.17a-c, 4.19a-c and 4.21a-c show the effect of quenching temperature, for three ionic strengths, on the structure of the agarose gel. Fig. 4.23 shows the average pore size calculated for these nine samples whereas Fig. 4.18, 4.20 and 4.22 show the pore size distributions of these samples. Average pore size (Fig. 4.23) for 0 m was 167 nm (0° C), 70 nm (10° C) and 153 nm (20° C). The respective values for 0.01 m were 84 nm (0° C), 115 nm (10° C), 140 nm (20° C) for while for 0.05 m were 80 nm (0° C), 87 nm (10° C), 100 nm (20°C). The standard deviation of the pore size distribution for 0.01 m (Fig. 4.18, 4.20 and 4.22) increased from 48 nm (0° C) to 71 (10° C) and 82 nm (20° C). For 0.05 m the standard deviation of the pore size distribution increased from 42 nm (0° C) to 65 nm (10° C) and 71 nm (20° C) while for 0 m no particular trend was observed since standard deviation decreased from 114 nm (0° C) to 50 nm (10° C), then increased to 97 nm (20° C).

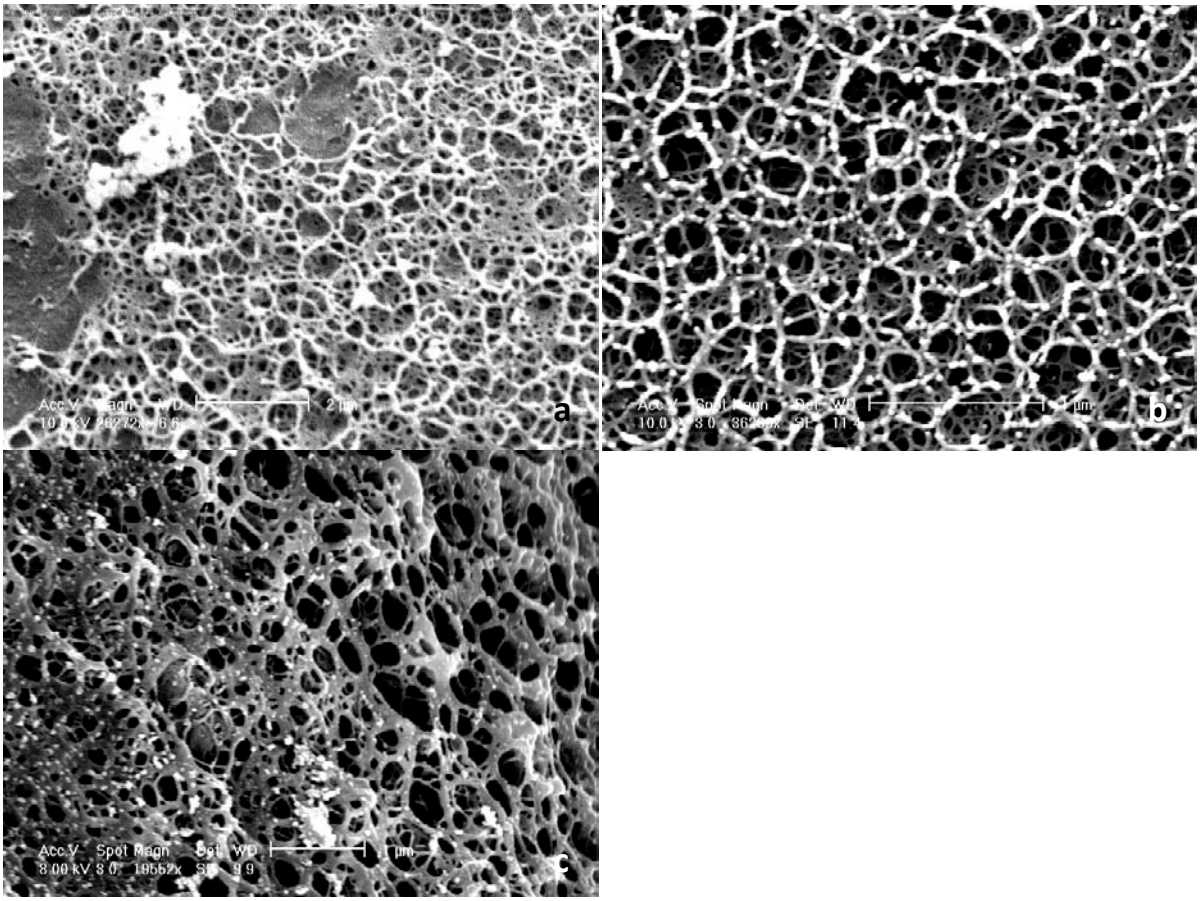

Figure 4.17. *Effect of quenching temperature on pore structure (ionic strength 0 m): (a) 0° C (scale bar 2 µm), (b) 10° C (scale bar 1 µm), (c) 20° C (scales bar 1 µm).*

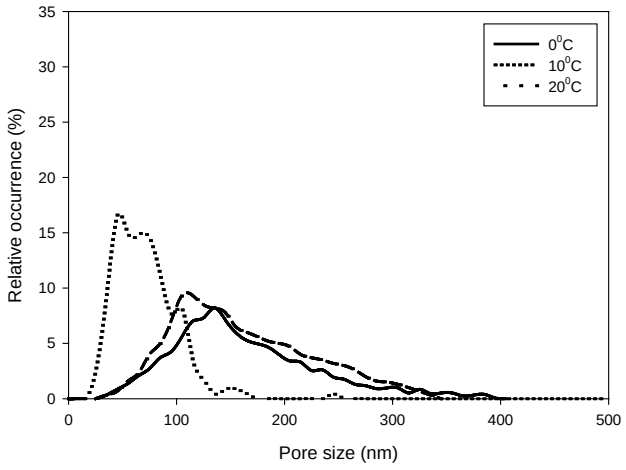

Figure 4.18. *Pore size distribution for three quenching temperatures (ionic strength: 0 m).*

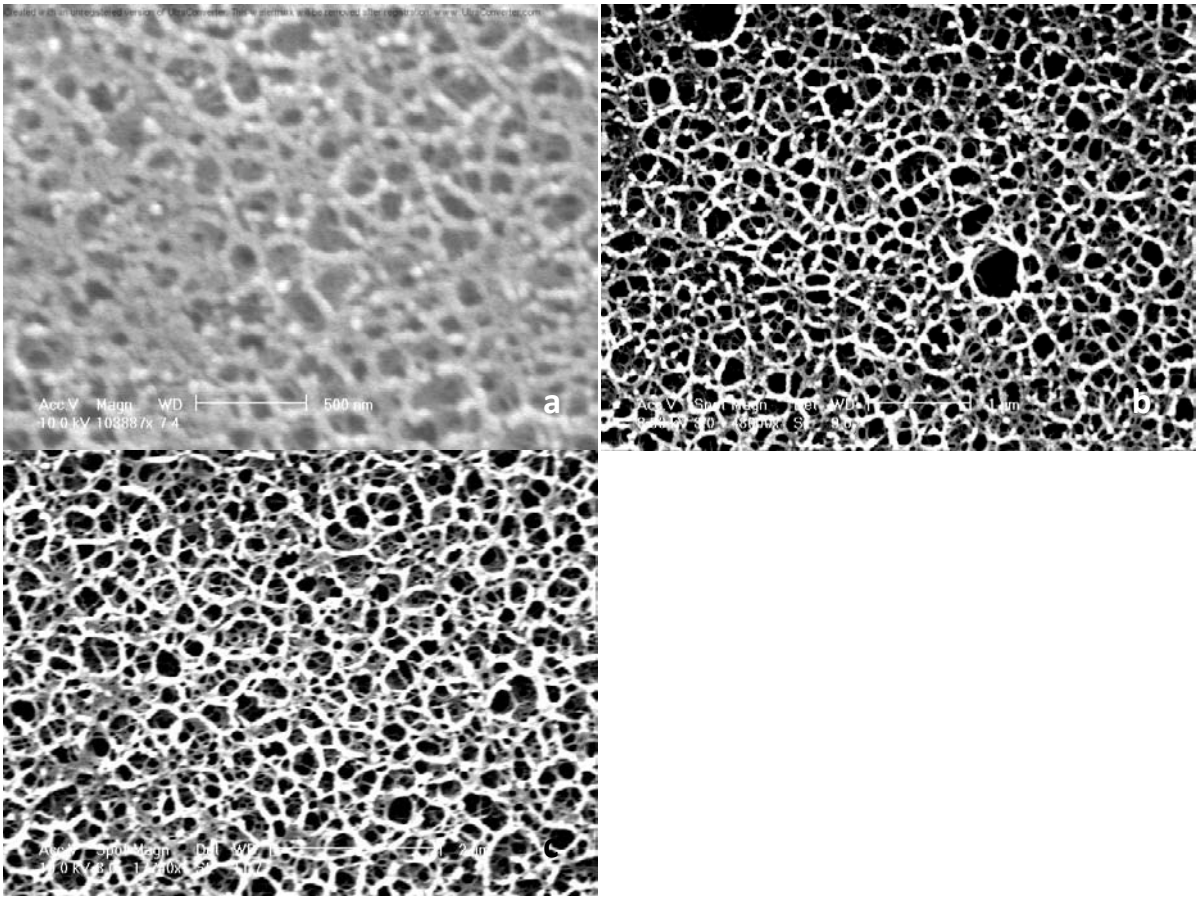

Figure 4.19. *Effect of quenching temperature on pore structure (ionic strength 0.01 m): (a) 0° C (scale bar: 500 nm), (b) 10° C (scale bar 1 µm) and (c) 20° C (scale bar: 2 µm).*

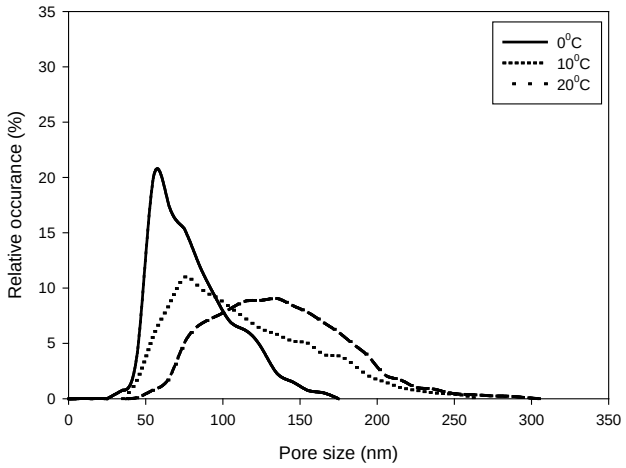

Figure 4.20. *Pore size distribution for three quenching temperatures (ionic strength: 0.01 m).*

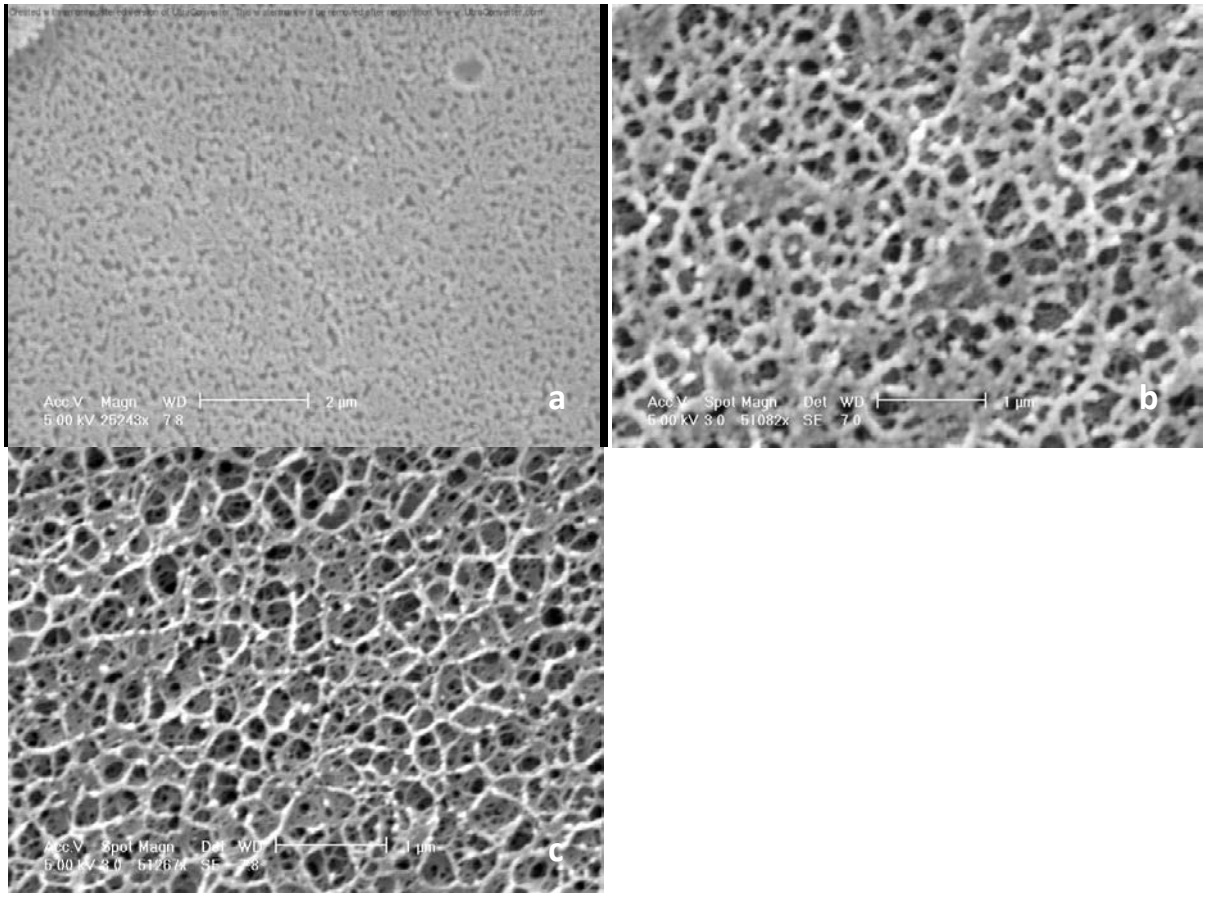

Figure 4.21. *Effect of quenching temperature on pore structure (ionic strength: 0.05 m) (a) 0°C (scale bar 2 µm), (b) 10° C (scale bar 1 µm), (c) 20° C (scale bar 1 µm).*

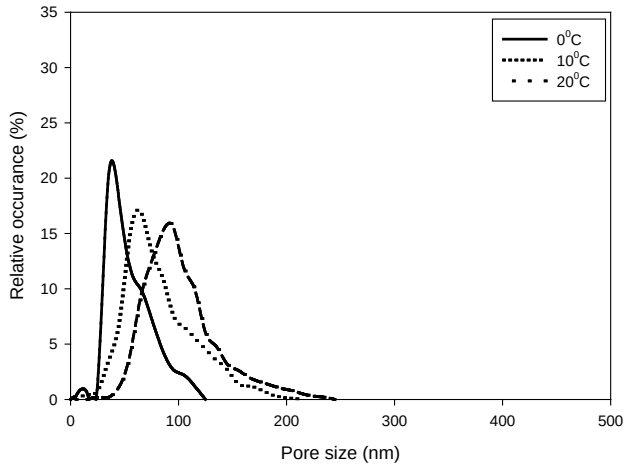

Figure 4.22: *Pore size distribution for two quenching temperatures (ionic strength: 0.05 m).*

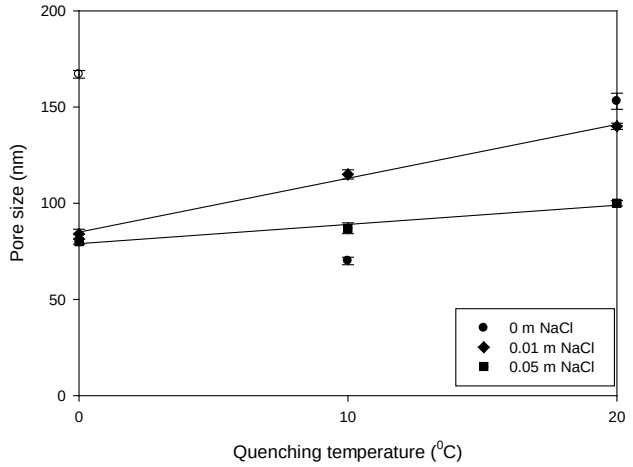

Figure 4.23: *Average pore size for thee ionic strengths, at three quenching temperatures.*

Similarly as observed with samples of increasing ionic strength examined with the cryo-SEM, the trends emerging from this set seem even more conflicting. In general though, samples with increasing salt content appear to have decreasing pore size, while the pore size of samples with high salt quenched at high temperature will show less decrease in that respect since the precipitation of salt on large pores will reduce their size to a lesser degree than on smaller pores (Fig. 4.19b-c, 4. 21b-c and regression lines on 0.01 m and 0.05 m in Fig. 4.23).

Despite the fact that numerical quantification of structural properties of agarose particles, especially of samples containing salt, cannot be obtained from cryo-SEM, owning to the extensive sample preparation and the sensitive nature of hydrogels, a useful conclusion may be drawn from SEM images: Fig. 4.24a shows the cross-section of a 20 µm particle, quenched at 0° C. The size of pores at the surface of this particle appears to be the same size as the pores located at the centre of the particle. Therefore, no temperature or gel

concentration gradient has being formed. As cooling conditions have a major effect on the pore size of agarose gels, it is possible that when particles are quenched at low temperature, very small or even blocked pores may be formed, preventing macromolecular diffusion in the interior of the particle. Additionally as no concentration gradient has been formed it can be concluded that agarose dissolution was successful, despite the viscous nature of the agarose solution. An example demonstrating inferior solution preparation is shown in Fig. 4.24d were ripples in the agarose structure are clearly visible, possibly caused by ionic strength gradients. Similarly, in Fig. 4.24b, where the surface of a particle from the same sample is shown one can clearly see inside the pores of the gel, which suggest that even particles manufactured at high quenching temperature were fully permeable.

In addition to the artefacts caused by salt precipitation during etching of the gel, the effectiveness of immersing samples into nitrogen slush in order to 'instantly' freeze them, thus prevent crystal formation, is challenged. By looking at the values of average pore sizes for samples with no salt (no salt precipitation artefacts, Fig. 4.2a and Fig. 4.23) quenched at different temperatures, one should be able to see, if not the same values, at least similar trends. Instead no correlation is observed between them suggesting that even in the absence of salt artefacts are also caused by ice crystal formation. In Fig. 4.24a the spherical shape of the agarose beads has been deformed by external ice crystal formation, whereas in Fig. 4.24c the surface of the particle has exploded leading to the enlargement of pore size and the flattening of the agarose fibres.

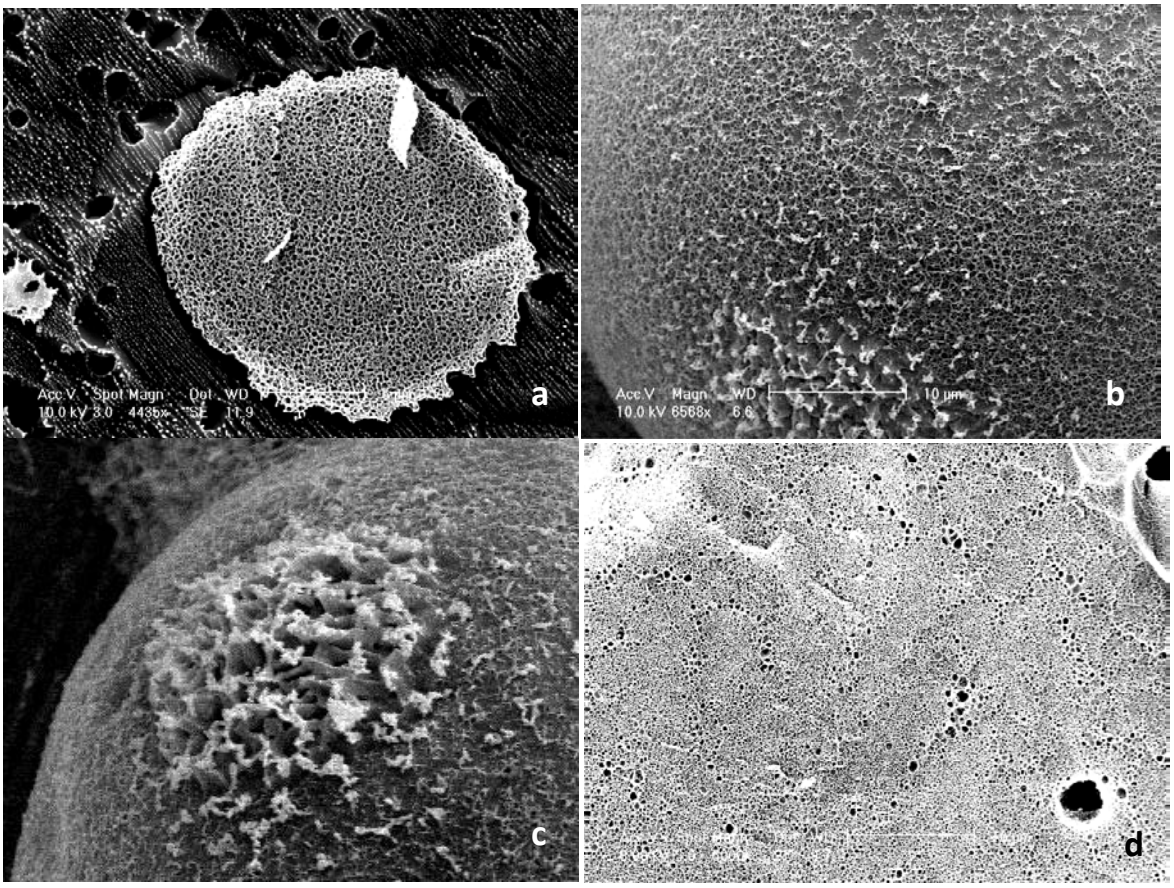

***Figure 4.24**. Sample 0 m, 0° C, (a) cross section of particle, (b) particle surface, (c) exploded particle , (d) ripples in the agarose structure possible caused by ionic strength gradients.*

4.2.3. Examination of Sepharose 4B and Sepharose CL-4B

Sepharose 4B and CL-4B were also examined with the SEM (Fig. 4.25). Average pore size for Sepharose CL-4B was slightly larger than of Sepharose 4B (141 nm over 130 nm). The shape of pore size distribution for these two samples was more or less the same. Despite the fact that the AFM showed the opposite (51 nm over 42 nm), the differences in both cases are minimal and can be attributed to experimental error. In addition, the standard deviation of the pore size distribution of both gels is larger (82 nm for Sepharose 4B, 74 nm for Sepharose CL 4B) when compared with values obtained from AFM (38 nm for Sepharose 4B,

39 nm for Sepharose CL 4B). Fig. 4.24a indicates that particles manufactured in this project have surface and interior pores of the same size it is reasonable to assume that the large difference in standard deviation is due to non-uniform freezing of the sample. On closer examination of Fig. 4.25 one can deduce that Sepharose 4B and Sepharose CL-4B do not contain any salt in their formulations as no salt appears to have precipitated on the agarose fibres during etching, confirming the observation stated in the AFM section, that Sepharose appears to have identical structural properties with 0 m quenched at 0° C.

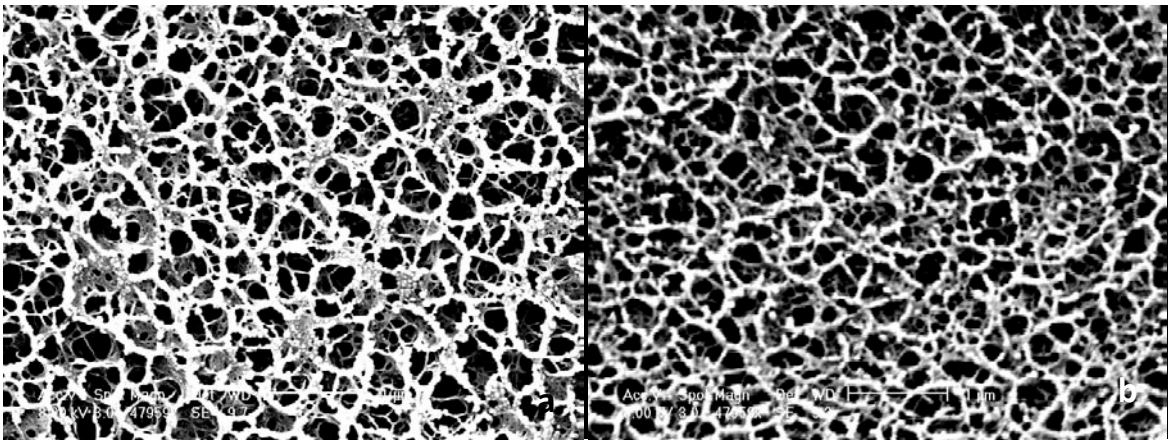

***Figure 4.25**. (a) Sepharose 4B (scale bar: 1 µm), (b) Sepharose 4B CL (scale bar: 1 µm).*

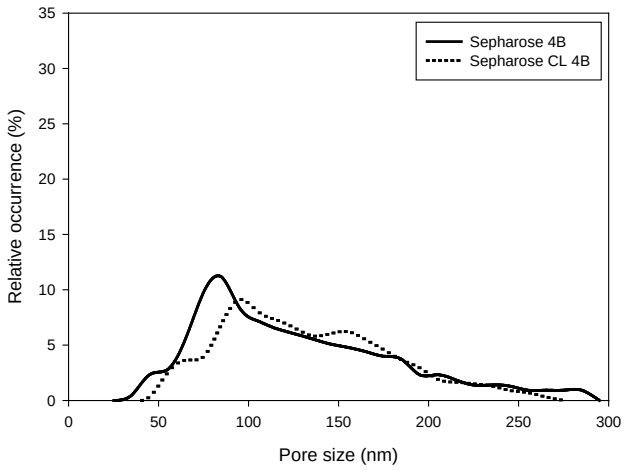

***Figure 4. 26**: Pore size distribution for Sepharose 4B and Sepharose CL-4B.*

Table 4.1. *Summary of AF and cryo-SE Microscopy results*

Method	Ionic strength	Quenching temperature	Pore size	Standard deviation	Surface roughness
AFM	(m)	(°C)	(nm)	(nm)	(nm)
	0.00	0	38	41	20
	0.01	0	40	45	30
	0.025	0	67	59	30
	0.05	0	128	74	30
	0.10	0	190	105	30
	0.00	10	101	85	100
	0.01	10	109	105	100
	0.05	10	172	120	100
	0.00	20	150	126	50
	0.01	20	169	140	100
	0.05	20	195	137	50
Sepharose 4B	n/a	n/a	51	38	100
Sepharose CL-4B	n/a	n/a	42	39	100
Cryo-SEM					
	0.00	0	167	114	-
	0.01	0	84	48	-
	0.025	0	110	53	-
	0.05	0	80	42	-
	0.10	0	-	-	-
	0.00	10	70	50	-
	0.01	10	115	71	-
	0.05	10	87	65	-
	0.00	20	153	97	-
	0.01	20	140	83	-
	0.05	20	100	71	-
Sepharose 4B	n/a	n/a	130	82	-
Sepharose CL-4B	n/a	n/a	141	74	-

CHAPTER 5

-

MECHANICAL PROPERTIES OF AGAROSE BEADS BY MICROMANIPULATION

5.1. Mechanical properties and pore size by Micromanipulation

Two different sets of experiments were carried out. In the first set, loading experiments were performed at two final deformations (10 and 30 %). The aim of these tests was to determine the range at which particles were fully elastic, to determine the compressive strength and Young's modulus, and to use the last to calculate the average pore size of the adsorbent. The second set included loading / holding experiments allowing the determination of the viscoelastic properties of the particles. Results from both sets, presented in graphical form, were obtained from the raw micromanipulation data acquired as described in section *2.5.6*. During compression of particles, the normal stress on the sphere is not uniform, but it varies from the maximum σ_{max} at the contact points between probe and particle to minimum σ_{min} in the cross-section of a particle placed half-way between the compressive surfaces. The full analysis of the spatial stress distribution is rather complex and in this case unnecessary, as only a comparison between samples is of interest in this work. Therefore the compressive strength of particles was compared in terms of average stress σ_{av}, or pseudo-stress, which is defined as the ratio of compressive force to the cross-section of an undeformed particle.

The theory for elastic spheres compressed between two flat rigid surfaces was first introduced by Hertz (Ding *et al*. 2007). For small deformations (up to 10 %), the relationship between force *F* (N) and deformation *h* (m) is described by the following equation:

$$F = \left[\frac{4}{3}\frac{R^{0.5}}{2^{1.5}}\frac{E}{1-\nu^2}\right]h^{1.5} \tag{5.1}$$

where: *R* is particle radius (m)

E is the Young's modulus (Pa)

v is the Poisson's ratio.

At higher deformations the Hertz equation fails. An extension of the Hertz theory has been developed by Tatara (Ding *et al*. 2007) where they introduced higher order terms in the force-displacement equation and suggested a semi-empirical relationship between force and deformation which is valid for up to 60 % deformation,

$$F = ah^{1.5} + bh^3 + ch^5 \tag{5.2}$$

where: *a* is the coefficient of the Hertz equation

b and *c* are material-depended constants, determined experimentally

5.1.1. Loading experiments

The Hertz model was used to describe the relationship between force and displacement for small deformation (10 %). Because this model is valid for small deformations only (up to 10 %) (Liu *et al*. 1998), the force-displacement relationship for large deformation (30 %) was

described by the Tatara model, which is valid for up to 60 % strain (Muller *et al.*, 2005). At least ten particles were compressed from each sample in order to obtain statistically representative results. An example of experimental data from a 100 µm in diameter particle fitted to both models in shown in Fig. 5.1.

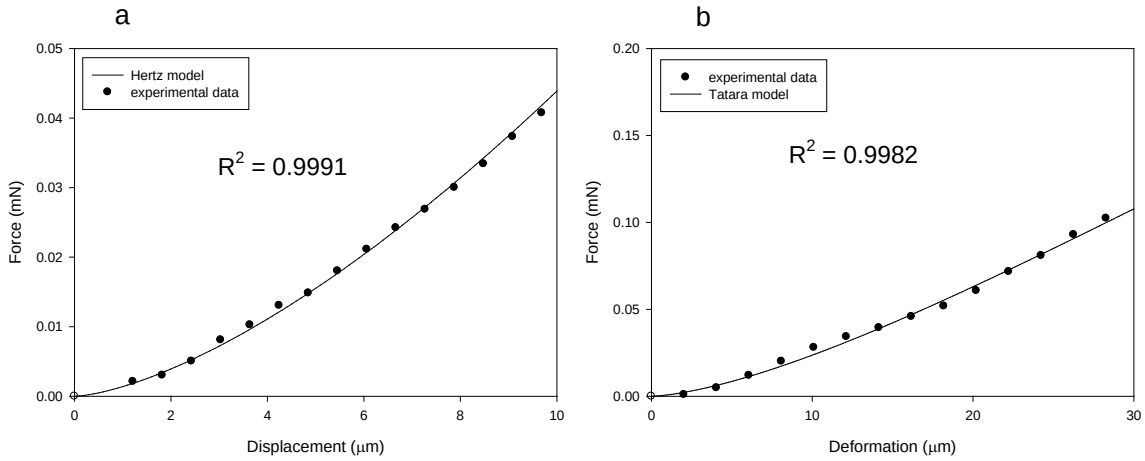

Figure 5.1*. (a) Small deformation (10 %) and (b) large (30 %) deformation for a 100 µm in diameter particle.*

At small deformation (10 %) (Fig. 5.2a, 5.3a) all curves practically overlap and there is no clear difference in the compressive strength of particles manufactured with increasing salt content and quenching temperatures. In particular, pseudo-stress for pure agarose was 0.00465 MPa, 0.00461 MPa for 0.01 m, 0.0641 MPa for 0.025 m, 0.00507 MPa for 0.05 m and 0.00622 MPa for 0.1 m. The respective values for samples quenched at increasing temperatures were: 0.00465 MPa for 0°C 0 m, 0.00507 MPa for 0° C 0.05 m, 0.00498 MPa for 20° C 0 m, and 0.00605 MPa for 20° C 0.05 m. Results suggest that 10% deformation was not sufficient to pronounce the structural differences caused by salting-out nor by slow cooling of the agarose gels. On the contrary, the difference between Sepharose 4B and Sepharose CL-4B (Fig. 5.4a) was far more pronounced (0.004057 MPa and 0.007924 MPa

respectively) even at such small deformation. At large strain (Fig. 5.2b, 5.3b) the differences between samples become obvious, for both increasing salt content and slow cooling. Samples manufactured with increasing ionic strength of the agarose solution, quenched at 0° C, showed a tendency to become stiffer with increasing salt content: Compressive strength was 0.0147 MPa for pure agarose, 0.0153 MPa for 0.01 m, 0.0168 MPa for 0.025 m, 0.0181 MPa for 0.05 m and 0.02 MPa for 0.1 m, an increase of the order of 135 % in compressive strength compared to pure agarose formulation. Similar increase in stiffness was observed in values of slowly cooled samples: 0.0147 MPa for pure agarose and 0.0181 MPa for 0.05 m at 0°C while for 20° C the respective values are 0.0190 MPa for 0 m and 0.0214 MPa for 0.05 m. The calculated error bars for both small and large deformations suggest that standard deviation is a function of and increases with deformation. The values obtained from compression of agarose beads are in good agreement with the literature (Mu *et al*. 2005). Large deformation of Sepharose 4B was of the same range with the 0° C, 0 m sample (0.0160 MPa and 0.0147 MPa respectively) (Fig. 5.4b). These two samples also had the same average pore size as found by the AFM, suggesting a similarity in manufacturing conditions and possibly in column performance with regards to pressure drop and bed compressibility. Large deformation of Sepharose CL-4B yielded the largest compressive strength observed between samples (0.0279 MPa), reflecting the significant increase in mechanical properties due to chemical cross-linking.

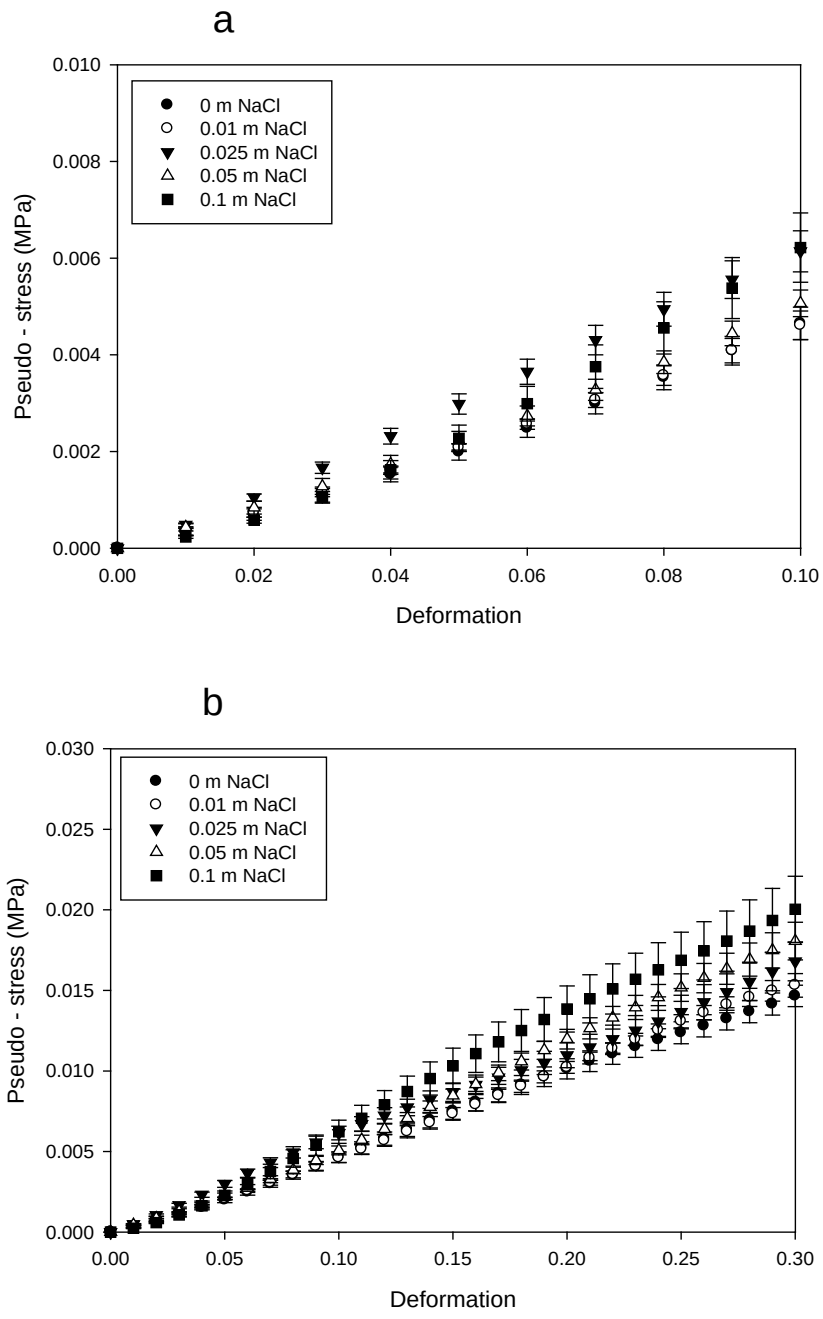

Figure 5.2. *(a) Small (10 %) and (b) large (30 %) deformation of agarose beads of increasing ionic strength quenched at 0° C.*

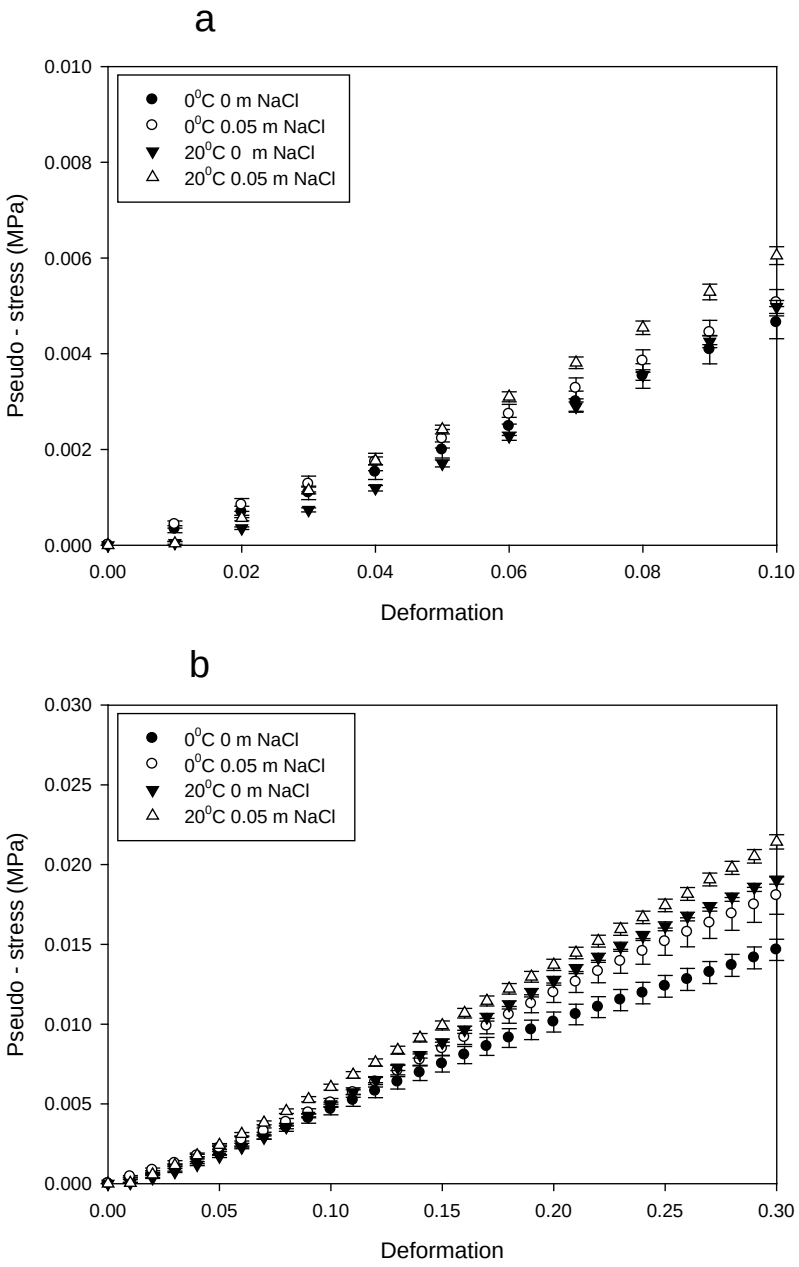

Figure 5.3. *(a) Small (10 %) and (b) large (30 %) deformation of samples quenched at two temperatures: 0° and 20° C, ionic strength: 0 m and 0.05 m.*

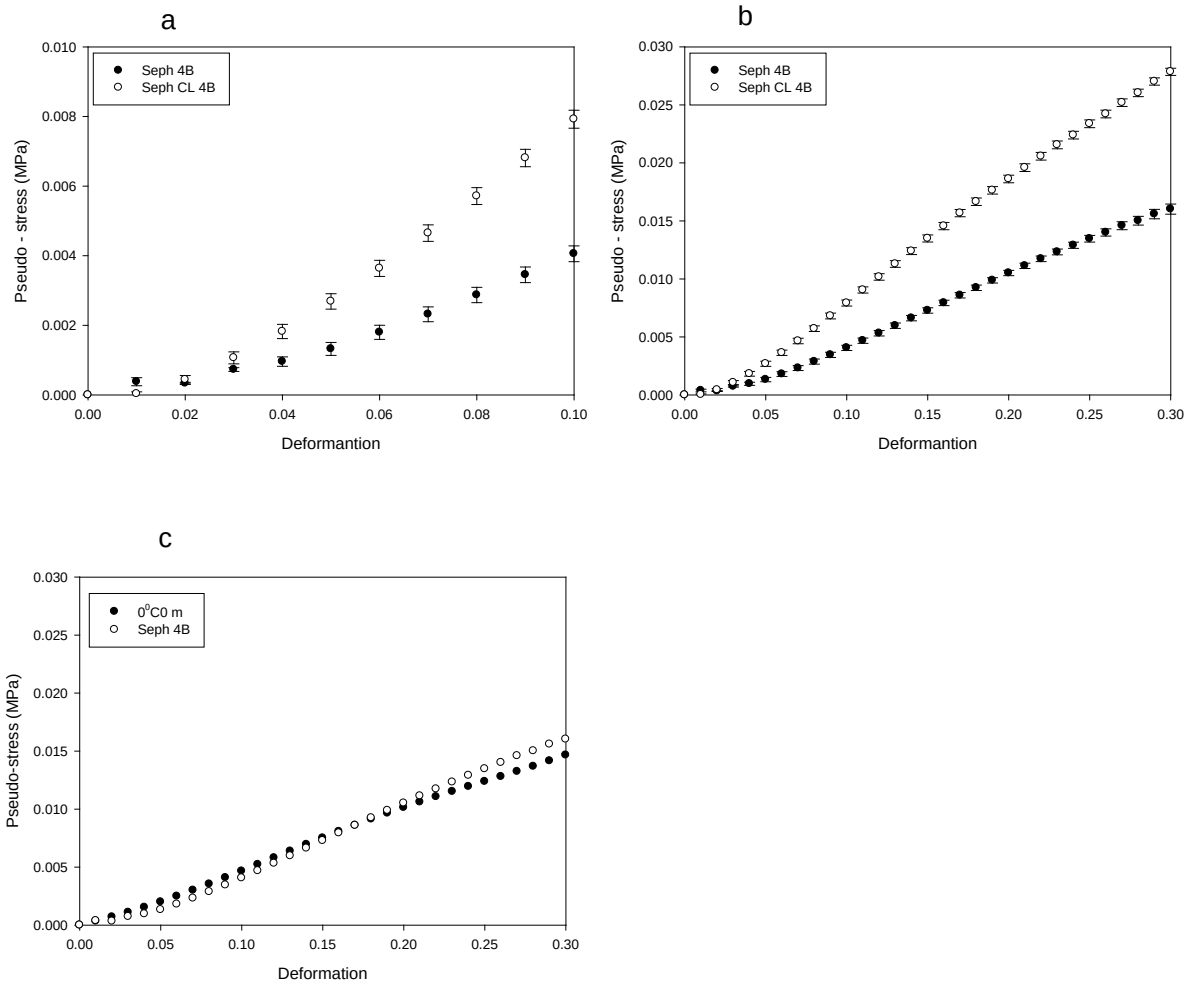

Figure 5.4*. (a) small (10 %), (b) large (30 %) deformation of Sepharose 4B and Sepharose CL-4B and (c) large (30 %) deformation of Sepharose 4B and 0° C 0 m sample.*

Although no unloading data were recorded, particles appeared to return to their original size as, there was no visible gap between the tip of the probe and the surface of particles, suggesting that beads were fully elastic at 10 % and 30 % deformation. Additionally, the range of deformations applied during loading tests was representative of the deformations chromatographic particles are exposed to during operation, with the latter being of the order of 15 % (Muller *et al*. 2005).

Young's modulus of particles was calculated from both small and large deformation data using the Hertz and Tatara models respectively. For said calculations it was assumed that the Poisson ratio of the particles was 0.5 (Mu *et al.* 2005). Values obtained using the Hertz model remained constant (0.29 MPa, standard deviation 0.015 MPa) with increasing ionic strength and quenching temperature (Fig. 5.5a, 5.5c). In addition, values obtained using this model resulted in large standard deviation of particles of the same sample (see error bars in Fig. 5.5a). However, when the Tatara model was used (Fig. 5.5b, 5.5d), Young's modulus increased with increasing salt content and quenching temperature, while values of individual particles were much closer to the mean of each sample (see error bars in Fig. 5.5b). Elastic modulus calculated using the Tatara model ranged from 0.155 MPa for 0° C, 0 m to 0.2950 MPa for 20° C, 0.05 m and where in reasonable agreement with the literature (Normand *et al*. 2000). The different values and trends obtained from these two models suggest that it is rather difficult to obtain accurate force measurements at such scale (30-150 μm) especially for small deformations (10 %). Furthermore, although the Hertz model has been shown experimentally to be valid for small deformations (Liu *et al*. 1998) the principal assumptions of this model, that the radius of contact area compared to that of the sphere is small and remains constant during compression (Zhang *et al*. 2007), should be taken in account, in light of the above results. Therefore the Tatara model appears to give a better description of the compression of these particles.

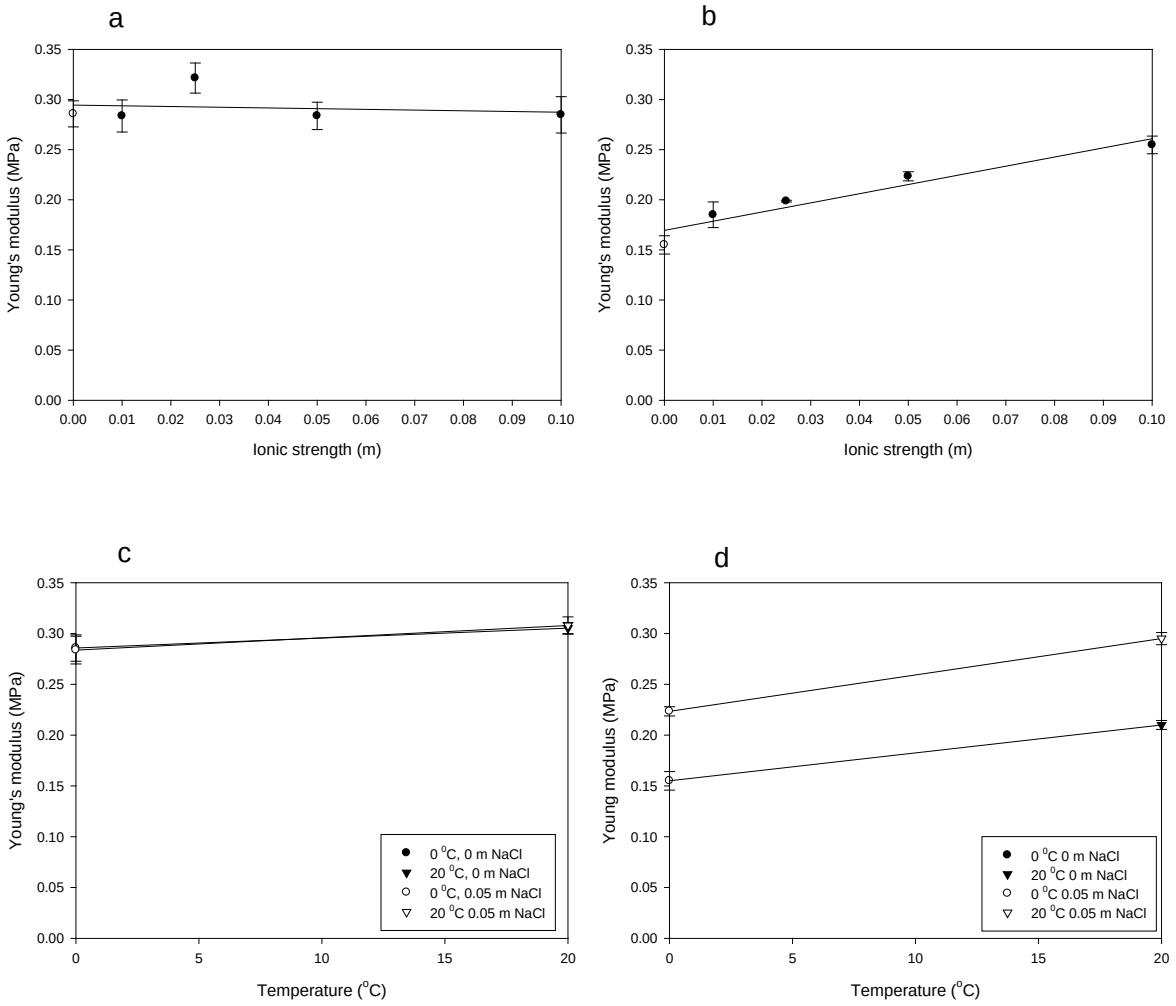

Figure 5.5. *Young's modulus for ionic strength calculated using (a) Hertz model, (b) Tatara model, Young's modulus for increasing quenching temperature calculated using (c) Hertz model, (d) Tatara model.*

The determination of the elastic modulus allows the calculation of the shear modulus of the particles from Eq. 5.3 (Mu *et al*. 2005, Yan *et al*. 2009). Since the Tatara model appears to describe the compression of agarose beads better than the Hertz model, values of elastic modulus obtained with this model were used for the calculation of the shear modulus. Table 5.1 shows the values of both moduli.

$$G = \frac{E}{2\,(1+v)} \tag{5.3}$$

where *G:* shear modulus (MPa)

v: Poisson ratio (0.5)

Table 5.1. *Young's and shear moduli*

Ionic strength (m)	**Quenching temperature** (°C)	**Young's modulus E (Hertz)** (MPa)	**Young's modulus E (Tatara)** (MPa)	**Shear modulus G (Tatara)** (MPa)
0.00	0.00	0.286	0.155	0.052
0.01	0.00	0.284	0.185	0.062
0.03	0.00	0.321	0.199	0.066
0.05	0.00	0.284	0.223	0.074
0.10	0.00	0.285	0.255	0.085
0.00	20.00	0.305	0.210	0.070
0.05	20.00	0.308	0.295	0.098

Once the compression strength and Young's and shear moduli are known, the maxima mechanical loads particles can be exposed to can be estimated. This is particularly useful since this type of information allows the determination of optimum working conditions during high-intensity post-processing steps such as filtration washing and chemical modification (cross-linking, activation) (Mu *et al*. 2005) as well as operation (chromatographic application).

Using relationships adopted from rubber elasticity theory (Anseth *et al*. 1996, Stenekes *et al*. 2000, Peppas *et al.* 2000) the calculation of the elastic modulus may provide a theoretical expression of the average pore size of a hydrogel:

$$M_c = \frac{3\rho RT}{E} \tag{5.4}$$

where: M_c is the molecular weight between crosslinks (kg mol^{-1})

ρ is the density (kg m^{-3})

R is the gas constant

T is the absolute temperature (°K)

E is the elasticity modulus (Pa)

The molecular weight between crosslinks M_c can be used to estimate the linear distance between two adjacent crosslinks, i.e. the average pore size of the gel, using the following equations (Peppas *et al.* 1985, Peppas *et al*. 2000):

$$\xi = a(r_0^2)^{1/2} \tag{5.5}$$

where: ξ is the average pore size (nm)

a is the elongation ratio of the polymer chains in any direction

$(r_0^2)^{1/2}$ is the root-mean-square, end-to-end of the polymer distance between two neighbouring crosslinks (nm)

For isotropically swollen networks, the elongation ratio *a* can be related to the polymer volume fraction using Eq. 5.6:

$$a = v_{2,s}^{-1/3} \tag{5.6}$$

where: $v_{2,s}^{-1/3}$ is the polymer volume fraction

The unperturbed end-to-end distance of the polymer chain between two adjacent crosslinks can be calculated using Eq. 5.7:

$$(r_0^2)^{1/2} = l(C_n N)^{1/2} \tag{5.7}$$

where: *l* is the length of the bond along the polymer backbone (nm)

C_n is the Flory characteristic ratio

N is the number of cross-links per chain

The number of cross-links per polymer chain can be calculated by the following equation:

$$N = \frac{2M_c}{M_r} \tag{5.8}$$

where: M_r is the molecular weight of the repeating unit from which the polymer is composed.

By combing Eq. 5.4-5.8 the following relationship is obtained:

$$\xi = l(v_{2,s}^{-1/3})(\frac{6C_n \rho RT}{M_r E})^{1/2} \tag{5.9}$$

Eq. 5.9 relates the elastic modulus of agarose obtained from micromanipulation data to molecular weight between crosslinks M_c and the polymer volume fraction $u_{2,s}$. With all other variables fixed, increasing the concentration of agarose (polymer volume fraction) in the gel results into more fibres per unit volume. Higher number of agarose fibres per unit volume indicates that more physical cross-linking events will occur per fibre (higher cross-linking density). Thus with increasing concentration of the polymer, smaller pore size and a narrow size distribution (Pernodet *et al*. 1997), as well as increased mechanical strength, are obtained. With increasing polymer concentration therefore, the cross linking density, given by Eq. 5.10 (Khonakdara *et al*. 2006), increases, which in turn decreases pore size and increases the value of elasticity modulus. The dependency of the elastic modulus on the cross-linking density exists because the elastic modulus is essentially a measure of the number of crosslinks per unit volume of the gel (De Gennes 1979, Khonakdara 2006)

$$v = \frac{\rho}{M_c} \tag{5.10}$$

where: v is the cross-linking density

Results from loading experiments show that with ionic strength and high quenching temperature the compressive strength (Fig. 5.2b, 5.3b) as well as the elastic modulus (Fig. 5.5b) of agarose beads increase. These trends are in good agreement with the literature (Mohammed *et al*. 1998, Mu *et al*. 2005, Maaloum *et al*. 1998). As it was previously shown (sections *4.1.1* and *4.1.2*), both ionic strength and high quenching temperature increase the pore size of agarose gels. This indicates that with ionic strength and / or slow cooling agarose

gels with large pore size and increased mechanical strength are obtained. Therefore, although cross-linking density decreases (less pores per unit area of AFM images with increasing salt content and / or slow cooling) and molecular weight between cross links increases (increase in pore size), the elastic modulus also increases. This is explained by considering the effect of ionic strength and / or slow cooling on the structure of the gel. Both process variables promote helix-helix aggregation and the formation of large pores and thick fibres. More agarose chains bound together suggest that the number of intramolecular hydrogen bonds per unit volume of the gel will be higher, thus having a large contribution to the rigidity of the gel structure (Yan *et al*. 2009). In other words, the increased aggregation of agarose fibres by salting-out and / or slow cooling arranges the same number of fibres (same polymer concentration in all samples) into a stronger network structure. If the increasing values of elastic modulus obtained from loading experiments were to be used in Eq. 5.9 the result would be decreasing pore size. This is because equations adopted from rubber elasticity theory do not account for the conformational effect of ionic strength and / or slow cooling on the gel (instead they account for a decrease in the elastic modulus through a reduction in the number of crosslinks per unit volume of the gel (De Gennes 1979, Khonakdara 2006)), therefore cannot be used to predict the average pore size of the particular agarose formulations.

A similar case describing what is found above is agarose gels consisting of chains of increasing molecular weight. It has been shown experimentally (Normand *et al*. 2000) that the elastic modulus of agarose gels increases with increasing molecular weight of the agarose chains. The authors suggested that this increase is a result of the increasing length (higher molecular weight) of the agarose chains which in turn provides a larger number of

available cross-linking sites per agarose chain, therefore promotes helix-helix aggregation and the formation of rigid structures. The same appears to hold true for increasing ionic strength and slow cooling.

Since the theoretical prediction of pore size of agarose beads manufactured in this project using equations adopted from rubber elasticity theory was not possible, a correlation between results obtained from large deformation of particles and pore size values obtained from the AFM was attempted. Fig. 5.6, a-b show the compressive strength of agarose beads at 30 % deformation and the calculated Young's modulus using the Tatara model plotted against average pore size as obtained by the AFM.

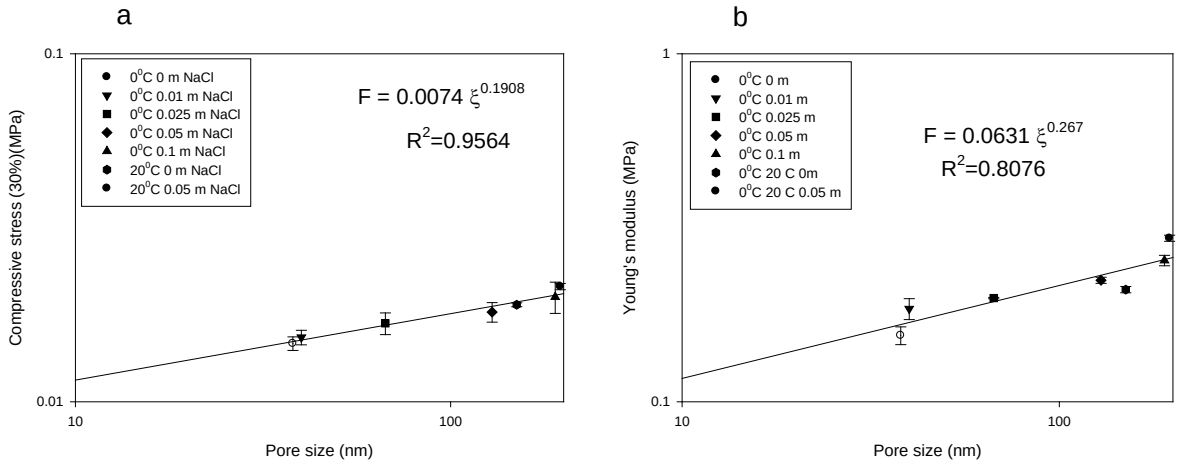

Figure 5.6. *Pore size by AFM vs. (a) compressive strength at 30 % and (b) Young's modulus using Tatara model*

It can be seen from Fig. 5.6 that compressive strength and Young's modulus increase linearly with the pore size of the gel. As previously discussed, this trend is a result of the contribution of intramolecular hydrogen bonds between agarose chains, on the rigidity of the gel structure (Yan *et al*. 2009). The larger the number of agarose chains aggregated

together, the larger the pore size and the better the mechanical strength. The correlation of loading experiments and AFM results, as well as the comparison of samples manufactured in this project with a benchmark product such as Sepharose 4B, allows one to deduce that particles manufactured with increasing salt content and / or slow cooling seem to have certain advantages (but also a disadvantage), in the purification of plasmids and viruses over currently existing commercial products designed for protein purification. The increased pore size of samples manufactured in this project can be exploited for the reversible accommodation of large bioproducts, by providing access to the interior of the adsorbent, thus increasing the apparent surface area for adsorption. Considering the soft nature of polysaccharides such as agarose and the reduced flow-rates associated with it (Jungbauer 2005), the improved mechanical properties of particles manufactured with increasing salt content and / or slow cooling suggest that the latter can be used at higher flow-rates than Sepharose 4B. Considering that crosslinking of the gel does not change the pore size or pore size distribution, the same can be argued for the preparative-grade counterparts of Sepharose. The disadvantage arising with the enlarging of the pore structure of agarose by said means is the possible band broadening during separation due to large pose size distribution. It has been shown experimentally (Kusukawa *et al*. 1999) in agarose gel for electrophoresis, that gels formed by rapid quenching gave sharper, more highly resolved bands of plasmid DNA compared to gels that had being allowed to gel at room temperature. This was explained on the basis of homogeneity of the pore size distribution and the way the latter affects the mobility and resolution of plasmid DNA within the gel.

Furthermore the correlation of AFM and loading experiments results suggest that the compression strength of agarose particles manufactured with increasing salt content and /

or slow cooling can be solely determined by AFM examination of samples, thus replacing the time-consuming micromanipulation experiments. The former, in combination with the practically minimal sample preparation of AFM, make this microscopy method a good candidate for the standard characterization of new agarose beads formulations, in terms of pore size and pore size distribution

5.1.2. Loading / holding experiments

Fig. 5.7a-c show the results of loading-holding experiments. The results in these figures were obtained from the raw data in a similar way as described for small and large deformation in section *2.5.6*. Particles were compressed to 50 % deformation and then held at this position for at least 35 s. It can be seen in the figure below that the relaxation force of these particles is of the order of 10 % of the total compressive force. Additionally, the curve describing the holding part of the compression is parallel to the x-axis, hence no relaxation occurs (Stenekes *et al*. 2000). These results indicate that no permanent changes occurred in the internal structure of the particles, even at 50 % deformation. Therefore, for engineering calculations particles can be treated as fully elastic. Similarly to loading experiments (section *5.1.1*), elastic behaviour was also demonstrated by the fact that particles returned to their original shape after compression and holding.

a

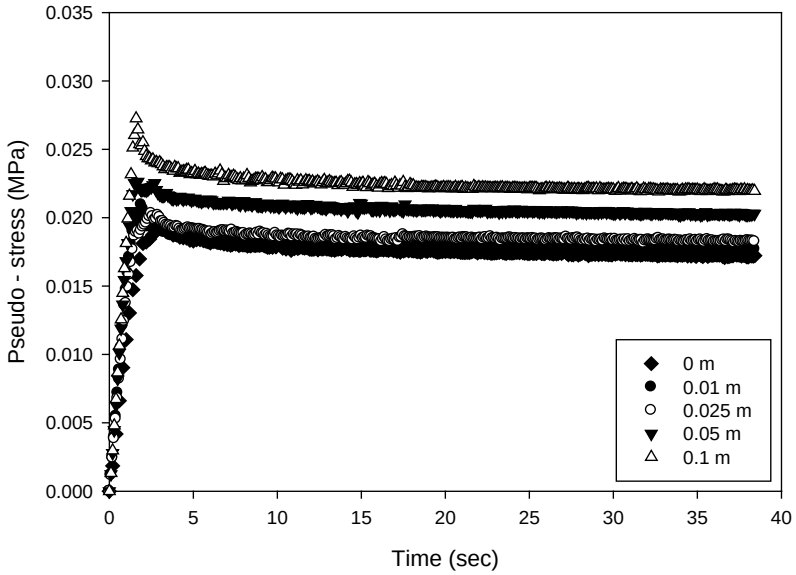
Pseudo - stress (MPa)
0.035
0.030
0.025
0.020
0.015
0.010
0.005
0.000
0
5
10
15
20
25
30
35
40
Time (sec)
0 m
0.01 m
0.025 m
0.05 m
0.1 m

b

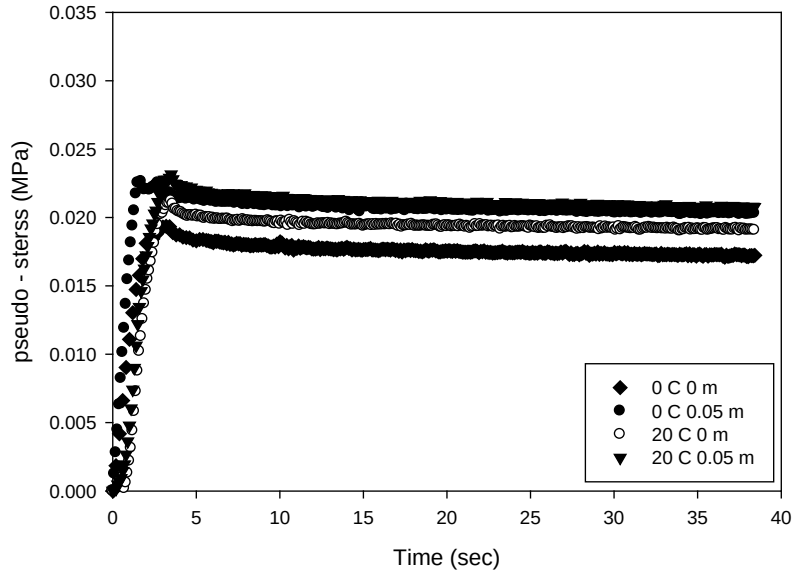
pseudo - sterss (MPa)
0.035
0.030
0.025
0.020
0.015
0.010
0.005
0.000
0
5
10
15
20
25
30
35
40
Time (sec)
0 C 0 m
0 C 0.05 m
20 C 0 m
20 C 0.05 m

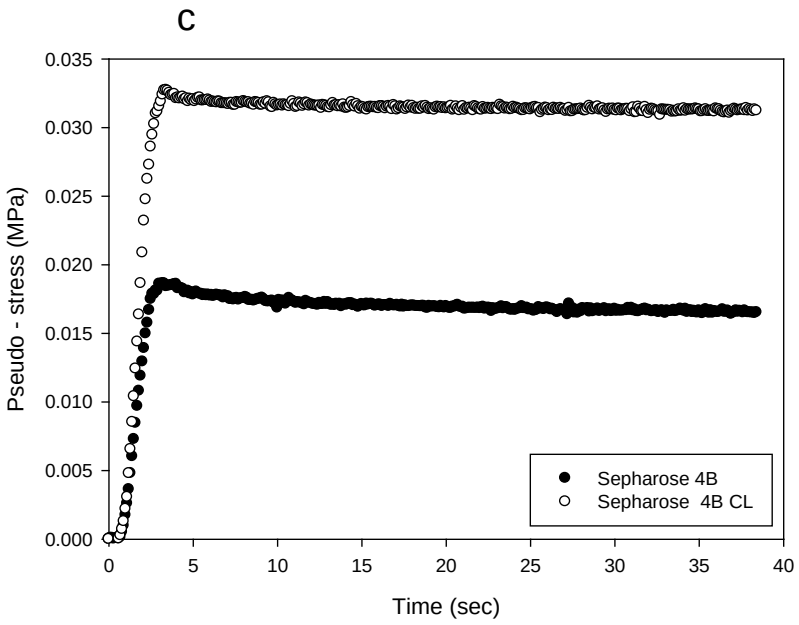

Figure 5.7. *Loading / holding experiments: (a) samples of increasing ionic strength, (b) samples cooled at different quenching temperatures, (c) Sepharose 4B and Sepharose CL-4B.*

CHAPTER 6

-

CONCLUSIONS AND RECOMMENDATIONS FOR FUTURE WORK

6.1. Conclusions for Chapters 3, 4 and 5

*6.1.1. Conclusions for **Chapter 3: Manufacturing and macroscopic characterization of agarose beads***

The effect of ionic strength of agarose solution and quenching temperature on the macroscopic properties of the adsorbent (particle size / particle size distribution) was investigated. Also, the effect of surfactant concentration and type, and energy dissipation rate on said properties was investigated.

Quenching temperature appears to have practically no effect on the macroscopic properties of the adsorbent, which suggests that droplets are covered by surfactant molecules and do not seem to coalesce and merge during quenching. However this may change if lower surfactant concentrations are to be used in combination with higher energy dissipation rates during emulsification. Also, coalescence of droplets can be promoted if the duration of droplet collision exceeds the film drainage time, conditions favoured in 'dead zones' characterized by low intensity during quenching or cooling. Therefore selection of emulsifying equipment for either batch or continuous production of the adsorbent must ensure the absence of such zones.

For the range of salt concentrations used (0-0.1 m NaCl) increasing the ionic strength of the agarose solution results in a mild fluctuation of D(0,9). This may be attributed to experimental errors during particle sizing, therefore assuming that salt does not affect particle size / size distribution. However, at higher salt concentrations, 'salting-out' of the hydrophilic head of the surfactant may occur, thus promoting recoalescence through diminishing electrostatic and steric repulsions between droplets. This will result in an increase in particle size therefore adjustment of energy dissipation rate may be needed to achieve the same particle size / size distribution.

Overall, for the concentrations of salt and range of quenching temperatures, it was demonstrated that the microscopic properties of the adsorbent can be controlled during manufacturing, without significantly affecting its macroscopic properties.

The presence of surfactants at the liquid-liquid interface of the emulsion greatly contributes toward the control of particle size / size distribution as well as increases process yield by lowering the interfacial tension and preventing coalescence. The high temperature of emulsification results in most of the surfactant added to the system being in the form of micelles in the bulk volume of the continuous phase. Consequently, only a small amount adsorbs at the liquid-liquid interface and the resulting particle size / size distribution strongly depends on the initial concentration, despite the relatively high amount used. This cannot be overcome in any way since the processing temperature is restricted by the gelling temperature of the agarose solution. Although process yield values of up to 50 % were reported here, with proper selection of emulsifier concentration and type, energy dissipation rate, and stator screen, higher yields may be achieved. Furthermore, although a

relatively narrow range of processing conditions was examined it is certain that the amount of surfactant added in the system can be reduced while emulsifying at higher energy dissipation rates. Thus a product of higher purity can be obtained as well as a small decrease in manufacturing cost can be achieved (less surfactant).

The comparison of different types of surfactant showed that a bulkier, more lipophilic (hydrophobic) molecule is more efficient in producing the desired particle size / size distribution, compared to a more lipophobic molecule. This was attributed to the large cross-sectional area of the lipophobic tail-group of the former and the properties associated with it, at given conditions.

*6.1.2. Conclusions for **Chapter 4: Atomic Force and cryo-Scanning Electron Microscopy characterization of agarose bead structure***

The effect of ionic strength of agarose solution and quenching temperature of the emulsion on the resulting pore size / size distribution of the adsorbent was investigated by Atomic Force and cryo-Scanning Electron microscopy. Despite the moderate availability of information on the effect of said parameters on agarose gels, this is the first account in the open literature of examining and numerically quantifying the effect of manufacturing conditions on the structural properties of beaded agarose intended for bioseparations. It is also the first account of the use of Atomic Force microscopy under wet state for examination of said properties of beaded agarose.

Increasing the ionic strength of agarose solution by adding salt results into 'salting-out' of the agarose fibres during gelation. This, in turn, promotes fibre aggregation and the formation of a structure with larger pore size and wider pore size distribution than of pure agarose. For the relatively narrow range of salt concentrations used (0-0.1 m NaCl) it was demonstrated that agarose beads with a five-fold increase in average pore size can be produced, while maintaining the same polymer concentration. It was also (theoretically) shown, that this effect is solely a function of ionic strength of solution and does not depend on the type of salt used. Decreasing the quenching temperature of the emulsion has a strikingly similar effect to salt, therefore the two process parameters can be combined if a wider structure is desired.

The examination of Sepharose 4B and Sepharose CL-4B revealed that, indeed chemical cross-linking does not change the original porous properties of the adsorbent in terms of dimensions. Therefore particles manufactured in this work can be chemically cross-linked to any degree to produce chemically and mechanically superior gels beads, while maintaining their original pore dimensions.

Overall, the results from this Chapter indicate that the agarose structure can be manipulated to a large extend to facilitate *intraparticle* diffusion of large-sized bioproducts in packed and/or expanded beds, such as viruses and plasmid DNA, without compromising mechanical strength (see below *Conclusions for Chapter 5*). Additionally there is no need for complicated and expensive manufacturing, such as the one encountered in superporous agarose by means of double emulsification or inclusion and subsequent dissolution of suitable porogene. Although the increase in average pore size of the gel is advantageous, the

widening of the pore size distribution is unfavourable as it is associated with broad elution peaks. For this reason such particles would be ideal at early stages of purification (see in *Introduction,* CIPP) where speed of operation and capacity of adsorbent for bioproduct are favoured at the expense of resolution.

The practically minimal sample preparation in combination with the ability to examine agarose gels in the wet state makes AFM a good method for the structural characterization of agarose beads in terms of pore dimensions. A drawback of AFM was the inability to examine the interior structure of the particles but this can be overcome with the development of an efficient fracturing / slicing method at wet state. The ability to examine both the surface and interior structure of the adsorbent is highly desirable in the controlled manufacturing of adsorbents as instances of under / over-processing can be identified and eliminated. On the contrary, the examination of agarose beads with the cryo-SEM may have provided information on the interior structure of the particles, but it was rather distorted by the extensive sample preparation, harsh examination conditions and salt precipitation. Therefore cryo-fixation is rather unsuitable for hydrogels.

6.1.3. Conclusions for ***Chapter 5: Mechanical properties of agarose beads by Micromanipulation***

The effect of ionic strength of and quenching temperature on the mechanical properties (compression strength at given deformations, Young's and shear moduli and viscoelastic properties) of the resulting particles was investigated by mechanical means. This is the first account in the open literature to quantify the effect of ionic strength on the mechanical

properties of single agarose beads intended for bioseparation. In addition, there is only one publication (Mu *et al*. 2005) available in the open literature concerned with effect of quenching temperature on the resulting mechanical properties of the adsorbent.

The Hertz and Tatara models were used to describe the force-deformation relationship of the particles at small (10 %) and large (30 %) deformation respectively. In addition, the two models allowed the determination of Young's and shear moduli of the particles. Loading experiments at small and large deformation showed that the compression strength of particles increases with ionic strength. The observed by AFM similarity between the effect of ionic strength and quenching temperature on the pore size / size distribution of the agarose beads was also reflected by the nearly identical mechanical properties of particles manufacture with salt and slow cooling. The values of these moduli obtained with the use of the Tatara model yielded more accurate values. This was attributed to the micron-sized scale of the experiment and the lower accuracy of small deformation measurements.

The increased compression strength of particles manufactured with salt and / or slow cooling is explained by the extended fibre aggregation the two parameters promote during agarose gelation. A larger number of aggregated fibres suggests that the number of intermolecular hydrogen bonds per unit volume of the gels will be higher, thus more rigid structures are obtained. In other words, increasing the ionic strength of solution and / or applying slow cooling, arranges the same number of fibres (same polymer concentration in all samples) into a more rigid gel structure.

Equations adopted from rubber elasticity theory could not be used to calculate the average pore size of the adsorbent. Based on these equations, the Young's modulus of a

polymer network is proportional to the number of physical cross-links per unit volume of the gel, i.e. the polymer concentration in the gel and consequently the average pore size of the adsorbent. In this work, increased pore size and values of Young's modulus were obtained by arranging the same number of fibres into a more rigid structure. Therefore, if values of Young's modulus obtained in this work were to be used in these equations, the result would be decreasing rather than increasing pore size.

Loading / holding experiments showed that even at 50 % deformation no permanent changes occurred in the internal structure of the particles as the measured relaxation force was of the order of 10 % while the trace describing the holding part of the experiment was parallel to the x-axis, suggesting full elasticity. Another point suggesting full elasticity of the agarose beads was the fact that particles appeared to return to their original shape after decompression.

Overall, results from this Chapter demonstrated that manipulating the structure of agarose by said means to produce adsorbents of wider pore structures is accompanied by improvement of mechanical properties. This is in contrast to the currently applied control of agarose structure, which is by lowering the polymer concentration in the gel when wider structures are desired. In addition, obtaining information on the mechanical properties of the absorbent, not only provides an insight on the performance of particles during operation but also, allows the optimization of post-manufacturing processing such as filtration-washing and chemical modification (cross-linking, activation).

6.2. Recommendations for future work

The following section includes recommendations and future work that could prove beneficial to the controlled manufacturing of agarose-based adsorbents.

6.2.1. Optimization of energy dissipation rate and surfactant concentration

As only a narrow range of energy dissipation rates and surfactant concentrations was used in this work, emulsification experiments should be carried-out at the maximum achievable energy dissipation rate of the device used. This suggests that the surfactant concentration in the system can be reduced to a minimum and therefore a product of higher purity can be obtained.

6.2.2. Interfacial tension measurements to determine surfactant equilibrium concentration after emulsification for oil recycling

One of the initial objectives of this work was the manufacturing of agarose beads without the use of surfactants. This is highly desirable for large scale manufacturing of agarose-based chromatographic adsorbents as the continuous phase, which is otherwise discharged a waste, can be recycled. Preliminary experiments showed that the use of surfactants cannot be avoided as the resulting particle size distribution was very wide, even at the highest energy dissipation rate, resulting into a very small process yield. In addition, instability of the system and irreproducibility of the results did not allow conclusions, from various experiments (stator geometry, introduction of agarose solution from different ports of the

emulsification vessel), to be drawn. Exploiting specific properties of the surfactant and mineral oil, such as different boiling points or the lowering of interfacial tension, to determine the equilibrium concentration of the surfactant in the continuous phase after emulsification, is proposed as a way to avoid discharging the latter. This will result in significant reduction in the manufacturing cost of the adsorbent.

6.2.3. Gelation temperature of agarose solution of increasing ionic strength and quenched at different temperatures

The pronounced aggregation of agarose chains (increased pore size) with ionic strength and slow cooling leads to the formation of rigid structures (gel) at higher temperature than of pure agarose; hence the gelation temperature of the agarose solution is increased. Therefore, as a complement to other characterization techniques, the increase in pore size with ionic strength and slow cooling can be indirectly observed by determining the gelation temperature of the agarose solution.

6.2.4. Broader ionic strength and quenching temperature ranges to achieve desired pore size dimensions for plasmids and viruses

The range of ionic strengths and quenching temperatures covered in this work resulted in a five-fold increase in average pore size of the adsorbent. As this range was relatively narrow it is certain that if a broader range is used, further increase in pore size can be achieved, therefore increasing plasmid or virus diffusivity into the interior of the adsorbent. In

addition, salts of different ionic strength should be used to confirm that the effect on the agarose fibres is indeed a function of ionic strength and does not depend on the type of salt used.

6.2.5. Plasmid adsorption capacity

Once the desired pore size allowing plasmid diffusion is achieved, experiments to determine the maximum adsorption capacity of the adsorbent should be carried out. This type of experiment can be performed in batch contactor and the results can be used to predict column performance of the adsorbent.

6.2.6. Column flow rate

Mechanical testing showed that the compression strength of particles prepared in this work is higher compared to that of a benchmark product. This suggests that these particles can be used at higher flow rates than the former but this assumption needs to be verified in a chromatography column. The same type of flow test should be applied to particles after cross-linking to determine the maximum flow rate of the enhanced structure.

6.2.7. Use of micro-tome to produce thin agarose bead sections

The use of AFM in this work only allowed the examination of the external surface of the agarose beads. This was due to the lack of proper slicing equipment that resulted in artefacts in the gel structure. Although both interior and exterior of the adsorbent were examined with the SEM the data obtained from these images is of questionable quality for reasons explained in *Chapter 4*. Given the effect of quenching temperature on the structure of the adsorbent, it is rather crucial to verify with a good characterization technique (such as AFM) that the pore size of the outer surface of the adsorbent is the same as the internal one. Therefore further work to obtained uniform slices of agarose beads should be attempted.

REFERENCES

Adachi Tadashi, Eiji Isobe (2004), "**Fundamental characteristics of synthetic adsorbents intended for industrial chromatographic separations**", *Journal of Chromatography A 1036, 33 – 44.*

Adachi Tadashi, Shingo Ando, Junya Watanabe (2002), "**Characterization of synthetic adsorbents with fine particle sizes for preparative – scale chromatographic separation**", *Journal of Chromatography A 944, 41 – 59.*

Amersham Biosciences (1996), "**Expanded Bed Adsorption Principles and Methods**" *18 – 1124 – 926 Edition AB, p.1.*

Amersham Biosciences (2000), "**Hydrophobic Interaction Chromatography Principles and Methods**" *18 – 1020 – 90 Edition AB, p.12.*

Amersham Biosciences (2002), "**Gel Filtration Principles and Methods**" *18 – 1022 – 18 Edition AI, p.10, 76.*

Amersham Biosciences (2004), "**Affinity Chromatography Principles and Methods**" *18 – 1022 – 29 Edition AD, p.10, 123, 125.*

Amersham Biosciences (2004), "**Ion Exchange Chromatography and Chromatofocusing Principles and Methods**" *11 – 0004 – 21 Edition AA, p.11, 42 – 45.*

Amsterdam Abraham, Zvi Er-el, Shmuel Shaltiel (1975), "**Ultrastructure of beaded agarose**", *Archives of Biochemistry and Biophysics 171, 673 – 677.*

Andersson Mikael, Mats Ramberg, Bo – Lennart Johansson (1998), "**The influence of the degree of cross – linking, type of ligand and support on the chemical stability of chromatography media intended for protein purification**", *Process Biochemistry 33, 47 – 55.*

Anseth Kristi S., Christopher N. Bowman, Lisa Brannon - Peppas (1996), "**Mechanical properties of hydrogels and their experimental determination**", *Biomaterials 17, 1647 – 1657.*

Anslyn Eric V., Dennis A. Dougherty (2006), "**Modern Physical Organic Chemistry**", *University Science Books, Edition: illustrated, p. 166.*

Anspach F. Birger, David Curbelo, Ralf Hartmann, Gunnar Garke, Wolf-Dieter Deckwer (1999), "**Expanded – bed adsorption in primary protein purification**", *Journal of Chromatography A, 865, 129 – 144.*

Araki Choji (1956), "**Structure of the agarose constituent of agar – agar**", *Bulletin of Chemical Society of Japan 29, 543 – 544.*

Arashiro Emerson Y., Nicole R. Demarquette (1999), "**Use of pendant drop method to measure interfacial tension between molten polymers**", *Materials Research 2 (1), 23 – 32.*

Asenjo Juan A., Barbara A. Andrews (2008), "**Mini – review Challenges and trends in bioseparations**", *Journal of Chemical Technology and Biotechnology 83, 117–120.*

Attwood T. K., B. J. Nelmes, D. B. Sellen (1988), "**Electron microscopy of beaded agarose gels**", *Biopolymers 27, 201 – 212.*

Aymard Pierre, David R. Martin, Kevin Plucknett, Tim J. Foster, Alan H. Clark, Ian T. Norton (2001), "**Influence of thermal history on the structure and mechanical properties of agarose gels**", *Biopolymers 59, 131 – 144.*

Balasundaram B., S.T.L. Harrison (2008), "**Influence of the extent of disruption of Baker's yeast on protein adsorption in expanded beds***", Journal of Biotechnology 133, 360 – 369.*

Barigou Mostafa (2003), **Course notes**, *University of Birmingham, UK.*

Baselt David (1993), "**The tip – sample interaction in atomic force microscopy and its implications for biological applications**", *PhD Thesis, California Institute of Technology, USA, p. 87.*

Binnig G., C. F. Quate, Ch. Gerber (1986), "**Atomic Force Microscopy**", *Physical Review Letters 56 (9), 930 – 933.*

Blewett Jennifer M. (2000), "**Micromanipulation of plant cell mechanical properties**", *PhD Thesis, University of Birmingham, UK, p.88.*

Bowen James (2005), "**NanoAdhesion: Investigating nanoscale adhesion using self – assembled monolayer**" *PhD Thesis, University of Birmingham, UK, p. 45 – 46.*

Buchmeiser Michael R. (2007), "**Polymeric monolithic materials: Syntheses, properties, functionalization and properties**", *Polymer 48, 2187 – 2198*.

Calabrese Richard V. Michael K. Francis, Ved P. Mishra, Supathorn Phongikaroon (2000), "**Measurement and analysis of drop size in a batch rotor-stator mixer**", *10th European Conference on Mixing.*

Chahal Parminder S, Marc G. Aucoin, Amine Kamen (2007), "**Primary recovery and chromatographic purification of adeno – associate virus type 2 produced by bacilovirus / insect cell system**", *Journal of Virological Methods 139, 61 – 70.*

Chui Martin M., Ronald J. Phillips, Michael J. McCarthy (1995), "**Measurement of the porous microstructure of hydrogels by nuclear magnetic resonance**", *Journal of Colloidal and interface science 174, 336 – 344*.

Colton J. Richard, David R. Baselt, Yves F. Dufrene, John – Bruce D Green, Gil U. Lee (1997), "**Scanning probe microscopy**", *Current Opinion in Chemical Biology 1997, 1 370 – 377.*

Connolly J., M. Singh, C.E. Buckley (2004), "**Determination of size and ordering of pores in mesoporous silica using small angle neutron scattering**", *Physica B 350, 224 – 226*.

Cuperus F.P., D. Bargeman, C.A. Smolders (1992), "**Critical points in the analysis of membrane pore structures by thermoporometry**", *Journal of Membrane Science 66, 45 – 53.*

Curling John (2007), "**Process chromatography: Five decades of innovation**", *BioPharm International 20, 10 – 19.*

Damrongsak Faroongsarng, Garnet E. Peck (2003), "**Thermal porosity analysis of croscarmellose sodium and sodium starch glycolate by differential scanning calorimetry**", *AAPS ParmaSciTech 4 (4), article 67.*

De Gennes P.G. (1979), "**Scaling Concepts in Polymer Physics**", *Cornell University Press, Ithaca NY, 1st edition, p. 221.*

Dennison Clive (2003), "**A Guide to Protein Isolation**", *Springer, 2nd edition, p. 75.*

DePhillips Peter, Abraham M. Lenhoff (2000), "**Pore size distributions of cation – exchange adsorbents determined by inverse size - exclusion chromatography**", *Journal of Chromatography A 883, 39 – 54.*

Ding P., I.T. Norton, Z. Zhang, A.W. Pacek (2007), "**Mechanical properties of gelatin – rich microparticles**", *Journal of Food Engineering 86, 307 – 314.*

Diogo M.M., J.A. Queiroz, D.M.F. Prazeres (2005), "**Chromatography of plasmid DNA**", *Journal of Chromatography A 1069, 3 – 22.*

Djabourov M., A. H. Clark, D. W. Rowlands, S. B. Ross-Murphy (1989), "**Small – angle x – ray scattering characterization of agarose gels and sols**", *Macromolecules 22 (1), 180 – 188.*

Doucet L. G. Ascanio, P. A. Tanguy (2005), "**Hydrodynamics characterization or rotor – stator mixer with viscous fluids**", *Chemical Engineering Research and Design 83 A10, 1186 – 1195.*

Egorov A. M., A. Kh. Vakhabov, V. Ya. Chernyak (1970), "**Isolation of agarose and granulation of agar and agarose gel**", *Journal of Chromatography 46, 143 – 148*.

Emanuele A., Di Stefano L., Giacomazza D., Trapanese M., Palma – Vitorelly M. B. (1991), "**Time-Resolved study of network self-organization from a biopolymeric solution**", *Biopolymers 31 (7), 859 – 868.*

Fatin-Rouge Nicolas, Konstantin Starchev, Jacques Buffle (2004), "**Size effects on diffusion processes within agarose gels**", *Biophysical Journal 86, 2710–2719.*

Gafonova Olga V., Harvey W. Yarranton (2001), "**The Stabilization of water-in-hydrocarbon emulsions by asphaltenes and resins**", *Journal of Colloid and Interface Science 241, 469 – 478.*

Gavrilescua Maria, Yusuf Chisti (2005), "**Biotechnology — a sustainable alternative for chemical industry"**, *Biotechnology Advances 23, 471 – 499.*

Giribabu K., P. Ghosh (2007), "**Adsorption of non-ionic surfactants at fluid-fluid interfaces: Importance in the coalescence of bubbles and drops**", *Chemical Engineering Science 62, 3057 – 3067.*

Griess Gary A., Kenneth B. Guiseley, Philip Serwer (1993), "**The relationship of agarose gel structure to the sieving of spheres during agarose gel electrophoresis**", *Biophysical Journal 65, 138 – 148.*

Grimaud E., J. C. Lecog, E. Boschetti, M. Corgier (1978), "**Comparison of gels for molecular sieving of proteins by electron microscopy and pore parameters determination**", *Journal of Chromatography 166, 37 – 45*.

Gustavsson Per – Erik, Klaus Mosbach, Kjell Nilsson, Per – Olof Larsson (1997), "**Superporous agarose as an affinity chromatography support**", *Journal of Chromatography A 776, 197 – 203.*

Gustavsson Per – Erik, Per – Olof Larsson (1996), "**Superporous agarose, a new material for chromatography**", *Journal of Chromatography A 743, 231 – 240*.

Gustavsson Per-Erik, Anders Axelsson, Per-Olof Larsson (1999), "**Superporous agarose beads as a hydrophobic interaction chromatography support**", *Journal of Chromatography A 830, 275 – 284.*

Gustavsson Per-Erik, Per-Olof Larsson (1999), "**Continuous superporous agarose beds for chromatography and electrophoresis**", *Journal of Chromatography A 832, 29 – 39.*

Gutenwik Jan, Bernt Nilsson, Anders Axelsson (2004), "**Effect of hindered diffusion on the adsorption of proteins in agarose gel using a pore model**", *Journal of Chromatography A 1048, 161 – 172.*

Hagel Lars, Magnus Ostberg, Torvald Andersson (1996), "**Apparent pore size distributions of chromatography media"**, *Journal of Chromatography A 743, 33 – 42.*

Hasse Ulrich, Fritz Scholz (2006), "**Tuning the size of silver deposits by templated electrodeposition using agarose gels**", *Journal of Solid State Electrochemistry 10, 380 – 382.*

Heeboll – Nielsen Anders (2002) "**High Gradient Magnetic Fishing**", *PhD Thesis, Technical University of Denmark, Denmark, p. 3*

Higuchi Akon Toshiro Iijima (1985), "**D.s.c. investigation of the states of water in poly(vinyl alcohol – co – itaconic acid) membranes**", *Polymer 26, 1833 – 1837*.

Hjerten Stellan (1971), "**Some new methods for the preparation of agarose**", *Journal of Chromatography 61, 73 – 80.*

Hoinkisa Ernst, Martin Ziehl (2003), "**A small - angle neutron scattering study of activated carbon fibres**", *Carbon 41, 2047 – 2056*.

http://wps.prenhall.com.

http://www.labfilters.pall.com/catalog/laboratory35870.asp.

http://www.soonersci.com/catalog/page46.html.

http://www.wiley.co.uk/genmed/clinical/.

Hubbuch Jurgen J. (2000), "**Development of Adsorptive Separation Systems for Recovery of Proteins from Crude Bioprocess Liquors**", *PhD Thesis, Technical University of Denmark, Denmark, p. 15.*

Jafari Seid Mahdi, Elham Assadpoora, Yinghe Heb, Bhesh Bhandari (2008), "**Re-coalescence of emulsion droplets during high-energy emulsification**", *Food Hydrocolloids 22 1191 – 1202.*

Jahanshahi Mohsen (2003), "**Integration and intensification of bioseparations: A role for pellicular solid phases in combinatorial cell disruption and fluidised bed adsorption**", *PhD Thesis, University of Birmingham, UK, p. 78.*

Jahanshahi Mohsen, Andrej W. Pacek, Alvin W. Nienow, Andrew Lyddiatt (2003), "**Fabrication by three – phase emulsification of pellicular adsorbents customised for liquid fluidized bed adsorption of bioproducts**", *Journal of Chemical Technology and Biotechnology 78, 1111 – 1120.*

Janson Jan – Christer, Jan – Ake Jonsson (1998) in "**Protein Purification: Principles, High Resolution Methods and Applications**", *Wiley – VCH, Inc. 2nd edition, p. 46.*

Janssen J.M., A. Boon, W.G.M. Agterof (1994), "**Influence of dynamic interfacial properties on droplet break-up in simple shear flow**" *AIChE Journal 40, 1929 – 1939.*

Johnson Erin M., David A. Berg, Rakesh K. Jain, William M. Deen (1995), "**Diffusion and partitioning of proteins in charged agarose gels**", *Biophysical Journal 68, 1561 – 1568.*

Joscelyne Simon M., Gun Tragardh (2000), "**Membrane emulsification – a literature review**", *Journal of Membrane Science 169, 107 – 117*.

Josic Djuro, James G. Clifton (2007), "**Use of monolithic supports in proteomics technology**", *Journal of Chromatography A 1144, 2 – 13.*

Jungbauer Alois (2005), "**Chromatographic media for bioseparation**", *Journal of Chromatography A 1065, 3 – 12.*

Kalyanpur Manohar (2000), in "**Downstream Processing of Proteins Methods and Protocols**", *Humana Press, Edition: Illustrated, p. 1 – 10.*

Karbstein Heike, Helmar Schubert (1995), "**Developments in the continuous mechanical production of oil – in – water macro – emulsions**", *Chemical Engineering and Processing 34, 205 – 211.*

Kepka Cecilia, Raf Lemmens, Jozsef Vasi, Tomas Nyhammar, Per-Erik Gustavsson (2004), "**Integrated process for purification of plasmid DNA using aqueous two – phase systems combined with membrane filtration and lid bead chromatography**", *Journal of Chromatography A 1057, 115 – 124.*

Khonakdara H.A., S.H. Jafari, U. Wagenknecht, D. Jehnichen (2006), "**Effect of electron-irradiation on cross-link density and crystalline structure of low- and high-density polyethylene**", *Radiation Physics and Chemistry 75, 78 – 86.*

Knox John H., Harald J. Ritchie (1987), "**Determination of pore size distribution curves by size – exclusion chromatography**", *Journal of Chromatography 387, 65 – 84.*

Kusukawa Noriko, Mikhail V. Ostrovsky, Mark M. Garner (1999), "**Effect of gelation conditions on the gel structure and resolving power of agarose-based DNA sequencing gels**" *Electrophoresis 20, 1455 – 1461.*

Laas T. (1998) in "**Protein Purification: Principles, High Resolution Methods and Applications**", *Wiley – VCH, Inc. 2nd edition, p.464.*

Ladisch M. R. (2001), "**Bioseparations Engineering**", *John Wiley & Sons, New York 1st edition, p. 2, 10, 515.*

Lambrich U., H. Schubert (1999), "**Emulsification using microporous systems**", *Journal of Membrane Science 257, 76 – 84.*

Levy Susana M., Ronan D. O' Kennedy, Parviz Ayazi - Shamlou Peter Dunnill (2003), "**Biochemical engineering approaches to the challenges of producing pure plasmid DNA**", *Trends in Biotechnology 18, 296 – 305.*

Li Ping, Guohua Xiu, Alirio E. Rodrigues (2003), "**Modelling separation of proteins by inert core adsorbent in a batch adsorber**", *Chemical Engineering Science 58, 3361 – 3371.*

Lightfoot E. N., J. S. Moscariello (2004), "**Bioseparations***", Biotechnology and Bioengineering 87 (3), 259 – 273.*

Liu K. K., D. R. Williams, B. J. Briscoe (1998), "**The large deformation of a single micro-elastomeric sphere**", *Journal of Physics D: Applied Physics 31, 294 – 303.*

Liu, T., Donald A. M., Zhang, Z. (2005), "**Novel manipulation in Environmental SEM for measuring the mechanical properties of single nano-particles**", *Materials Science and Technology 21 (3), 289 – 294.*

Ljunglof Anders, Peder Bergvall, Ramagauri Bhikhabhai, Rolf Hjorth (1999), "**Direct visualisation of plasmid DNA in individual chromatography adsorbent particles by confocal scanning laser microscopy**", *Journal of Chromatography A 844 129 – 135*.

Lobo Lloyd, Aileen Svereika, (2003), "**Coalescence during emulsification 2: Role of small molecule surfactants**" *Journal of Colloidal and Interface Science 261, 498 – 507.*

Lobo Lloyd, Aileen Svereika, Mridula Nair (2002), "**Coalescence during emulsification 1: Method development**" *Journal of Colloid and Interface Science 253, 409 – 418.*

Lucassen – Reynders E.H., K. A. Kuijpers (1992), "**The role of interfacial properties in emulsification**", *Colloids and Surfaces 65, 175 – 184.*

Lyddiatt A. (2002), "**Process Chromatography: Current constrains and future options for the adsorptive recovery of bioproducts**" *Current Opinion in Biotechnology 13, 95 – 103.*

Lyddiatt Andrew, Deirdre A. O'Sullivan (1998), "**Biochemical recovery and purification of gene therapy vectors**", *Current Opinion in Biotechnology 9, 177 – 185.*

Ma Guanghui, Fangling Gong, Guohua Hu, Dongxia Hao, Rong Liu, Renwei Wang (2005), "**Multi – scale structure in emulsion and microsphere complex systems**", *China Particuology 3 (6), 296 – 303.*

Maaloum Mounir, Nadine Pernodet, Bernard Tinland (1998), "**Agarose gel structure using atomic force microscopy: gel concentration and ionic strength effects**", *Electrophoresis 19, 1606 – 1610.*

Malmqvist (1978), "**Degradation of agarose gels and solutions by bacterial agarase**", *Carbohydrate Research 62, 337 – 348.*

Malvern Instruments Ltd. (1997), "**Sample Dispersion and Refractive Index Guide**" *MAN 0079, Version 3.1.*

Manno M., A. Emanuele, V. Martorana, D. Bulone, P. L. San Biagio, M. B. Palma-Vittorelli, M. U. Palma (1999), "**Multiple interactions between molecular and supramolecular ordering"**, *Physical Review E 59 (2), 2221 – 2230.*

Mashmoushy H., Z. Zhang, C. R. Thomas (1998), "**Micromanipulation of the mechanical properties of baker's yeast cells**", *Biotechnology Techniques 12, 925 – 929.*

McClements D.J. (2005), "**Food Emulsions: Principles, Practices, and Techniques**", *CRC Press 2nd edition, p.261 – 262.*

McRobbie Donald W. (2007), "**MRI, from Picture to Proton**", *Cambridge University Press 2nd edition, p.155.*

Medin Anders S., Jan – Christer Janson, Bo Nordin (1995), "**Studies on agarose gels with scanning electron microscopy**", *Uppsala University, Uppsala, Sweden.*

Milliken W. J., H.A. Stone and L.G. Leal (1993), "**The effect of surfactant on the transient motion of newtonian drops**", *Physics of Fluids A 5 1, 69 – 79.*

Milliken W. J., L. G. Leal (1994), "**The influence of surfactant on the deformation and breakup of a viscous drop: The effect of surfactant solubility**" *Journal of Colloid Interface Science 166, 275 – 285.*

Mohammed Z. H., M. W. N. Hember, R. K. Richardson, E. R. Morris (1998), "**Kinetic and equilibrium processes in the formation and melting of agarose gels**", *Carbohydrate Polymers 36, 15 – 26.*

Mohan Shashi, Ganesan Narsimhan (1997), "**Coalescence of protein-stabilized emulsions in high – pressure homogenizer**", *Journal of Colloidal and Interface Science 192, 1 – 15.*

Mu Y., A. Lyddiatt, A.W. Pacek (2005), "**Manufacture by water – in – oil emulsification of porous agarose beads: Effect of processing conditions on mean particle size, size distribution and mechanical properties**", *Chemical engineering and Processing 44, 1157 – 1166.*

Muller E., J. – T. Chung, Z. Zhang, A. Sprauer (2005), "**Characterization of mechanical properties of polymeric chromatographic particles by micromanipulation**", *Journal of Chromatography A 1097, 116 – 123.*

Myers Kevin J., Mark F. Reeder, David Ryan (2001), "**Power draw of a high-shear homogenizer**", *The Canadian Journal of Chemical Engineering 79, 94 – 99.*

Narayanan Janaky, Jun – Ying Xiong, Xiang Yiang Liu (2006), "**Determination of agarose gel pore size: Absorbance measurements vis a vis other techniques**", *Journal of Physics: Conference Series 28, 83 – 86.*

Narsimhan Ganesa, Parul Goel (2001), "**Drop Coalescence during Emulsion Formation in a high - pressure homogenizer for tetradecane-in-water emulsion stabilized by sodium dodecyl sulfate**", *Journal of Colloid and Interface Science 238, 420 – 432.*

Nedelec Jean Marie, Jean Pierre E. Grolier, Mohamed Baba (2006), "**Thermoporosimetry: A powerful tool to study the cross – linking in gel networks**", *Journal of Sol – Gel Science and Technology 40, 191 – 200.*

Normand Valery, Didier L. Lootens, Eleonora Amici, Kevin P. Plucknett, Piere Aymard (2000), "**New insight into agarose mechanical properties**", *Biomolecules 1, 730-738.*

Nucci Nathaniel V., Jane M. Vanderkooi (2008), "**Effects of the Hofmeister series on the hydrogen bond network of water**", *Journal of Molecular Liquids 143, 160 – 170.*

Ogawa Tomoharu, Kouichi Takamura, Masumi Koishi, Tamotsu Konto (1972), "**Studies on microcapsules. XIII: Effect of Span 85 and pH of aqueous phase of the formation of polyamide microcapsules**", *Bulletin of the Chemical Society of Japan 45, 2329 – 2331.*

Opawele Foyeke O., Diane J. Burgess (1998), "**Influence of interfacial properties of lipophilic surfactants on water – in – oil emulsions**", *Journal of Colloidal and Interface Science 172, 142 – 150.*

Overbeek J. T. G., P.L. de Bruyn, F. Verheckx (1984) in "**Surfactants**", *Academic Press London p. 125 – 127.*

Pacek A. W., Michael Baker, A. T. Utomo (2008), "**Flow pattern, periodicity and energy dissipation in a batch Rotor stator mixer**", *Sixth International Symposium on Mixing in Industrial Process Industries – ISMIP VI Niagara on the Lake, Niagara Falls, Ontario, Canada.*

Padron G. (2001), "**Measurement and comparison of power-draw in rotor stator mixers**", *MSc Thesis, University of Maryland, USA, p.29.*

Padron G. (2005), "**Effect of surfactants on drop size distribution in a batch rotor-stator mixer**", *PhD Thesis, University of Maryland, USA, p. 34 – 35, 99, 145.*

Park Tae Gwan, Allan S. Hofmann (1993), "**Sodium chloride – induced phase transition in non-ionic poly(*N* – isopropylacrylamide) Gel**" *Macromolecules 26, 5045 – 5048.*

Peixoto C., T.B. Ferreira, M.J.T. Carrondo, P.E. Cruz, P.M. Alves (2006), "**Purification of adenoviral vectors using expanded bed chromatography**", *Journal of Virological Methods 132, 121 – 126.*

Peltonen Leena, Jouni Hirvonen, Jouko Yliruusi (2001), "**The behavior of sorbitan surfactants at the water – oil Interface: Straight – chained hydrocarbons from pentane to dodecane as an oil phase**", *Journal of Colloid and Interface Science 240, 272 – 276.*

Peppas N. A., Moynihan H. J., Lucht L. M. (1985), "**The structure of highly cross-linked poly(2-hydroxyethyl methacrylate hydrogels.**" , *Journal of Biomedical Materials 19, 397 – 411.*

Peppas N. A., P. Bures, W. Leobandung, H. Ichikawa (2000), "**Hydrogels in pharmaceutical formulations**", *European Journal of Pharmaceutics and Biopharmaceutics 50, 27 – 46.*

Pernodet Nadine, Mounir Maaloum, Brnard Tinland (1997), "**Pore size of agarose gels by atomic force microscopy**", *Electrophoresis 18, 55 – 58.*

Perreur Chistelle, Jean – Pierre Habas, Alain Lapp, Jean Peyrelasse (2006), "**Salt influence upon the structure of aqueous solutions of branched PEO–PPO–PEO copolymers**", *Polymer 47, 841 – 848.*

Peters, D. C. (1992) in "**Mixing in the Process Industries**", *Butterworth – Herman 2nd edition, p. 295 – 296.*

Pines E, W. Prins (1973) "**Structure-property relations of thermoreversible macromolecular hydrogels**", *Macromolecules 6, 888 – 895.*

Pluen Alain, Paolo A. Netti, Rakesh K. Jain, David A. Berk (1999), "**Diffusion of macromolecules into agarose gels: Comparison of linear vs. globular configurations**", *Biophysical Journal 77, 542 – 552.*

Poole F. Colin (2003), "**The essence of chromatography**", *Elsevier Science B.V., 1st edition, p.874.*

Porath Jerker, Jan – Christer Janson, Torgny Laas (1971), "**Agar derivatives for chromatography, electrophoresis and gel – bound enzymes: I. Desulphated and reduced cross – linked agar and agarose in spherical bead form**", *Journal of Chromatography 60, 167 – 177*.

Porath Jerker, Torgny Laas, Jan – Christer Janson (1975), "**Agar derivatives for chromatography, electrophoresis and gel – bound enzymes: III. Rigid agarose gels cross – linked with divinyl sulphone (DVS)"**, *Journal of Chromatography 103, 49 – 62.*

Przybycien Todd M, Narahari S Pujar, Landon M. Steele (2004), "**Alternative bioseparation techniques: life beyond packed bead chromatography**", *Current Opinion in Biotechnology 15, 496 – 478.*

Qualli Lahoussine, Joachim Kohlbrecher, Konstantin Startchev, Jacques Buffle (2001), "**Fractal structure of agarose gel: Effects of the ionic strength of the solvent and cooling rate during gel formation**", *SINQ Proposal Number II/00 S – 22.*

Saito Hazime, Motoko Yokoi, Junko Yamada (1990), "**Hydration – dehydration – induced conformational changes of kappa – and iota – carraggenans as studied by high-**

resolution, solid – state C – nuclear magnetic resonance spectroscopy", *Carbohydrate Research 199, 1 – 10.*

Schmidt – Traub H. (2005), "**Preparative Chromatography**", *Wiley – VCH, p. 25, 28.*

Schnabel R., P. Langer (1991), "**Controlled – pore glass as a stationary phase in chromatography**", *Journal of Chromatography 544, 137 – 146*.

Serwer Philip, Gary A. Griess (1991), "**Methods for producing agarose gels having variable pore size**", *United States Patent, no. 5,009,759.*

Shinoda Kozo, Hironobu Kunieda (1977) in "**Microemulsions – Theory and Practice**", *Academic Press, Inc. p. 80.*

Shiu Carlo (2000), "**Mechanical properties of bacteria***", PhD Thesis, University of Birmingham, UK, p. 105.*

Silverson Machines Ltd (2005), "**Installation, Operation and Maintenance Instruction Manual For Sealed Unit Laboratory Mixers**", *LAB – 014 – BASE, ISSUE 6*

Snyder L. R., J. J. Kirkland (1979), "**Introduction to Modern Liquid Chromatography**", *John Wiley & Sons Inc. 2nd Edition, p. 28.*

Solomon T. (2001), "**The definition and unit of ionic strength**", *Journal of Chemical Education 78-12, 1691 – 1692.*

Srinorakutara T. (1997), "**Mechanical Strength of Yeasts***", PhD Thesis, University of Birmingham, UK, p. 12 – 13.*

Stenekes Robert, Stefaan C. De Smedt, Joseph Demeester, Guangzhi Sun, Zhibing Zhang, Wim E. Hennink (2000), "**Pore sizes in hydrated dextran microspheres**", *Biomacromolecules 1, 696 – 703*.

Stickel J.J., A. Fotopoulos (2001), "**Pressure – flow relationships for packed beds of compressible chromatography media at laboratory and production scale**", *Biotechnology Progress 17, 744 – 751.*

Stone H.A., L.G. Leal (1990), "**The effects of surfactants on drop deformation and breakup**", *Journal of Fluid Mechanics 220, 161 – 86.*

Sulthana Shireen B., S.G.T. Bhat, A.K. Rakshit (1996), "**Thermodynamics of micellization of a non-ionic surfactant Myrj 45: effect of additives***", Colloids and Surfaces A: Physicochemical and Engineering Aspects 111, 57 – 65.*

Sun H., X. Li, G. Ma, Z. Su (2005), "**Polystyrene – type uniform porous microsphere enables high resolution and low-pressure chromatography of natural products — a case study with icariin purification**", *Chromatographia 61, 9 – 15.*

Suwa K., Yamamoto K., Akashi M., Takano K., Kunugi S. (1998), "**Effects of salt on the temperature and pressure responsive properties of poly-(*N*- vinylisobutyramide) aqueous solutions**", *Colloid Polymer Science 276, 529 – 533.*

Tadros Tharwat F. (2005), "**Applied Surfactants: Principles and Applications**", *Wiley – VCH, Edition: illustrated, p.10.*

Taisne Laurent, Pieter Walstra, Bernard Cabane (1996), "**Transfer of oil between emulsion droplets**", *Journal of Colloid and Interface Science 184, 378 – 390.*

Tako Masakuni, Sanehisa Nakamura (1988), "**Gelation mechanism of agarose**", *Carbohydrate Research 180, 277 - 284.*

Tcholakova Slavka, Nikolai D. Denkov, Thomas Danner (2004), "**Role of surfactant type and concentration for the mean drop size during emulsification in turbulent flow**", *Langmuir*, *20 (18), 7444 – 7458.*

Theodossiou Irini, Michael Søndergaard, Owen R.T. Thomas (2001), "**Design of expanded bed supports for the recovery of plasmid DNA by anion exchange adsorption**", *Bioseparation 10, 31 – 44.*

Thwaites Eric, Simon C. Burton, Andrew Lyddiatt (2001), "**Impact of the physical and topographical characteristics of adsorbent solid-phases upon the fluidised bed recovery of plasmid DNA from Escherichia coli lysates**", *Journal of Chromatography A 943, 77 – 90.*

Tiainen Peter, Per-Erik Gustavsson, Anders Ljungol, Per-Olof Larsson (2007), "**Superporous agarose anion exchangers for plasmid isolation**", *Journal of Chromatography A 1138, 84 – 94.*

Trathnigg Bernd, Martin Veronik, Alexei Gorbunov (2006), "**Looking inside the pores of a chromatography column: I. Variation of the pore volume with mobile phase composition**", *Journal of Chromatography A 1104, 238 – 244.*

Troy David B., Paul Beringer (2005), "**Remington: The Science and Practice of Pharmacy**", *Lippincott Williams & Wilkins, 21st Edition: illustrated, p. 299.*

Unger Klaus, Jurgen Schick – Kalb, Karl Friedrich Krebs (1973), "**Preparation of porous silica spheres for column liquid chromatography**" *Journal of Chromatography 83, 5 – 9.*

Utomo A., M. Bakerb, A.W. Pacek (2009), "**The effect of stator geometry on the flow pattern and energy dissipation rate in a rotor – stator mixer**", *Chemical Engineering Research and Design 87, 533 – 542.*

Van Os Nico M. (1997), "**Non-ionic surfactants – Organic chemistry**", *CRC Press, Edition: illustrated p. 59.*

Vankova Nina, Slavka Tcholakova, Nikolai D. Denkov, Ivan B. Ivanov, Vassi D. Vulchev, Thomas Danner (2007), "**Emulsification in turbulent flow 1. Mean and maximum drop diameters in inertial and viscous regimes**", *Journal of Colloid and Interface Science 312, 363 – 380.*

Vladisavljevic Goran T., Masataka Shimizu, Tadao Nakashima (2004), "**Preparation of monodispersed multiple emulsions by multi – stage premix membrane emulsification**", *Journal of Membrane Science 244, 97 – 106.*

Waki S., J. D. Harvey, A. R. Bellamy (1982), "**Study of agarose gels by electron microscopy of freeze fracture surfaces**" *Biopolymers 21, 1909 – 1926.*

Walcarius A, C. Despas, J. Bessiere (1998), "**Molecular sieving with amorphous monodispersed silica beads**", *Microporous and Mesoporous Materials 23, 309 – 313.*

Walstra Pietre (1993), "**Principles of emulsion formation**", *Chemical Engineering Science 48 (2), 333 – 349.*

Wang C.X., L. Wang, C.R. Thomas (2003), "**Modelling the mechanical properties of single suspension – cultured tomato cells**", *Annals of Botany 93, 443 – 453*

www.abtbeads.com.

www.bioscience-beads.com.

www.chromdata.net/ChromMedia.php?id=100&PageID=Ligand.

www.financialreports.merck.de/servlet/PB/menu/1139910/index.html.

www.isis.rl.ac.uk/largescale/loq/documents/sans.htm.

www.jeolusa.com/sem/docs/sem_guide/tbcontd.html.

www.nanoscience.com/education/AFM.html.

www.purdue.edu/REM/rs/sem.htm.

www1.gelifesciences.com.

www1.gelifesciences.com/APTRIX/upp01077.nsf/Content/bioprocess.

Yamamotoa T., S.R. Mukaib, K. Nitta, H. Tamon, A. Endo, T. Ohmori, M. Nakaiwa (2005), "**Evaluation of porous structure of resorcinol – formaldehyde hydrogels by thermoporometry**", *Thermochimica Acta 439, 74 – 79.*

Yan Yan, Zhibing Zhang, Jason R. Stokes, Qing-Zhu Zhou, Guang-Hui Ma, Michael J. Adams (2009), "**Mechanical characterization of agarose micro-particles with a narrow size distribution**", *Powder Technology 192, 122 – 130.*

Yan Yao, Abraham Lenhoff (2004), "**Determination of pore size distribution of porous chromatographic adsorbents by inverse size – exclusion chromatography**", *Journal of Chromatography A 1037, 273 – 282*.

Yoonsun Yang, Seong-Won Nam, Nae Yoon Lee, Youn Sang Kim, Sungsu Park (2008), "**Superporous agarose beads for solid support for microfluidic immunoassay**", *Ultramicroscopy 108, 1384 – 1389.*

Zana Raoul, Eric W. Kaler (2007), "**Giant Micelles**", *CRC Press, Edition: illustrated p. 485.*

Zhang Yanjie, Paul S. Cremer (2006), "**Interactions between macromolecules and ions: the Hofmeister series**", *Current Opinion in Chemical Biology 10, 658 – 663.*

Zhang Z, M.A. Ferenczi, A.C. Lush, C.R. Thomas (1991), "**A novel micromanipulation technique for measuring the bursting strength of single mammalian cells"**, *Applied Microbiology and Biotechnology 36, 208 – 210.*

Zhang Z. L., H. Kristiansen, J. Liu (2007), "**A method for determining elastic properties of micron-sized polymer particles by using flat punch test**", *Computational Materials Science 39, 305 – 314.*

Zhang Zhanren, Simon Burton, Sharon Williams, Eric Thwaites, Andrew Lyddiatt (2001), "**Design and assembly of solid-phases for the effective recovery of nanoparticulate bioproducts in fluidised bed contactors**", *Bioseparation 10, 113 –132.*

Zhou Qing-Zhu, Guang-Hui Ma, Zhi-Guo Su (2009), "**Effect of membrane parameters on the size and uniformity in preparing agarose beads by premix membrane emulsification**", *Journal of Membrane Science 326, 694 – 700.*

Zhou Qing-Zhu, Lian-Yan Wang, Guang-Hui Ma, Zhi-Guo Su (2007), "**Preparation of uniformed – sized agarose beads by microporous membrane emulsification technique**", *Journal of Colloid and Interface Science 311, 118 – 127.*

Zhou Qing-Zhu, Lian-Yan Wang, Guang-Hui Ma, Zhi-Guo Su (2008), "**Multi – stage premix membrane emulsification for preparation of agarose microbeads with uniform size**", *Journal of Membrane Science 322, 98 – 104*.

Zhou Xin, Yan Sun, Zheng Liu (2007), "**Superporous pellicular agarose – glass composite particles for protein adsorption**", *Biochemical Engineering Journal 34, 99 – 106.*